Volume 18, Number 1

January, 1965

SOVIET ATOMIC ENERGY

АТОМНАЯ ЭНЕРГИЯ
(ATOMNAYA ÉNERGIYA)

TRANSLATED FROM RUSSIAN

CONSULTANTS BUREAU

NEW BOOKS | CONSULTANTS BUREAU / PLENUM PRESS

REVIEWS OF PLASMA PHYSICS

A systematic, multi-volume review of the present status of plasma theory, serving both as an introduction for students and for researchers entering the field, and as a convenient, authoritative, up-to-date presentation of current knowledge for workers in plasma physics. This continuing series, prepared by internationally known Soviet experts in specific fields, is under the editorship of Academician M. A. Leontovich, of the Kurchatov Institute of Atomic Energy. Each volume contains a number of integrated tutorial reviews, covering in depth and in breadth specific aspects of the theory of the given field of plasma physics. In many cases, new material is presented. Translated by Herbert Lashinsky, University of Maryland.

Volume 1: A comprehensive introduction to "classical" plasma physics, contains authoritative papers on: Orbit Theory, by D. V. Sivukhin; Collisions in Fully Ionized Plasma, by B. A. Trubnikov; Plasma Transport Phenomena, by S. I. Braginskii; and Plasma Thermodynamics, by A. A. Vedenov. Much of the material in the first two papers is presented here for the first time. Although the theoretical analyses are quite advanced, the experimental aspects of the subject are kept firmly in view throughout. This is especially true of the article on transport phenomena, in which the kinetic approach is developed in parallel with qualitative physical descriptions of transport phenomena, including some of the less familiar "transverse" thermal transport effects in plasma in magnetic fields. Many physical examples and applications of the theory are given.

336 pages $12.50

Volume 2: Contains four review papers concerned primarily with the problem of plasma confinement: Magnetic Field Geometries; Plasma Equilibrium in Magnetic Fields; Hydromagnetic Plasma Stability; and Motion of Charged Particles in Electromagnetic Fields.

Approx. 300 pages $12.50

Volume 3: Devoted to plasma waves, includes: Electromagnetic Waves in a Plasma; Oscillations of an Inhomogeneous Plasma; Introduction to the Theory of a Weakly Turbulent Plasma; and Symmetric Magnetohydromagnetic Flow and Helical Waves in a Circular Plasma Cylinder.

Approx. 300 pages $12.50

Volume 4: Contains three papers: Hydrodynamic Descriptions of a Highly Rarefield Plasma; Collective Phenomena in Collisionless Plasma Shock Waves, and Coulomb Collisions in Fully Ionized Plasma. The latter paper contains new material on the relevance of this topic in mirror machines, provided by the author (D. B. Sivukhin) for the English edition.

Approx. 290 pages $12.50

Volume 5: To be published late in 1965 in the Soviet Union is to comprise a comprehensive review of radiation phenomena in plasma. An English translation will be published promptly.

LEBEDEV PHYSICS SERIES

Complete English translations of the Proceedings ("Trudy") of the famed Lebedev Physics Institute of the USSR Academy of Sciences published as Consultants Bureau Special Research Reports. Series edited by D. V. Skobel'tsyn. The first three volumes in this distinguished series of ten Special Research Reports in translation, beginning with Volume 25, are:

OPTICAL METHODS OF INVESTIGATING SOLID BODIES

"Trudy" Volume 25

Includes papers by N. D. Zhevandrov (on polarized luminescence of crystals), V. P. Cheremisinov (on vibrational spectra and structure of oxides in the crystalline and glassy states) and L. A. Vainshtein (on calculation of cross sections for excitation of atoms and ions by electron impact).

194 pages 1965 $22.50

COSMIC RAYS

"Trudy" Volume 26

Contains an account of experimental investigations into nuclear and electromagnetic interactions at high and ultra-high energies. Theoretical articles on problems of the passage of high-energy electrons and photons through matter are included, as well as some results of the investigations into cosmic rays by means of artifical earth satellites.

262 pages 1965 $27.50

RESEARCH IN MOLECULAR SPECTROSCOPY

"Trudy" Volume 27

Devoted to spectroscopic investigations into matter in various states of aggregation by the methods of Raman scattering and infrared absorption. A special section is devoted to the methodological problem of correcting measured quantities for instrumental errors. Great attention is paid to the investigation of the temperature dependence of such spectroscopic quantities as the profile, width, and integrated intensity of Raman lines and absorption bands.

214 pages 1965 $22.50

CONSULTANTS BUREAU / PLENUM PRESS 227 W. 17th St., New York, N. Y. 10011

SOVIET ATOMIC ENERGY

A translation of **ATOMNAYA ÉNERGIYA**
A publication of the Academy of Sciences of the USSR

Volume 18, Number 1 January, 1965

CONTENTS

Annual Subscription: $95 **Single Issue: $30** **Single Article: $15**

CONTENTS (continued)

The Russian date "Podpisano k pechati" of this issue was 12/19/1964. This is equivalent to "approved for printing." Publication did not occur prior to this date, but must be assumed to have taken place reasonably soon thereafter.

Publisher

THE SEVENTIETH BIRTHDAY OF ACADEMICIAN A. L. Mints

Translated from Atomnaya Énergiya, Vol. 18, No. 1,
pp. 3-4, January, 1965

Aleksandr L'vovich Minch

January 8 marked the passage of 70 years since the birth of Hero of Socialist Labor, Academician Aleksandr L'vovich Mints—the Direction of the Radio Engineering Institute, Academy of Sciences of the USSR.

Alexandr L'vovich Mints is widely known in our country and abroad as a prominent scientist and engineer, talented organizer, and director of the development and installation of high-power broadcasting stations and gigantic charged particle accelerators.

In the Civil War, Aleksandr L'vovich was an active fighter for the victory of Soviet power, taking part in the battles in the Caucasus, on the Polish and Crimean fronts as a member of the legendary first mounted army, in the capacity of the Radio Division.

After the end of the Civil War, A. L. Mints continued serving for some time in the Red Army, occupying a position of command in the advanced communications War College in the Scientific Research Communications Institute, and then, around 1924, he turned to the development and installation of high-power radio station in the Soviet Union, the installation of which to some extent or other was not connected with the name of Alexandr L'vovich. At that time, he was responsible for the design of new high-power radio stations, and was in charge of construction. A. L. Mints developed and built dozens of radio stations and radio centers in the Soviet Union, starting with the 20 kilowatt ASPopov radio station (1925-1927), and ending with the superhigh-power 1200-kilowatt radio station (1941-1943). This period clearly exhibited one of the basic characteristics of A. L. Mints — the effort to bring his scientific developments to practical application in the shortest possible time. The scientific work of A. L. Mints embraces literally all fields of high-power radio equipment: the theory and development of methods for designing radio telephone modulation systems, the development, investigation, and installation of new antenna systems for long and short-wave radio stations, the development of new vacuum tube devices, and much, much else.

In 1930-1932, A. L. Mints proposed and brought to practical realization a completely new unit system, which has been used up to the present time in building all the large radio stations in the USSR as well as abroad.

To a considerable extent, as the result of A. L. Mints' work, Soviet high-power radio work occupied a leading place in the world even in those years. The advanced ideas which A. L. Mints carried out in high-power radio stations exerted an enormous effect on the development of Soviet radio engineering, as well as the radio industry.

Building radio stations and radio centers revealed the brilliant organizational abilities of A. L. Mints, who showed in practice that the time required to build and adjust large radio engineering installations may be greatly reduced by a correct and exact organization of the work.

The creative and organizational abilities of Alexandr L'vovich were brilliantly revealed in the period which marked the beginning of construction of the first large charged particle accelerators in the USSR. In 1946, a group of specialists headed by A. L. Mints, M. G. Meshcheryakov, and D. V. Efremov took over the construction of the first high-power proton accelerator in the USSR — the 500-MeV synchrocyclotron in Dubna (later its energy was raised

to 680 MeV). The accelerator was built in an unusually short time, and began to operate in 1949. Then, likewise in Dubna, a group from the radio engineering laboratory of the Academy of Sciences of the USSR, together with other institutes, engaged in the development and construction of what was at that time the largest proton accelerator – the 10-BeV synchrophasotron, which was started up in 1957. Building accelerators required the solution of very difficult radio engineering problems: In the synchrocyclotron, the frequency of a high-power oscillator had to increase by a factor of two during a very short oscillation cycle (3 msec), while in the synchrophasotron, the frequency had to be changed by as much as a factor of 10 according to a definite law, and at the same time the value of the frequency had to be maintained with an accuracy of $3 \cdot 10^{-4}$ at all times. These very complicated problems were solved, not only successfully and elegantly from the engineering point of view, but with a high degree of reliability.

In later years, the range of A. L. Mints' scientific interests continued to increase. In addition to radio electronic systems for the ring-type stiff focusing 7-BeV proton accelerator (started up in 1961 at the Institute of Theoretical and Experimental Physics) and the 70-BeV one (installed in the Institute of High-Energy Physics of the GKAÉ), Alexandr' L'vovich directed the development and building of the 30-MeV linear electron accelerator at the I. V. Kurchatov Atomic Energy Institute, the 20-MeV and 100-MeV linear proton accelerators, and other machines.

Since 1962, development of a project for building a gigantic ring-type proton accelerator for energies of 1000 BeV has been going on under A. L. Mints' direction. This project includes new ideas among them, ideas for the cybernetization of the acceleration processes so that the accelerator has been given the name cybernetic. At the same time a model of this accelerator is being built for an energy of 1 BeV.

Since 1958, at the suggestion of academician I. V. Kurchatov, a group from the Radio Engineering Institute of the Academy of Sciences, USSR, headed by A. L. Mints, has started work on high-frequency plasma equipment. In 1959, work began on the investigation of the ionosphere, of space near the earth, and of interplanetary plasma.

The years that Academician A. L. Mints spent on building accelerators were also the years of the founding and development of the Radio Engineering Institute of the Academy of Sciences, USSR, which grew from a small laboratory into a large scientific research center. A. L. Mints was the organizer of this center, and is its permanent director. To the comparatively young group at the institute, A. L. Mints communicates his characteristic scientific boldness, persistence in the achievement of a goal, and clearly defined organization, as well as organic unity in profound theoretical analysis of the most complex questions of present day radio engineering and experimental physics and the practical realization of scientific ideas.

A. L. Mints has educated many talented young scientists, known for their work, among them not a few State and Lenin prize winners, candidates and doctors of science.

During the 45 years of his scientific, engineering, and social activity, A. L. Mints published more than 100 scientific and engineering science papers, books and pamphlets, made more than 30 inventions in various fields of radio engineering and electronics, and has presented more than 70 papers, popular scientific, and publicizing articles.

A. L. Mints carries on a large amount of social work, and is a member of the Scientific Councils of several institutes, a member of the Bureau of the Division of General and Applied Physics, Academy of Sciences of the USSR, as well as an honorary member of the ASPopov Scientific and Technological Radio Engineering and Electrical Communications Society.

The Scientific and Engineering accomplishments of A. L. Mints are highly esteemed by the Communist Party of the Soviet Union, and by the Soviet Government. He has been awarded three orders of Lenin, two orders of The Red Banner of Labor, the Order of the Red Star, and medals. He has received the high distinction of Hero of Socialist Labor, and has been distinguished by two state prizes of the first grade, and by the Lenin prize. The Presidium of the Academy of Sciences of the USSR has awarded A. L. Mints the ASPopov Gold Medal.

The high devotion to principle, ability as an organizer, profound feeling of responsibility, and great self criticism, scientific boldness and ability to act, harmoniously blended in Alexandr L'vovich with a fine and spritual relation to his fellow workers, have given him great and well deserved authority.

Academician A. L. Mints is a splendid example of a prominent Soviet Scientist, Engineer and Organizer.

HIGH-FREQUENCY OSCILLATIONS EXCITED ON INTERACTION OF AN ELECTRON BEAM WITH PLASMA

UDC 533.9

A. K. Berezin, Ya. B. Fainberg, L. I. Bolotin, and G. P. Berezina

Translated from Atomnaya Énergiya, Vol. 18, No. 1,
pp. 5-14, January, 1965
Original article submitted June 4, 1964

Some results of experiments on the observation and study of oscillations excited in a beam and plasma as a result of their interaction are presented. The experiments were made under conditions in which $\omega_0 < \omega_H$, where ω_0 is the electron Langmuir frequency of the plasma, and ω_H is the electron cyclotron frequency. The conditions of excitation of the waves in the plasma were determined, together with their frequency spectra, phase velocities, and gain factors, the intensity of the electric field, and the absolute values and spectral distribution of the power of the oscillations excited. The experimental results for the frequencies, gain factors, and phase velocities of the oscillations excited in the plasma are in satisfactory agreement with calculated data.

As shown earlier in [1-3], on passing a heavy-current pulsed electron beam (current 5 to 8.5 A, energy 15 keV, pulse length 3.6 μsec) through a plasma in a longitudinal magnetic field (intensity 400 to 1320 Oe), under certain conditions it loses a considerable part of its initial energy (10 to 25%). In these experiments the plasma is created by the beam itself. It follows from theoretical considerations [4, 5] that this energy must pass into excitation of oscillations in the beam and plasma, and also into heating them.

As we know [4-6], in the case described in the present paper, forward waves (normal dispersion) should be excited. For large electron beam densities, frequencies associated with the electronic Langmuir oscillations of the beam must be excited together with Langmuir electronic frequencies of the plasma.

The measurements were made under standing and traveling wave conditions for current 5 and 8.5 A in a longitudinal magnetic field of intensity 720 to 1320 G. In the first case, a metal reflector plate (current collector) was placed at the end of the chamber, and in the second an adiabatic absorbing load (graphite cone 12 cm long).

Study of Oscillations Excited in the Plasma

The block diagram of the apparatus is shown in Fig. 1. Let us examine some of the components in more detail.

For recording the H_φ-, H_ρ-, H_z-components of the hf field, the oscillations are detected by a loop, and for recording the E_z component by a half-wave dipole situated in the plasma and oriented in the appropriate direction, connected via a movable coaxial cable to a power-calibrated resonance wavemeter (band half-width ~1.5 Mc).

Changing the wavemeter over to frequency and recording the power variation of the signal detected, the frequency spectrum of the oscillations excited in the plasma could be obtained for a fixed position of the loop or dipole inside the chamber. By moving the coaxial cable bearing the loop or dipole in the direction of motion of the electron beam and recording the variation in the hf power of the oscillations excited in the plasma for given frequency, the intensity distribution of the corresponding components of these hf oscillations could be obtained.

In order to eliminate vibration, the coaxial cable bearing the loop or dipole was moved inside a guide (copper tube 4 × 6 mm, with a side slot along the whole length). The guide was fixed inside the chamber near to the edge, parallel to the axis of the system. The movable cable came out of the side slot in the guide and ended in the loop (area ~1 cm^2) or half-wave dipole. The loops and dipole were placed at a distance of 10 mm from the beam bound-

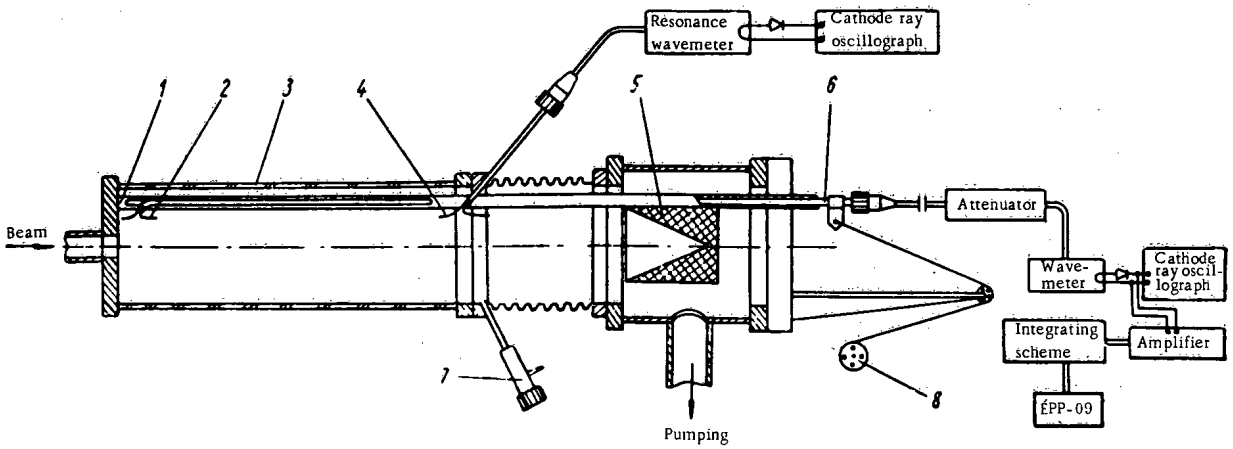

Fig. 1. Block diagram of apparatus for studying oscillations excited in the plasma under standing and traveling wave conditions: 1) Guide; 2) loop or dipole; 3) chamber; 4) fixed dipole; 5) current collector; 6) movable coaxial cable; 7) leak; 8) synchronous motor.

ary. The coaxial cable passed through to the outside by a way of a special vacuum seal, and was connected via a calibrated attenuator to a power-calibrated resonance wavemeter. The signal from the output of the wavemeter fell simultaneously on to an oscillograph and a wide band amplifier, then to a cathode follower with integrating circuit, and then to an automatic electronic potentiometer ÉPP-09. The envelope of the hf oscillations was observed on the oscillograph screen and its amplitude measured (to an accuracy of 5%). Calibration of the wavemeter for given frequency (in an assigned frequency range) consisted of the following. Oscillations of known power from a standard signal generator operating under continuous conditions fell on the wavemeter with crystal detector, the steady voltage at the output being measured. The generator power was determined with a low-power meter (IMM-6) to an accuracy of 7 to 10%. Such calibration was carried out before and after measuring the hf power of the oscillations excited. Only measurements for which the calibration did not alter during the experiment were taken into account.

On measuring the power in this way, the total error was ±17 to 20%, the error associated with the calibration of the wavemeter being ±7 to 10%, and that in determining the attenuator factors being ±10%.

The magnetic field strength of the corresponding components of the hf oscillations were calculated from the formula

$$\tilde{H} = \frac{10^8 \sqrt{P\rho}}{\omega S}, \qquad (1)$$

where P is the hf power collected by the loop in W, ρ is the input resistance of the wavemeter (ρ = 75 Ω), S is the area of the loop in cm^2 ($S = 1\ cm^2$), and ω is the oscillation frequency in cps.

The most intense oscillations in the plasma were excited in the range 825 to 835 Mc (half-width 50 to 70 Mc) in the pressure range 4 to $7 \cdot 10^{-4}$ mm Hg. An example of such an oscillogram taken for a frequency of 825 Mc appears in Fig. 2.

From measurements of the hf field distribution in standing wave conditions, the phase velocities were determined; measurements under traveling wave conditions gave the gain coefficient of the excited oscillations.

The relative phase velocity β was calculated as follows:

$$\beta = \frac{\lambda_g}{\lambda_0}, \qquad (2)$$

where λ_g and λ_0 are the wavelengths in the plasma and free space respectively. The gain factor γ was calculated from the relation

$$\gamma = \frac{1}{2(z_2 - z_1)} \ln \frac{P_2}{P_1} = \frac{1}{(z_2 - z_1)} \ln \frac{\tilde{H}_2}{\tilde{H}_1}, \qquad (3)$$

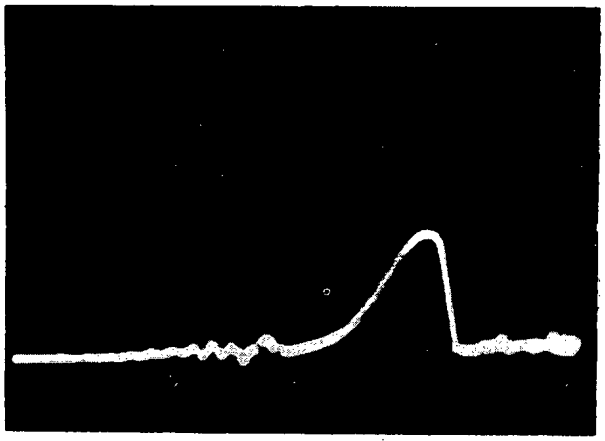

Fig. 2. Variation of the amplitude of the hf oscillations with time. Oscillation frequency 825 Mc; voltage pulse length 3.6 μsec; scale 1 μsec.

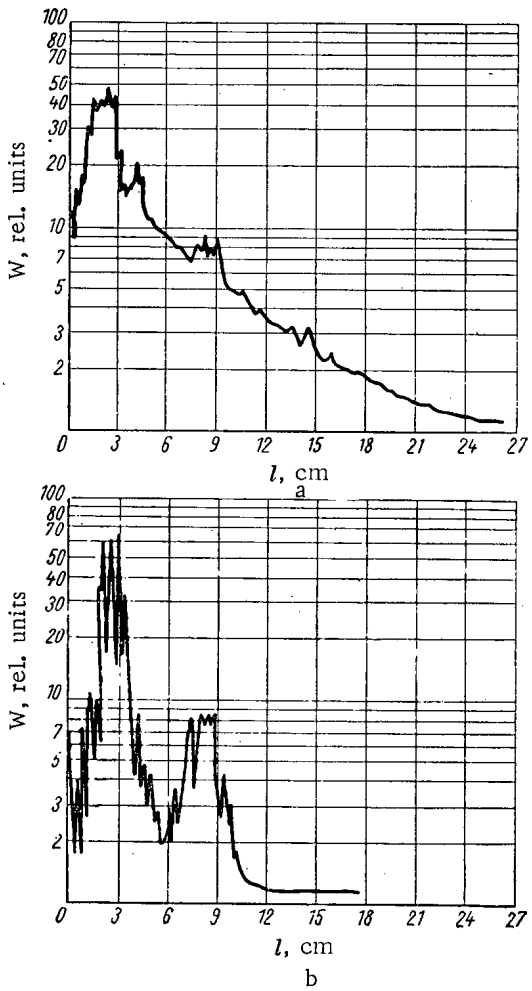

Fig. 3. Graphs showing the spatial distribution of the H_ρ-component of the hf field at frequency 835 Mc. The electron beam has current 5 A and energy 15 keV; the pressure of the working gas is $6 \cdot 10^{-4}$ mm Hg, and the magnetic field intensity 1320 G; a) traveling waves; b) standing waves. The beam moves from right to left.

where $\tilde{H}_1$ and $\tilde{H}_2$ are the field intensities of the propagating wave at points z_1 and z_2, while P_1 and P_2 are the corresponding hf powers.

Graphs of the distribution of the H_ρ-components of the electromagnetic hf field along the direction of motion of the beam (z axis) at frequency 835 Mc under standing wave conditions are presented for various magnetic field strengths (1320, 960, and 720 G) in [2], in Fig. 7a,b, and c. In these graphs, the axis of ordinates represents the hf power proportional to H_ρ^2 (in relative units) collected by a loop suitably oriented and situated at a given point along z. The axis of abscissas represents the distance (in cm) reckoned from the end of the region of interaction.

Figures 3a and b show distributions of the H_ρ-component of the hf field in the plasma along the direction of motion of the beam for both standing and traveling waves.

Analogous graphs were obtained for the H_φ-, H_z-, and E_z-components of the hf field in the plasma.

The slight peaks on the curve of Fig. 3a may be explained by the fact that, owing to the imperfect loading, together with absorption, there is a partial reflection of the wave (cone length 12 cm, i.e., approximately equal to the wavelength in the system at frequency 835 Mc). Measurements show that on an average the wavelength of the oscillations in the plasma is ~10 to 12 cm, i.e., $\beta \approx 0.3$ (oscillation frequency 835 Mc).

Below we give the gain factors as a function of the longitudinal magnetic field intensity (frequency 835 Mc):

Magnetic field intensity, G	Gain factor, cm^{-1}
1320	0.21
960	0.23
720	0.26

On changing the current and velocity of the beam, the gain factors also change, increasing with increasing beam current and decreasing beam velocity.

Thus, in the present experiments, when an electron beam interacts with a plasma, slow electromagnetic waves are excited in the latter, and these rise in intensity along the direction of motion of the beam. The magnetic field intensity of these oscillations at the end of the chamber, calculated from formula (1), reaches 0.3 to 0.4 G. Variation of the longitudinal magnetic field intensity from 1320 to 720 G hardly affects the frequency of the oscillations, but alters their intensity substantially: as the magnetic field intensity rises that of the oscillations falls.

The frequency spectra were measured in the frequency range 400 to 3200 Mc at the end of the region of

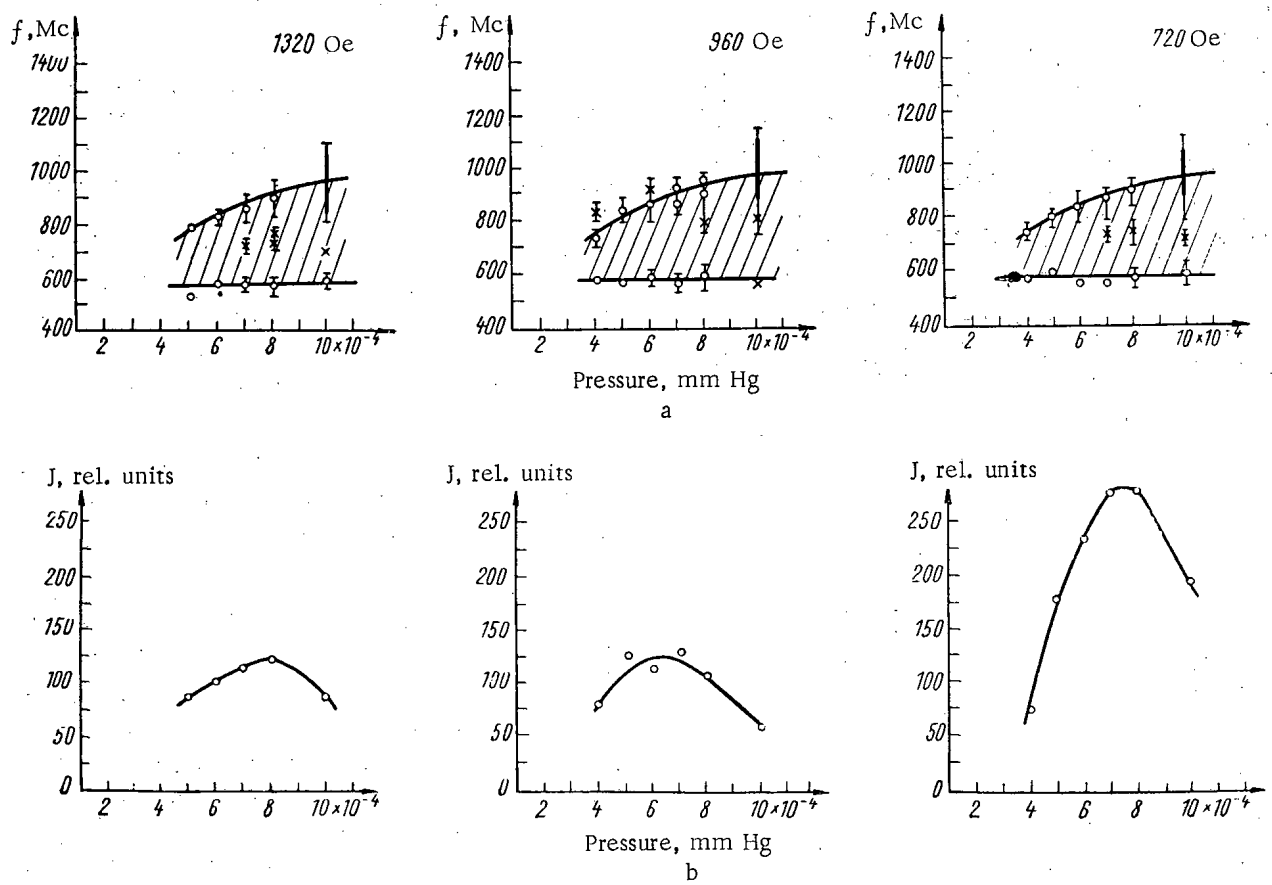

Fig. 4. a) Excited frequencies f_1 and f_2 and spectral half-widths, and b) maximum intensity of excited oscillations as functions of air pressure in the plasma chamber for a 5-A, 15-keV electron beam for various longitudinal magnetic field intensities.

interaction of the beam with the plasma. For pressures below $8 \cdot 10^{-4}$ mm Hg, the frequency spectra have two (sometimes three) sharp maxima. For the high pressure region ($8 \cdot 10^{-4}$ to $2 \cdot 10^{-3}$ mm Hg) there is a characteristic plateau in place of the maxima.

From the data obtained, we constructed graphs on which the values of the excited frequencies, the spectral half-widths, and the maximum intensity of the excited oscillations are given as functions of air pressure in the plasma chamber, current (5 and 8.5 A), and longitudinal magnetic field intensity (720, 960, and 1320 G). The beam energy was 15 keV. The graphs for the 5 A current are shown in Fig. 4a and b. The graphs for the 8.5 A current are of the same form.

The frequency ranges between the intensity maxima are shaded in this figure. The frequency of one of the intensity maxima (f_1) depends on the air pressure in the plasma chamber, increasing as this rises. On the other hand, the frequency of the second maximum (f_2) is independent of pressure, remaining almost constant; further, $f_1 > f_2$. We should note that $f_2 \approx \Omega_0/2\pi$, where Ω_0 is the electronic Langmuir frequency of the beam.

As seen from the graphs given in Fig. 4, the spectral half-widths of the excited frequencies rise on increasing the air pressure in the plasma chamber. This may evidently be explained by the fact that these half-widths are directly proportional to the frequency of collisions in the plasma, which increases on raising the pressure of the working gas.

With increasing velocity of the electron beam, the frequency f_1 rises.

Figure 4b shows the maximum intensity of the oscillations at frequency f_1 as a function of the air pressure in the plasma chamber. From these graphs we may draw the following conclusions: 1) the intensity of the excited oscillations reaches a maximum at pressures 4 to $7 \cdot 10^{-4}$ mm Hg; 2) on increasing or decreasing the pressure rela-

TABLE 1

Current, A	α	A*, Mc	$\Omega_0/2\pi$, Mc
5	0.53	450	560
8.5	0.44	600	730

tive to the optimum value the intensity of the excited oscillations falls; 3) on lowering the longitudinal magnetic field intensity from 1320 to 720 G the intensity of the oscillations rises. Measurements also show that on raising the velocity of the electron beam the intensity of the excited oscillations falls. Similar laws were observed for experiments in both standing and traveling wave conditions.

Since in our case the plasma density N is proportional to the air pressure in the chamber, we constructed graphs relating f_1^2 to the plasma density for fixed current and energy of the electron beam. Such graphs appear in Fig. 5a and b for currents 5 and 8.5 A respectively. The values of plasma density as a function of air pressure in the chamber were taken from Fig. 3 of [2]. The plasma density was measured by two methods: by means of a hf interferometer ($\lambda_g \approx 3.2$ cm), and by means of a method based on the use of the dispersion properties of plasma waveguides.

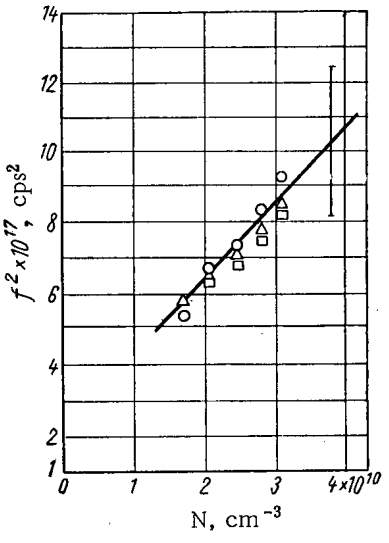

a

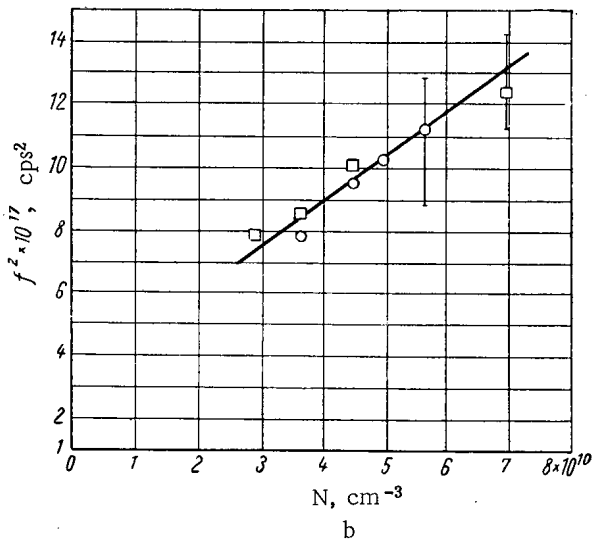

b

Fig. 5. Variation of the square of the excited frequencies in the plasma (f_1^2) as a function of plasma density for an electron beam of energy 15 keV and current (a) 5 and (b) 8.5 A: □) 1320 G; ○) 960 G; △) 720 G.

As we know, there is a cutoff band in our waveguide between the limits ω_0 and ω_H [for the case $\omega_H > \omega_0$ (see Fig. 9, curve –o–)]. Hence after determining the frequency corresponding to the beginning of the cutoff we may find the plasma density [2]. We may therefore suppose that the squares of the excited frequencies (f_1^2) vary in direct proportion to the electron density of the plasma. The excited frequencies rise on increasing the current in the electron beam.

The equation of the straight lines shown in Fig. 5a and b may be written in the form

$$f_1^2 = \alpha^2 f_0^2 + (A^*)^2, \qquad (4)$$

where α is the coefficient of proportionality between f_1 and f_0, A* is the frequency of the excited oscillations in the absence of plasma ($f_0 = 0$), and $f_0 = \omega_0/2\pi$. From the calculations made we obtain the values given in the table (remember that Ω_0 is the electronic Langmuire frequency of the beam).

As seen from the table, the values $A_1^* = 450$ Mc and $A_2^* = 600$ Mc are in agreement with the values of the Langmuir frequency for the electrons in the beam for the above current values. If we neglect a small correction in the investigated frequency region A* to f_1, the frequency of the excited oscillations f_1 is $0.53 f_0$ for a 5 A current and $0.44 f_0$ for an 8.5 A current.

We also studied oscillations with frequencies in the 2400 Mc range. These oscillations were only observed under standing wave conditions. The measurements showed that these hf oscillations in the plasma had only H_z- and H_ρ-components. The intensity distribution of the oscillations along the z axis at frequency 2405 Mc for current 5 A and energy 15 keV with magnetic field intensity 1320 G is shown in Fig. 6. As seen from the graph, the intensity variation of the oscillations along the z axis at frequency 2405 Mc differs from the distributions found earlier. The radiation consists of narrow lines (two or three lines with a half-

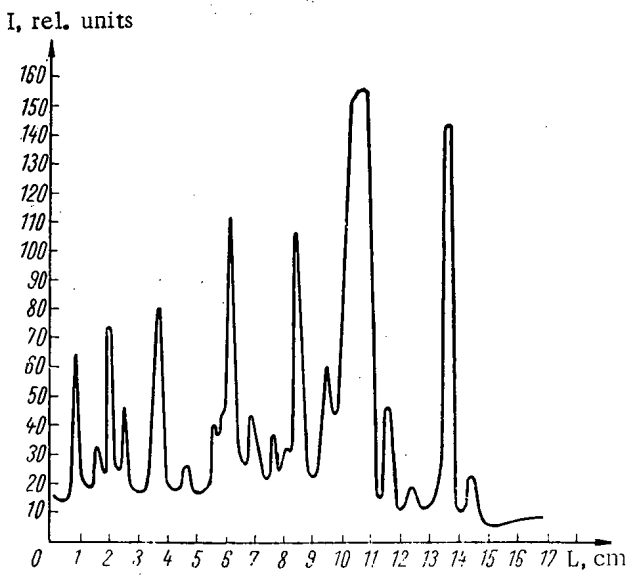

Fig. 6. Distribution of the H_ρ-component of the hf field in the plasma along the axis of the system at frequency 2405 Mc. Beam energy 15 keV, current 5 A, longitudinal magnetic field intensity 1320 G. Direction of beam motion in the oscillogram right to left.

width of the order of 3 to 5 Mc). The maximum field intensity of these oscillations is 0.05 to 0.15 G. The frequency of the oscillations is almost independent of the pressure of the working gas in the chamber and the magnetic field intensity, but depends greatly on the current and velocity of the electron beam, rising as these increase.

Thus we may conclude that the excitation of oscillations in the frequency region 2400 Mc depends on the boundary conditions, while in the range 825 to 835 Mc it is independent of these. The most distinctive feature of the oscillations at frequency 825 Mc is the fall in their intensity on lowering the magnetic field strength.

Analogous measurements were made using argon and hydrogen as working gas instead of air. The dependence of H_ρ on z for air and argon was much the same if the working gas pressure in the chamber was roughly the same and other experimental conditions were identical. In order to obtain the same kind of oscillations after admitting hydrogen to the chamber, its pressure had to be raised to $5 \cdot 10^{-3}$ mm Hg (i.e., to some six times the value for air). These results maybe explained by noticing that the specific ionization coefficients $\varepsilon(V)$ in air and argon are roughly the same, while for hydrogen the value is six or seven times smaller [7].

Study of Oscillations Excited in the Electron Beam After Passing through the Plasma

The block diagram of the apparatus for studying these oscillations is shown in Fig. 7. The electron beam (not modulated at the input), after interacting with the plasma, passed through a helical junction, by means of which hf power in the beam was selected.

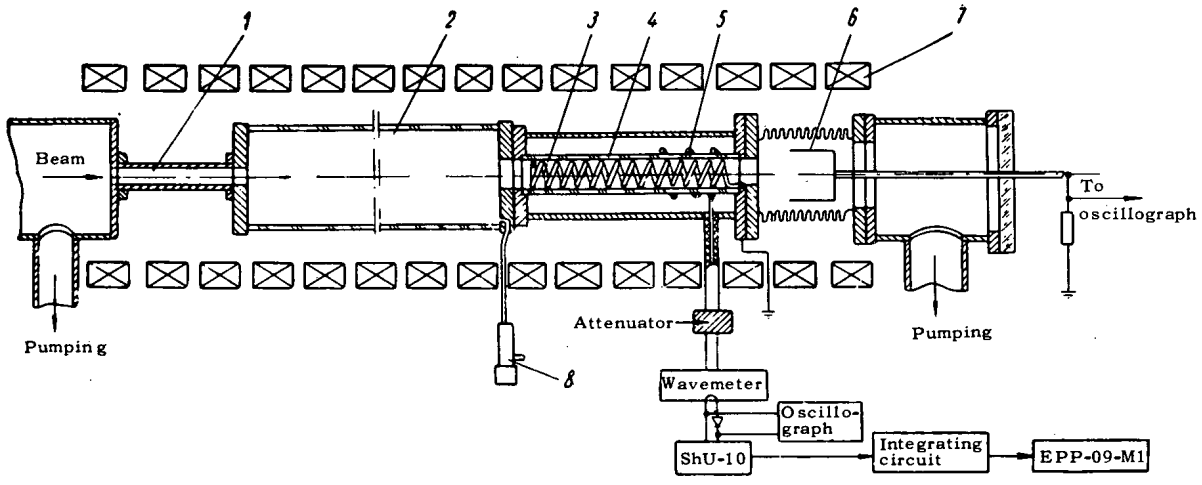

Fig. 7. Block diagram of the apparatus for studying oscillations excited in the beam: 1) Tube for creating pressure drop; 2) chamber; 3) inner helix of helical junction; 4) glass tube; 5) outer helix; 6) current collector; 7) solenoid for creating longitudinal magnetic field; 8) leak.

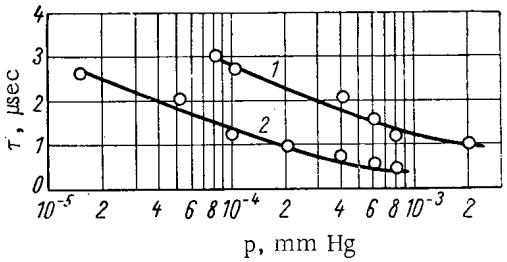

Fig. 8. Time of appearance of oscillations excited in the beam as a function of the pressure of the working gas: 1) Frequency 825 Mc; b) frequency ~2400 Mc.

The helical junction was made in the following way. Inside a vacuum-sealed glass tube of internal diameter 18 mm was placed a helix of 1.5 mm diameter molybdenum wire. The pitch of the helix was chosen so that the phase velocity of a wave propagated along the helix should be equal to the velocity of the electron beam passing inside the same helix. On the outside, the helix was surrounded by a second, shorter helix with turns in the opposite direction. This latter was connected to a coaxial cable, the wave resistance of which was 75 Ω. At one end, the inner helix was connected to an electrode at zero ("ground") potential. The ends of the glass tube were covered with a layer of aquadag. Thus electrons falling on the ends of the glass tube and the inner helix spiral flowed to ground. The length of the helical junction was ~15 cm. The standing wave voltage coefficients (SWVC) of the input into these helical junctions did not exceed 2.0 in the frequency range 650 to 5000 Mc. These measurements were made on systems without an electron beam. Beyond the helical junction was placed a collector, and the electron beam fell into this. The experiments were mainly carried out with a 5-A electron beam of 15-keV energy at a pressure of $6 \cdot 10^{-4}$ mm Hg, and a longitudinal magnetic field intensity of 1320 G.

Measurements showed that the spectra of the frequencies excited in the beam were analogous to the earlier described spectra of oscillations excited in the plasma under the same conditions. The power of the oscillations was determined by a method similar to that described earlier, using fixed attenuators and a calibrated wavemeter.

As the measurements showed, the absolute power of the oscillations at frequency 825 Mc was of the order of 150 to 200 W, and at frequency 2400 Mc some 1 to 2 kW. The total power of the oscillations radiated in the 825-Mc frequency range was 3 to 4 kW pulsed. Thus, the total power of the radiation recorded in the beam was 6 to 8 kW pulsed.

Estimates show that, for the above beam and plasma parameters, the electric field strength of the excited wave at the end of the beam-plasma interaction region ($f \sim 825$ Mc) equals 0.5 to 0.6 kV/cm. The properties of the oscillations excited in the beam in the frequency region ~825 Mc are analogous to those of the oscillations excited in the plasma and described earlier.

The time at which the oscillations excited in the beam at frequencies in the range 825 to 1100 and ~2400 Mc appeared was also determined. This time was determined from oscillograms similar to those shown in Fig. 2. The time was reckoned from the beginning of the voltage pulse applied to the cathode of the electron gun up to the maximum amplitude of the high frequency envelope. A graph showing the variation of the time of appearance of the oscillations with the air pressure is shown in Fig. 8. As seen from the graph, oscillations at frequency 2400 Mc are excited in the beam earlier than oscillations in the frequency range 825 to 1100 Mc. With increasing pressure, the time of excitation of the oscillations in the beam diminishes.

Discussion of Results Obtained and Comparison with Theoretical Data

Let us compare the experimental results obtained with theory. As indicated in [3-6], the interaction of an electron beam with plasma situated in a longitudinal magnetic field may result in the development of instabilities in both beam and plasma owing to the Cherenkov-Vavilov and anomalous Doppler effects. In order to determine the possible spectrum of excited frequencies and gain factors we used a dispersion equation describing the interaction of a bounded electron beam with a bounded plasma situated in a longitudinal magnetic field, obtained by M. F. Gorbatenko [6].[1] In the case in which the radius of the plasma column b equals the radius of the beam a, the dispersion equation has the form

$$1+\frac{1}{u^2-x^2}+\frac{\varepsilon}{u^2-(y-x)^2}+N'y^2\left[1-\frac{1}{x^2}-\frac{\varepsilon}{(y-x)^2}\right]=0, \tag{4}$$

where

$$N'=\frac{b^2\omega_0^2}{\lambda_p v^2},\quad \varepsilon=\frac{\Omega_0^2}{\omega_0^2},\quad u^2=\left(\frac{\omega_H}{\omega_0}\right)^2,\quad y=\frac{k_3 v}{\omega_0},\quad x=\frac{\omega}{\omega_0}$$

[1] All the succeeding calculations were also made by M. F. Gorbatenko.

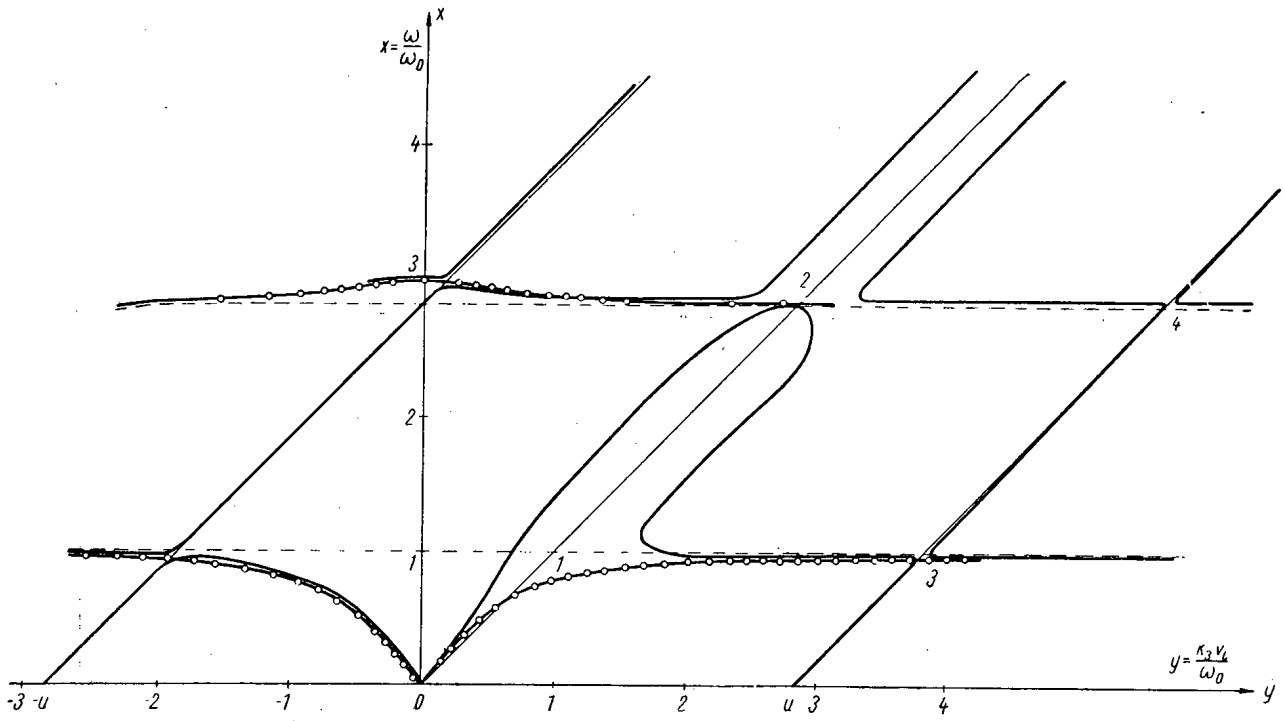

Fig. 9. Solution of dispersion equations: —○—○— for plasma; —— for beam with plasma (values of parameters indicated in text).

(here $k_3 = \omega / v_\phi$, v = beam velocity, v_ϕ = constant lying within the limits 2.4 to 3.8). Dispersion relations for our beam and plasma parameters are given in Fig. 9, where $u^2 = 8$, $N' = 2$, $\varepsilon = 0.125$, which corresponds to $N \approx 2 \cdot 10^{10}$ cm^{-3}, H = 1200 G, current = 5 A, $v \approx 6 \cdot 10^9$ cm/sec, and b = 2.5 cm.

It follows from an analysis of the dispersion equation that in our case the regions of excitation of the oscillations are situated close to the frequencies ω_0 and ω_H. In the ω_0 region the excitation may be caused by the Cherenkov-Vavilov effect (region 1) and anomalous Doppler effect (region 3) on the forward wave. In the ω_H region excitation may be caused by the Cherenkov-Vavilov effect (region 2) and the anomalous Doppler effect (region 4) on the backward wave.

The growth increments (imaginary part of x) calculated for these regions in our case have the following values: for region 1 the maximum growth increment equals 0.26, for region 2 it is 0.12, for region 3 it is 0.07, and for region 4 it is 0.06.

Thus the growth increment has the largest value in region 1, in which the oscillations are excited by the Cherenkov-Vavilov effect on the forward wave (normal dispersion). The frequency f_1 of these oscillations is close to the electronic Langmuir frequency of the plasma f_0, but not coincident with this ($f_1 \sim 0.6 f_0$) owing to the bounded state of the beam and plasma and the influence of the strong magnetic field.

The experimentally measured frequency of the oscillations most amplified is $f_1 \sim 0.53 f_0$ for a current of 5 A (see Fig. 5a and table), in very good agreement with calculated data. The frequency of the most amplified oscillations was also measured for an 8.5 A current; this equals $0.44 f_0$ (see Fig. 5b and table).

It follows from the calculations that in our case slow electromagnetic waves with a wavelength of about 7.2 cm in the plasma (frequency 835 Mc) must be excited. The measured wavelength in the plasma is 10 to 12 cm ($\beta \approx 0.3$) (see Fig. 3a). Thus slow waves with a phase velocity approximately equal to the beam velocity ($v_\phi \approx v$) are in fact excited in the present experiments.

The calculated value of the gain factors for the conditions ruling in the experiment equals 0.32 cm^{-1}; the experimental values lie between 0.21 and 0.26 cm^{-1} (see above). Thus the gain factors are also in agreement with calculated values.

As indicated in [8, 9], on interaction between an electron beam and plasma a convective (transport) instability should be developed. The graphs of Fig. 3a and b confirm the validity of this principle.

During the measurements we failed to observe any marked excitation of frequencies in the neighborhood of the electron cyclotron frequency ω_H. This corresponds to theory, since in our case the increments in this region of frequencies equals 0.12, which is considerably less than that for frequencies in the neighborhood of ω_0 (0.26). Hence the oscillations excited in the frequency range ~800 to 1100 Mc are longitudinal waves in the beam and plasma caused by the Cherenkov-Vavilov effect (forward waves). The experimental results agree with the main theoretical principles.

Together with oscillations in the frequency range 800 to 1100 Mc, for certain conditions oscillations of frequency 2400 Mc are also excited. The frequency of these oscillations is practically independent of the plasma density. In time, they develop earlier than the oscillations in the frequency range 800 to 1100 Mc (see Fig. 8). Their frequency does not depend on the longitudinal magnetic field strength, but depends on the velocity of the electron beam. The intensity of the oscillations in the region of 2400 Mc, in contrast to the plasma oscillations, rises on increasing the longitudinal magnetic field strength.

It should be mentioned that the excitation of oscillations at frequencies of 2400 Mc only takes place in the case in which a reflecting metal surface is placed at the end of the region in which beam and plasma interact. All this strongly suggests that such oscillations are caused by the electron beam itself, not depending on the parameters of the plasma. It may be assumed that in the present case parametric excitation of oscillations takes place. Additional measurements must nevertheless be made in order to decide the question completely.

It follows from the measurements made in [1-3] that, for current 5 A, energy 15 keV, and pressure 4 to $6 \cdot 10^{-4}$ mm Hg, the electron beam loses up to 18% of its initial energy as a result of interaction with the plasma (~13 kW pulsed). This energy goes into excitation of oscillations in the beam and plasma, and also into "heating" these. As measurements show, the power of the excited oscillations is 8 kW pulsed, i.e., at least 60% of the total beam energy loss.

We must note, however, that in the experiments carried out the coupling of the beam with the helical junction, and hence the power of the excited oscillations was not optimal, so that it is quite possible that only part of the power in the hf oscillations was taken off from the electron beam during its passage through the helical junction, and hence the power of the excited oscillations may be in fact higher. Some part of the energy goes into heating the beam and plasma.

The authors express their thanks to M. F. Gorbatenko for carrying out the calculations.

LITERATURE CITED

1. A. K. Berezin, et al., Atomnaya énergiya, 14, 249 (1963).
2. A. K. Berezin, et al., Collection: Plasma Physics and Problems of Controlled Thermonuclear Synthesis [in Russian] (Kiev, Izd. AN UkrSSR, 1963), Vol. 3, p. 125.
3. A. K. Berezin, et al., Atomnaya énergiya, 18, No. 3 (1965).
4. Ya. B. Fainberg, Dissertation [in Russian] (FIAN SSSR, 1960); Atomnaya énergiya, 11, 313 (1961).
5. V. D. Shapiro and V. I. Shevchenko, ZhÉTF, 42, 1515 (1962); V. D. Shapiro, ZhÉTF, 44, 613 (1963); Dissertation [in Russian] (OIYaI, Dubna, 1963).
6. M. F. Gorbatenko, Zh. tekhn. fiz., 33, 173, 1070 (1963); Dissertation [in Russian] (Khar'kov Gos. Univ., 1964).
7. A. Engel' and M. Shteenbek, Physics and Technology of the Electrical Discharge in Gases [in Russian] (Moscow-Leningrad, ONTI, 1935), Part 1.
8. P. Sturrock, Phys. Rev., 112, 1488 (1958).
9. Ya. B. Fainberg, V. I. Kurilko, and V. D. Shapiro, Zh. tekhn. fiz., 31, 633 (1961).

INTERACTION OF PLASMOIDS WITH AN ELECTROMAGNETIC WAVE

(UDC 621.384.623)

V. I. Veksler, I. R. Gekker, É. Ya. Gol'ts, G. A. Delone, B. P. Kononov, O. V. Kudrevatova, G. S. Luk'yanchikov, M. S. Rabinovich, M. M. Savchenko, K. A. Sarksyan, K. F. Sergeichev, V. A. Silin, and L. É. Tsopp

Translated from Atomnaya Énergiya, Vol. 18, No. 1, pp. 14-18, January, 1965
Original article submitted April 22, 1964

Some preliminary results of a study of plasma acceleration in circular waveguides are presented. The study was made in the 10-cm range on systems with H_{01} and H_{11} type waves and various plasma injectors. Plasmoids with initial particle concentration 10^{12} cm^{-3} and above were injected with an initial velocity of $5 \cdot 10^6$ cm/sec from a spark source, or formed directly on the waveguide axis by means of a plasma source with pressure drop, the working vacuum in the accelerator being 10^{-7} to 10^{-6} mm Hg. Diagnostics were conducted by means of electric probes uhf methods, and an electrostatic particle energy analyzer. The plasma was contained by auxiliary external magnetic fields of various configurations. Accelerated ions of energy greater than 10 keV were obtained.

A proposal was made in 1954 [1] to use the coherent interaction of charged particles with an electromagnetic wave for accelerating plasma. Subsequent theoretical studies showed that, on fulfilment of certain conditions, prolonged acceleration of plasmoids could be achieved, their form and dimensions remaining unchanged [2, 3].

In the present investigation, the initial stage of acceleration and the behavior of the plasma in the waveguide in the presence of a strong electromagnetic wave were studied experimentally. No attempt was made in these experiments to secure stable acceleration of the plasmoids or reach high energies of accelerated particles. Two systems were prepared; these differed in the type of accelerating wave used and the method of plasma injection. External magnetic fields were used to reduce the diffusion of plasma to the walls of the waveguide. Plasmoids were created in the waveguide at a vacuum of 10^{-7} to 10^{-6} mm Hg, both with a spark injector [4] and a pressure-drop plasma source [5]. The investigations thus made enabled us to obtain the first experimental data on the radiation acceleration of plasma.

Acceleration of Plasma in an H_{01} Wave

The choice of the H_{01} wave was determined by the following considerations:

1. The field configuration of the H_{01} wave is such that it permits metal rods of small cross section to be introduced along the radius and along the axis without seriously distorting the field pattern. This enables us to place the plasma gun and probes inside the accelerating waveguide.
2. The H_{01} wave is a wave of the lower type and quite easily excited.
3. The electric field configuration of the H_{01} wave eliminates the occurrence of uhf discharges to the waveguide walls.

In order to achieve radiation acceleration of plasma in an H_{01} wave, the system shown schematically in Fig. 1 was constructed. Power from the uhf generator passes into the waveguide tract through a ferrite valve into a King-type wave transformer. Here the H_{01} type wave in the rectangular waveguide is transformed into an H_{01} type wave in the circular waveguide. The accelerating waveguide is formed by a stainless steel tube with wall thickness 1 mm. This kind of tube ensures low damping of the uhf waves (around 0.2 dB), and screens the external pulsed magnetic field very little. Between the accelerating waveguide and the transformer lies a vacuum-tight uhf window. The

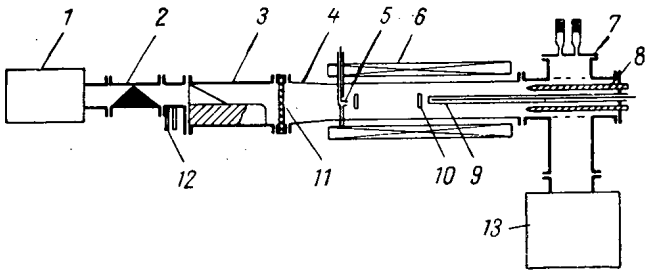

Fig. 1. H_{01} wave accelerator (schematic): 1) uhf generator; 2) ferrite valve; 3) wave transformer 4) accelerating waveguide; 5) spark plsma injector; 6) magnetic system; 7) pumping section; 8) uhf absorbing load; 9) screened electric probe; 10) diagnostic window; 11) vacuum-tight uhf window; 12) section with two detector heads; 13) high-vacuum line.

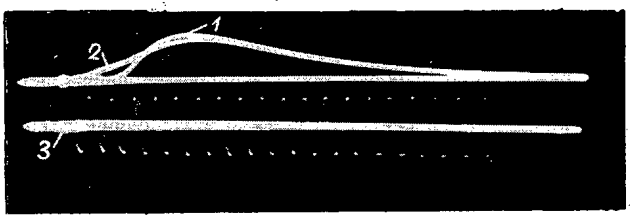

Fig. 2. Screened electric probe ion current oscillograms: 1) uhf power switched off; 2) uhf power switched on; 3) calibrating signal, period 2 μsec.

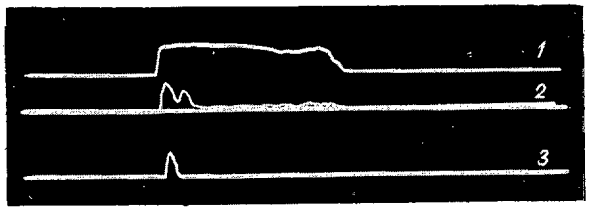

Fig. 3. Signals from an uhf probe placed at the window of the accelerating waveguide (time base 23 μsec): 1) Envelope of uhf-pulse without the plasma; 2) the same on discharging the plasma gun; 3) signal from gun.

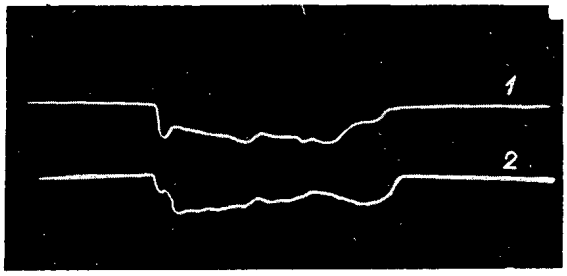

Fig. 4. Signals from two detector heads displaced by a distance of 10 cm (time base 17 μsec): 1) First head; 2) second head.

accelerating waveguide is terminated by an absorbing uhf load coinciding with the pumping section. Windows for plasma diagnostics are set in the accelerating waveguide tube.

The 10-cm wave uhf generator operates on a single pulse 8 μsec long. The mean power flow density through the cross section of the accelerating waveguide is not greater than $8 \cdot 10^3$ W/cm^2. The standing wave coefficient (voltage) of the whole waveguide system of the accelerator (without plasma) is not worse than 1.3.

A plasma injector of the spark type is introduced along the radius into the center of the waveguide and has a symmetrical "counterweight," reducing distortion of the fundamental wave. The maximum current through the gun in the aperiodic condition is 1.8 kA for a duration of 0.3 μsec. The spark gun creates a plasma containing around 50% ions of atomic hydrogen. The total number of ions is 10^{15} to 10^{16}.

In order to reduce the passage of plasma to the walls of the accelerating waveguide, both a longitudinal magnetic field and also a magnetic field created by a system of straight conductors parallel to the waveguide axis, fed by currents moving in alternate directions, are employed. During the motion of the plasma in the accelerating waveguide (20 μsec), the magnitude of the magnetic fields remains practically unaltered.

The accelerated ions are recorded by means of screened electric probes [6] introduced from the end of the waveguide. Figure 2 shows a superposition of two oscillograms giving the probe ion currents for uhf power "on" and "off"; the longitudinal magnetic field here equalled 300 G, and the gun to probe distance was 45 cm. We see from Fig. 2 that switching on the accelerating field leads to a shift in the velocity distribution of particles in the bunch in the direction of higher velocities.

It was not possible to determine the total number of accelerated particles using the probe method, since this can only separate out particles with velocities exceeding the maximum particle velocity in the absence of the uhf accelerating field. Estimates showed that there were not less than 10^{12} accelerated particles, the maximum velocity of some of the ions exceeding 10^8 cm/sec. It should be noted that these experimental values agree satisfactorily with calculations in order of magnitude, if we assume that the momentum of the uhf wave is transferred completely to the plasma. Varying the number of particles created by the plasma injector by an order of magnitude (by varying the conditions of the spark gun) does not greatly affect the number of accelerated particles.

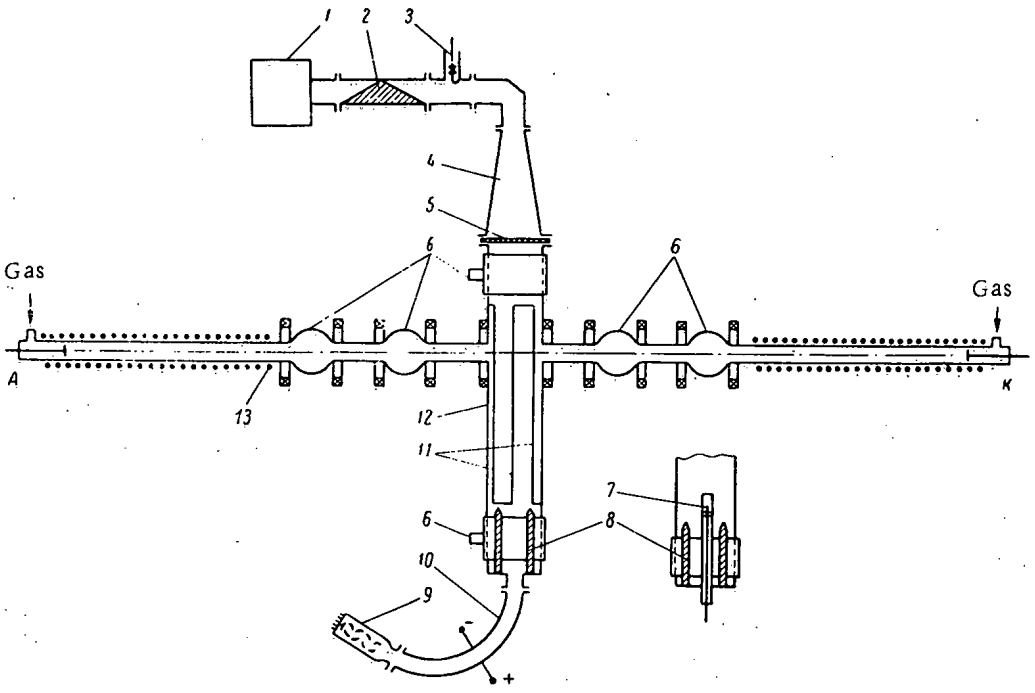

Fig. 5. Principle of H_{11} wave accelerator: 1) uhf generator; 2) ferrite valve; 3) detector head; 4) wave transformer ($H_{10}^{\square} \rightarrow H_{11}^{\bigcirc}$); 5) vacuum-tight uhf window; 6) high vacuum pumping line; 7) electric probe; 8) absorbing uhf-load; 9) electron multiplier; 10) electrostatic (127°) particle energy analyzer; 11) magnetic system; 12) accelerating waveguide; 13) pressure-drop plasma source.

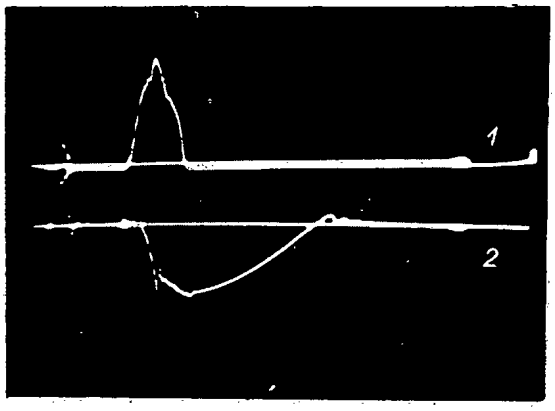

Fig. 6. Oscillograms (time base 6.4 μsec): 1) uhf envelope; 2) signal from electric probe.

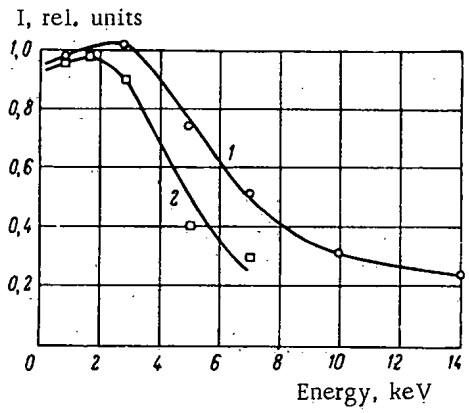

Fig. 7. Energy spectrum of accelerated ions: 1) uhf wave power $P = P_{max}$; 2) $P = 0.5 P_{max}$.

Operation with the magnetic field created by the system of straight conductors required the introduction of a glass tube inside the metal accelerating waveguide, since, as experiments proved, the plasma losses during motion in a metal tube with this field were large (two orders in density lost in a distance of 1 cm). This is connected with the fact that the polarization of the plasma arising from the presence of the transverse magnetic field is taken by the metal walls, and polarization currents flow constantly in the plasma, retarding its motion. The introduction of a glass tube leads to the insulation of the plasma from the metal walls.

The results obtained on accelerating plasma by an uhf wave in this field were analogous to those described earlier.

By means of an uhf probe (detector head) set at the diagnostic windows of the accelerating waveguide, it was observed (Fig. 3) that, after discharge of the plasma gun, the waveguide practically cut off, that is a "block" was set up for the uhf-wave independently of the external magnetic field. This was confirmed by measurements made with the help of two detector heads [7] in respect of uhf power reflected from the plasma. The presence of the reflected wave appeared in the form of modulation of signals sent from the detector heads (Fig. 4). Analysis of the experimental data showed considerable reflection of the uhf wave from the bunch, reaching some 90%.

Acceleration of Plasma in an H_{11} Wave

The intensity polarized H_{11} wave is a wave of the lower type in a circular waveguide. A possible failing of the H_{11} wave is the considerable electric field strength at the waveguide wall, facilitating the development of uhf breakdown. On the waveguide axis, in a condition well removed from critical, the H_{11} wave takes on a form close to a plane wave, and in certain cases this may make for easier comparison between experimental and computed data.

Figure 5 shows the principle of a system for accelerating plasma in an H_{11} wave. The uhf generator is the same as that in the arrangement of Fig. 1. Excitation of the linearly polarized H_{11} wave is effected by smooth transition from a rectangular waveguide. The accelerating waveguide also consists of a stainless steel tube 1 mm thick. The magnetic field is formed by a system of six straight conductors with currents flowing in alternate directions.

A pressure-drop source is used to form the plasma. The principle of this source is described in [5]. A plasma pinch with particle concentration above 10^{12} cm^{-3} is formed in a discharbe between electrodes A and K (see Fig. 5) in a longitudinal magnetic field. The pressure of the hydrogen admitted at the anode A and cathode K equals 10^{-2} mm Hg. The pressure in the accelerating waveguide is 10^{-6} mm Hg. The pressure difference is maintained by means of four diffusion pumps. After the plasma pinch has been formed, the A-K voltage is switched off and the magnetic field of the straight conductors is switched on (the time of growth of the field is 25 μsec). After the magnetic field has reached a value of the order of 10^3 G (at the stops) and the plasma is squeezed away from the walls, the uhf field is switched on. A displacement of the standing waves takes place in the waveguide as the plasma moves. This is recorded by a detector head (see Fig. 5). The observed modulation of the uhf oscillation envelope is analogous to that shown in Fig. 4.

The accelerated particles were recorded by an electric probe screened from the uhf field (asymmetrical double probe); this was introduced on the side of the uhf-load and could be moved along the waveguide axis.

Figure 6 shows an oscillogram of the uhf oscillation envelope and signal from the electric probe situated at a distance of 30 cm from the point of injection. In the absence of the uhf wave, no signals are observed from the probe. From the delay in the arrival of the plasma we may estimate its mean translational velocity, which in order of magnitude is 10^7 cm/sec.

In order to measure the energy of the accelerated ions, an electrostatic analyzer rotating the particles through 127° was used together with an electron multiplier as ion detector. The analyzer enables us to measure ion energies within the range 1 to 100 keV; it is placed at the end of the accelerating waveguide, 70 cm from the injector.

Figure 7 shows the detector current as a function of the energy of the recorded ions. With increasing uhf power the energy spectrum shifts towards higher energies. On increasing the sensitivity of the system, ions with energies up to 50 keV were recorded.

Conclusions

As a result of the experiments described, radiation acceleration of plasma was established. Accelerated ions were obtained in both systems, independently of the type of wave in the waveguide and the form of the plasma injectors. The energy of the accelerated ions increased on raising the uhf power. The total number of accelerated particles is of the order of 10^{12}, which corresponds to the momentum of the uhf wave transferred to the plasma. The maximum energy of the accelerated particles is up to 50 keV.

Regarding the small value of the mean energy obtained in the experiments, there is a number of explanations. First, our plasma injectors give a very large number of particles (up to 10^{15} to 10^{16}) which, for a given uhf field power, cannot all be markedly accelerated. The background of unaccelerated particles blocks the waveguide. Secondly, almost all the hf power is reflected from the plasma. Thus the acceleration region is small (a few cm), and the length of the accelerating waveguide (30 to 100 cm). Thirdly, a wave of the H_{11} type evidently cannot

exert a stabilizing influence on the size and direction of motion of the bunch, as would be expected from theory, owing to the large dimensions of the bunch [2]. The results obtained for the acceleration of plasma in waves of the H_{01} and H_{11} types are similar to one another (a wave of the H_{01} type should not stabilize the dimensions of the bunch in the direction of acceleration). This is also explained by the action of the background particles in screening the uhf wave. Higher energies can evidently be obtained not only by increasing the uhf power but also by forming compact bunches at the beginning of the acceleration.

The use of inhomogeneous fields [3] for stabilizing the transverse dimensions of the bunches justified itself completely. We had hardly any plasma losses to the walls of the waveguide on using quadrupole or sextupole magnetic fields. Up to the present, however, we have not succeeded in stabilizing the longitudinal dimensions by means of an inhomogeneous field [3]. This is explained by the low initial velocity of the bunch and its small conductivity. It would appear that, in the initial stages of acceleration at least, we should use two types of wave simultaneously in the circular waveguide, as was proposed earlier [2].

Thus the preliminary experiments carried out offer a basis for developing a fairly clear program to increase the energy and number of accelerated particles.

LITERATURE CITED

1. V. I. Veksler, CERN, Symposium, Geneva (1956), Vol. 1, p. 80; Atomnaya énergiya, 2, 427 (1957).
2. M. L. Levin, M. S. Rabinovich, and G. A. Askar'yan, Proc. Internat. Conf., CERN (1959).
3. G. A. Askar'yan, et al., Nucl. Fusion, Suppl., Part 2, 797 (1962).
4. W. Bostic, Phys. Rev., 104, 292 (1956).
5. B. P. Kononov and K. A. Sarksyan, Zh. tekhn. fiz., 31, 1294 (1961).
6. K. D. Sinel'nikov, et al., Plasma Physics and Problems of Controlled Thermonuclear Synthesis [in Russian] (Kiev, Izd. AN Ukr.SSR, 1962), p. 102.
7. A. Bloch, F. Fisher, and G. Hunt, Proc. IEE, 100, 93 (1953).

DETERMINING THE PERTURBATIONS OF THE PARAMETERS IN THE MAGNETIC AND ACCELERATING SYSTEMS OF AN ELECTRON SYNCHROTRON ON THE BASIS OF AN ANALYSIS OF INFORMATION REGARDING THE BEAM

(UDC 621.384.60)

I. P. Karabekov

Translated from Atomnaya Énergiya, Vol. 18, No. 1,
pp. 18-22, January, 1965
Original article submitted May 13, 1964

A method of selecting and analyzing information regarding the center of gravity of the beam in the cross section of an accelerator vacuum chamber is proposed; on the basis of this, the deviation of certain fundamental parameters of the electron synchrotron may be obtained.

The various components making up an accelerator can only be constructed with finite accuracy. Thus the parameters of the magnetic and accelerating systems also can only hold to a certain accuracy around their calculated values. The deviation of these parameters by more than the permissible values leads to a considerable loss of particles. Hence the question of measuring the parameters of the magnetic and accelerating systems from beam data and also stabilizing them (by introducing special corrections) demands special attention in setting up modern accelerators. At the present time, methods of controlling the frequency of the accelerating voltage from information regarding the radial position of the beam [1, 2], methods of measuring and stabilizing the frequency of betatron oscillations [3, 4], and a method of correcting the space harmonics of the magnetic field from beam data [3, 5] have been or are being developed. Also being developed are methods of correcting the magnetic field before injection in order to make the start-up of the first rotation of the beam automatic [6]. Different arrangements of the mutual disposition of the sensory beam elements and controlling devices are considered, as well as the number of controllable sections of orbit required [7].

The distortion of the beam trajectory depends on many factors associated with the deviation of various accelerator parameters from their nominal values. For effective correction of the beam trajectory and reduction of particles loss during acceleration, it is important to determine the distortion arising correctly, i.e., to separate out the perturbations corresponding to the various parameters. The possibility of separating the perturbations due to different parameters on the basis of an analysis of beam information and of determining the operations required to correct these perturbations enables us to make the tolerances laid on various components of the accelerator less stringent, so making construction cheaper and more rapid.

In the present paper, methods of handling beam information and determining therefrom the perturbation of certain leading parameters of the magnetic and accelerating systems are discussed.

Determining the Value of the Field Perturbation of the Magnetic Sections of the Accelerator, and Corrective Operations for Compensating These

Let us suppose that we know the coordinates of the trajectory of the center of gravity of the beam and its derivative with respect to azimuth at the ends of the magnetic section at points θ_1 and θ_2. Let us assume that our magnet has no field deviation; then the motion of the particles within the magnet in question must be described by the differential equation

$$r'' - \left(\frac{l}{2\pi\rho}\right)^2 n(\theta)\, r = 0, \tag{1}$$

where l is the length of the period of the magnetic system; ρ the radius of curvature in the magnets, $n(\theta)$ the field falloff index. Hence

$$r = C_0 F + C_0^* F^*, \quad r' = C_0 F' + C_0^* F^{*\prime}, \tag{2}$$

where F and F^* are the Floquet function and its complex conjugate, C_0 and C_0^* are complex conjugate constants, and θ varies by 2π within the limits of the gradient period.

Solving the algebraic system of equations (2) with respect to C_0 at points θ_1 and θ_2, we obtain

$$C_{01} = \frac{r_1 F_1^{*\prime} - r_1' F_1^*}{-2i}, \tag{3}$$

$$C_{02} = \frac{r_2 F_2^{*\prime} - r_2' F_2^*}{-2i}, \tag{4}$$

in which C_{01} is identically equal to C_{02} for $\Delta H / H_0 = 0$. The existence of some perturbation, however, destroys this identity:

$$\Delta C = C_{02} - C_{01} = \frac{r_2 F_2^{*\prime} - r_2' F_2^* - r_1 F_1^{*\prime} + r_1' F_1^*}{-2i}. \tag{5}$$

At the same time, the quantity ΔC, as we know already [8], is associated with the value of the perturbation $(\Delta H / H_0)\theta$ via the expression

$$\Delta C = \left(\frac{l}{2\pi}\right)^2 \frac{1}{2i} \int_{\theta_1}^{\theta_2} F^* \frac{\Delta H}{\rho H_0}(\theta)\, d\theta. \tag{6}$$

Let us measure r_1, r_2, r_1', and r_2' and determine ΔC from (5). Expression (6) connects the quantity ΔC with the perturbation $(\Delta H / H_0)\theta$ in the unit; this connection, however, is clearly not unequivocal. What is important in practice is not the exact measurement of the function $(\Delta H / H_0)\theta$, but the determination of such equivalent corrective perturbations as will restore the condition $\Delta C = 0$, i.e., make the unit perturbation-free. (The deviation of the beam inside the unit must not be too great.) Since ΔC, generally speaking, is a complex quantity, two parameters are required in order to compensate it. Let us divide the unit into two parts (these may, for example, be focusing and defocusing parts). Then expression (6) may always be written in the form

$$\Delta C = \left(\frac{l}{2\pi}\right)^2 \frac{1}{2i\rho} \left(\frac{\Delta H_1}{H_0}\right)_{eq} \left\{ \int_{\theta_1}^{\theta_n} F^*\, d\theta + K \int_{\theta_n}^{\theta_2} F^*\, d\theta \right\}, \tag{7}$$

where $(\Delta H_1 / H_0)_{eq}$ is the required equivalent perturbation created by the first correcting coil, and K is the ratio between the values of the perturbations created by the first and second correcting coils. By due choice of the signs and magnitudes of $(\Delta H_1 / H_0)_{eq}$ and K, the right-hand sides of formulas (5) and (7) may be made equal.

Equating the arguments of the complex expressions in (5) and (7), we obtain

$$K = -\frac{Im\left[\int_{\theta_1}^{\theta_n} F^*\, d\theta\right] - Re\left[\int_{\theta_1}^{\theta_n} F^*\, d\theta\right] \frac{Im(Z)}{Re(Z)}}{\frac{Im(Z)}{Re(Z)} Re\left[\int_{\theta_n}^{\theta_2} F^*\, d\theta\right] - Im\left[\int_{\theta_n}^{\theta_2} F^*\, d\theta\right]}, \tag{8}$$

where

$$Z = r_2 F_2^{*\prime} - r_2' F_2^* - r_1 F_1^{*\prime} + r_1' F_1^*.$$

Correspondingly the quantity $(\Delta H_1 / H_0)_{eq}$ is determined by the expression

$$\left(\frac{\Delta H_1}{H_0}\right)_{eq} = \frac{r_2 F_2^{*\prime} - r_2' F_2^* - r_1 F_1^{*\prime} + r_1' F_1^*}{\left(\frac{l}{2\pi}\right)^2 \frac{1}{\varrho}\left\{\int_{\theta_1}^{\theta_n} F^* d\theta + K\int_{\theta_n}^{\theta_2} F^* d\theta\right\}}, \tag{9}$$

where θ_n is the coordinate of the middle of the block.

For the simple case in which $\Delta H/H_0$ = const over the whole length of the block, K = 1 and $(\Delta H_1/H_0)_{eq} = \Delta H/H_0$. Formulas (8) and (9) do not depend on normalization and the initial phase of the Floquet function. Still more important, the results of determining $(\Delta H_1/H_0)_{eq}$ and K do not depend on the number of passages of the beam through the magnet over which the quantities r and r' measured by the signal electrodes are averaged. This enables us to increase the precision of determining $(\Delta H_1/H_0)_{eq}$ and K for a given precision of measuring the momentary values of r and r'.

In order to determine the sensitivity of the method, calculations were made for the Erevan annular electron accelerator ÉKU with the FOFDOD magnetic structure; the radius of curvature of the magnets was ~25 m, and the mean ring radius ~30 m. Calculations showed that use of the values of r and r' measured at the ends of the block yielded a reliable value of $\Delta H/H_0 = 0.5\%$ for the perturbation. Thus, the occurrence of a deviation $\Delta H/H_0 = 0.5\%$, constant over the length of the bloc, leads to a change of $\Delta r_2 = 1.21$ mm and $\Delta r_2' = 1.18$ mm/rad in the coordinate at the exit from the block. The coordinates of the beam axis are conveniently measured at the ends of the magnetic block, since the derivatives with respect to azimuth do not alter in the free spaces. For greater reliability in the determination of the derivatives we may then use information from sensing devices situated at the entrance and exit of two neighboring blocks. The fair distance between these points ensures good precision in determining r'. Thus for the ÉKU accelerator for the length of the free space between the blocks $\Delta\theta = 0.86$ rad and $\Delta H/H_0 = 0.5\%$, $\Delta r'\Delta\theta = 1.00$ mm. The value of the derivatives may be made more exact by additional measurements in the free spaces. The method enables us to determine and compensate perturbations in the magnetic system caused by imprecise installation of the blocks and chance displacements. In the case in which the beam-sensing elements are fixed in the vacuum chamber, such perturbations will be sensed as phase shifts of the Floquet function.

In order to distinguish the case of loss of beam inside the magnetic block from that of its emergence with zero parameters, we must use the total signal from the sensing elements situated at the end of the block. If the over-all signal at the block entrance is zero, then a special signal proportional to the maximum possible displacement of the center of gravity of the beam at the block exit must be applied to the analyzing device. From this signal and the measured values of r_1 and r_1' we may determine the values of $(\Delta H_1/H_0)_{eq}$ and K. For successive correction of the blocks, however, this case in not very probable. Thus, for the ÉKU, loss of the beam inside the block in the case of zero entrance parameters ($r_1 = 0$, $r_1' = 0$) means a field deviation of $\Delta H/H_0 \approx 30\%$ in the block.

Determining the Magnitude of the Frequency Deviation of Betatron Oscillations

Suppose we know for certain that in one of the magnetic blocks the magnitude of the perturbation is constant along the whole length. If r_1, r_1' and r_2, r_2' are the measured values of the coordinates and the derivatives of the beam center of gravity at the ends of this magnetic block, then the value of $K \equiv 1$ determined from Eq. (8) is independent of the value of $\Delta H/H_0$. Let us suppose that the frequency of the betatron oscillations varies by $\Delta\nu$. Here we obtain a new distribution of the Floquet function with respect to azimuth, leading to an additional distortion of the beam trajectory. If the values of r_1 and r_1' remain the same as for $\Delta\nu = 0$, the r_2 and r_2' acquire certain increments Δr_2 and $\Delta r_2'$. If the new values of r_2 and r_2' are put into expression (8), the value of K will differ from unity. Let us examine the variation with $\Delta\nu$ of the phase of the expression

$$Z = \tilde{r}_2 F_2^{*\prime} - \tilde{r}_2' F_2^* - r_1 F_1^{*\prime} + r_1' F_1^*. \tag{10}$$

The new values of the Floquet function and its derivative for a change of $\Delta\nu$ in the frequency of the betatron oscillations will to a first approximation be given by the expressions:

$$\varphi = Fe^{i\Delta\nu\theta} \approx F + i\Delta\nu\theta F,$$
$$\varphi' = i\Delta\nu F e^{i\Delta\nu\theta} + F' e^{i\Delta\nu\theta} \approx F'(1 + i\Delta\nu\theta) + i\Delta\nu F. \tag{11}$$

From the measured values of r_1 and r_1' and the new values of the Floquet function, we determine $\tilde{r}_2$ and $\tilde{r}_2'$. Making some fairly simple mathematical transformations and rejecting terms containing $\Delta\nu^2$, we obtain

$$\tilde{r}_2 = r_{2\,\mathrm{fr}} + r_{2\,\mathrm{fo}} - Re\{K(r_1 r_1') + L(\Pi)\}\Delta\nu, \tag{12}$$

$$\tilde{r}_2' = r_{2\,\mathrm{fr}}' + r_{2\,\mathrm{fo}}' - Re\{N(r_1 r_1') + E(\Pi)\}\Delta\nu, \tag{13}$$

where $r_{2\,fr}$ and $r_{2\,fr'}$ are the values of the coordinate of the center of gravity and its derivative at the point θ_2 for $\Delta\nu = 0$ and $\Delta H/H_0 = 0$ ("free"), and $r_{2\,fo}$ and $r_{2\,fo'}$ are the "forced" solutions at the point θ_2 for $\Delta\nu = 0$; $K(r_1, r_1')$ and $N(r_1, r_1')$ are functions determined by the values of r_1 and r_1', and $L(\Pi)$ and $E(\Pi)$ are functions determined by the magnitude of the perturbation in the magnetic block. These functions have the form

$$K(r_1 r_1') = -\frac{1}{2}[(r_1 F_1^{*\prime} - r_1' F_1^*) F_2(\theta_2 - \theta_1) - r_1 F_1^* F_2], \tag{14}$$

$$N(r_1 r_1') = -\frac{1}{2}\{[F_2 + F_2'(\theta_2 - \theta_1)][r_1 F_1^{*\prime} - r_1' F_1^*] - r_1 F_1^* F_2'\}, \tag{15}$$

$$L(\Pi) = \frac{F_2 \Pi}{2}\left(\int_{\theta_1}^{\theta_2} F^*\theta\, d\theta - \theta_2 \int_{\theta_1}^{\theta_2} F^*\, d\theta\right), \tag{16}$$

$$E(\Pi) = \frac{1}{2}\left[(\theta_2 F_2' - F_2)\ \Pi \int_{\theta_1}^{\theta_2} F^*\, d\theta - F_2'\,\Pi \int_{\theta_1}^{\theta_2} F^*\theta\, d\theta\right]. \tag{17}$$

Here

$$\Pi = \left(\frac{l}{2\pi}\right)^2 \frac{1}{\varrho} \cdot \frac{\Delta H}{H_0}. \tag{18}$$

Substituting expressions (12) and (13) into (10), rejecting terms containing $\Delta\nu^2$, and allowing for the condition

$$r_{2\,\mathrm{fr}} F_2^{*\prime} - r_{2\,\mathrm{fr}}' F_2^* - r_1 F_1^{*\prime} + r_1' F_1^* = 0, \tag{19}$$

we obtain

$$Z = r_{2\,\mathrm{fo}} F_2^{*\prime} - \Delta\nu Re\{K(r_1 r_1') + L(\Pi)\} F_2^{*\prime} - r_{2\,\mathrm{fo}}' F_2^* + \Delta\nu Re\{N(r_1 r_1') + E(\Pi)\} F_2^*. \tag{20}$$

Let us form the ratio of the imaginary part of expression (20) to the real part. Expanding the resultant expression in series in powers of $\Delta\nu$ and restricting consideration to the term containing the first power of $\Delta\nu$, we obtain:

$$\frac{Im(Z)}{Re(Z)} = \frac{r_{2\,\mathrm{fo}}\ ImF_2^{*\prime} - r_{2\,\mathrm{fo}}'\ ImF_2^*}{r_{2\,\mathrm{fo}}\ ReF_2^{*\prime} - r_{2\,\mathrm{fo}}'\ ReF_2^*} + \Delta\nu T(r_1 r_1' \Pi). \tag{21}$$

An expression for $T(r_1 r_1' \Pi)$ can easily be found by making some simple transformations. In expression (21)

$$\frac{r_{2\,\mathrm{fo}}\ ImF_2^{*\prime} - r_{2\,\mathrm{fo}}'\ ImF_2^*}{r_{2\,\mathrm{fo}}\ ReF_2^{*\prime} - r_{2\,\mathrm{fo}}'\ ReF_2^*} = \frac{Im\left\{\int_{\theta_1}^{\theta_2} F^*\, d\theta\right\}}{Re\left\{\int_{\theta_1}^{\theta_2} F^*\, d\theta\right\}} = \mathrm{const}. \tag{22}$$

Thus for the EKU accelerator this quantity equals -0.195. The function $T(r_1, r_1' \Pi)$ is a linear function of the principal coordinates, their derivatives, and the value of the perturbation. Hence the value averaged over many rotations of the beam is $\langle T(r_1, r_1' \Pi)\rangle = T(\Pi)$, i.e., constitutes a certain constant determined by the magnitude of the perturbation specially introduced into the block. Substituting expression (21) into (8) and averaging over many turns, we determine the deviation of K from unity. This deviation may, for a known value of $T(\Pi)$, be graduated in units of $\Delta\nu$.

Determining the Amplitude and Frequency Coherent Phase Oscillations

In electron synchrotrons calculated for a particle energy of the order of several BeV, owing to the high multiplicity of the high frequency voltage the direct method of measuring the amplitude and frequency of coherent phase oscillations presents considerable difficulty. This information may be obtained far more simply by measuring the coherent deviation of the particle energy from the equilibrium value arising for phase oscillations. It is known [8] that for $E_S \gg mc^2$

$$\frac{d\Phi}{dt} = q\omega_0\alpha \frac{\Delta E}{E_s}(t), \tag{23}$$

where q is the multiplicity of the frequency of the accelerating voltage, ω_0 is the frequency of rotation of the particles in the orbit, and α is the logarithmic derivative of the length of the orbit with respect to momentum. Let us suppose that the momentary phase of the accelerating voltage for which the center of gravity of the beam passes through the middle of the accelerating gap under the influence of an external perturbation, is given by the expression

$$\Phi = \Phi_s + \Delta\varphi \cos \Omega t, \tag{24}$$

where Φ_S is the value of the equilibrium phase, $\Delta\varphi$ the amplitude of the phase oscillation, and Ω the oscillation frequency. On this assumption, expression (23) will have the form

$$-\Delta\varphi\Omega \sin \Omega t = q\omega_0\alpha \frac{\Delta E}{E_s}(t). \tag{25}$$

Let us measure the coordinates and their derivatives with respect to azimuth at the ends of one magnetic block and determine the value of the total perturbation arising as a result of deviations of the magnetic field values in the block and the mean particle energy in the beam:

$$r_2F_2^{*\prime} - r_2'F^* - r_1F_1^{*\prime} + r_1'F_1^* = \left(\frac{l}{2\pi}\right)^2 \frac{1}{\varrho} \int_{\theta_1}^{\theta_2} F^* \frac{\Delta H}{H_0}(\theta)\, d\theta - \left(\frac{l}{2\pi}\right)^2 \frac{\Delta E}{\varrho E_s} \int_{\theta_1}^{\theta_2} F^*\, d\theta.$$

The deviation of the magnetic field in the blocks during the acceleration cycle changes considerably more slowly than the coherent deviation of the particle energy, owing to the phase oscillations. Hence the duly separated high frequency component of expression (24) determines the amplitude and frequency of the oscillation of $(\Delta E/E)t$. The frequency of the variation of $(\Delta E/E_0)t$ may be measured by many well known methods. The amplitude of the phase oscillations will be connected with the maximum deviation of the beam energy by the expression

$$\Delta\varphi = \frac{q\omega_0\alpha}{\Omega} \cdot \frac{\Delta E}{E_0}\max. \tag{26}$$

In conclusion, the author considers it his pleasant duty to thank S. M. Rubchinskii, É. L. Burshtein, A. A. Vasil'ev, Yu. F. Orlov, S. A. Kheifets, and V. M. Kharitonov for discussion of the work, and M. A. Garzoyan for help in carrying it out.

LITERATURE CITED

1. A. A. Vasil'ev, A. A. Kuz'min, and Yu. S. Ivanov, Pribory i tekhnika éksperimenta, No. 4, 111 (1962).
2. É. L. Burshtein, Yu. S. Ivanov, and A. A. Kuz'min, Pribory i tekhnika éksperimenta, No. 4, 102 (1962).
3. É. L. Burshtein, et al., Atomnaya énergiya, 12, No. 2 (1962).
4. A. A. Vasil'ev, A. A. Kuz'min, and V. A. Uvarov, Pribory i tekhnika éksperimenta, No. 4, 134 (1962).
5. A. A. Vasil'ev, Transactions of the International Conference on Accelerators, Dubna, 1963 [in Russian] (Moscow, Atomizdat, 1964), p. 871.
6. A. A. Vasil'ev, Dokl. AN SSSR, 148, 577 (1963).
7. A. I. Dzergachard, V. A. Karpov, See [5], p. 867.
8. S. A. Khaifets, The Electron Synchrotron [in Russian] (Erevan, Izd. AN Arm.SSR, 1963).

PHASE STABILITY OF A SYSTEM OF PARTICLES IN SELF-REGULATED ACCELERATORS

(UDC 621.384.60)

É. A. Zhil'kov and A. N. Lebedev

Translated from Atomnaya Énergiya, Vol. 18, No. 1, pp. 22-28, January, 1965
Original article submitted February 13, 1964

The problem of the phase stability of a sytem of particles in a cyclic accelerator with frequency autocorrection of the accelerating field along the beam is considered. The stability of nonlinear synchrotron oscillations is investigated by the kinetic-equation method for arbitrary characteristics of the self-regulating system. Some general stability criteria are obtained.

One of the most promising routes in the development of cyclic accelerators is the wide application of beam autocontrol systems, which permit a considerable reduction to be made in the allowance for different parameters of the magnet and high-frequency systems [1, 2]. In practice the most important and at present most widely used system of this type is the system of automatic frequency trimming of the accelerating field by radial (or phase) shift of the accelerated particles, thus permitting considerable increase in the stability of coherent synchrotron oscillations relative to various perturbations. An investigation, which was carried out in linear approximation [3], showed that the frequency of coherent synchrotron oscillations, i.e., oscillations of the beam center, is increased by a factor of $(1 + K)^{1/2}$ where K is the amplification factor in the self-regulation cycle with respect to the radial shift of the beam. In addition, it was proved possible to achieve strong damping of the coherent oscillations.

The oscillations around the beam center, discussed in [3] in linear approximation, are not subject to the effect of self-adjustment and have the normal frequency of synchrotron oscillations. Naturally, the nonlinear nature of the phase motion should alter this picture, leading to coupling of the beam-center oscillations and the free oscillations around it. The representation of the nature of this coupling can be obtained in this case if the first moments of the distribution are considered as in [4] and, more rigorously, in the first and second sections of this paper.

However, for the subsequent statement of the problem the discussion should center on the stability of a system having a large, almost infinite number of degrees of freedom corresponding to a large number of accelerated particles. It is shown below that this investigation can be carried out by the kinetic-equation method with self-consistent interaction. It was found possible to obtain a very general characteristic equation, useful for a wide class of regulatory systems and giving in principle an answer to the problem as posed.

The paper has been limited to the investigation of certain general properties of this equation which are independent of the choice of the feedback circuit parameters. The calculation of an actual system, requiring computation of a number of purely radiotechnological considerations, will be carried out in a separate report.

1. Statement of the Problem

In order to describe the synchrotron oscillations of an individual particle, we shall use the canonical conjugate variables

$$\varphi;\ u = \frac{2\pi\Omega_0}{eV\sin\varphi_s}\int_{E_s}^{E}\frac{dE}{\omega(E)}, \tag{1.1}$$

where $\omega(E)$ is the rotational frequency of a particle with energy E; V and φ are the amplitude and phase, respectively, of the accelerating potential; Ω_0 is the frequency of the linear synchrotron oscillations in the absence of self-regulation. We shall neglect the explicit time dependence of the parameters Ω_0, V, etc.

If we choose $\tau = \Omega_0 t$ as an independent variable, then the synchrotron oscillation equation can be written in the form

$$\left.\begin{aligned} \dot{u} &= F(\varphi) = \frac{\cos\varphi - \cos\varphi_s}{\sin\varphi_s}, \\ \dot{\varphi} &= u + \Delta(\tau), \end{aligned}\right\} \tag{1.2}$$

where $\Delta(\tau)$ is the correcting adjustment to the frequency of the accelerating field, associated with the energy of the self-regulation system and expressed in units of Ω_0.

According to Eq. (1.2) the kinetic equation which describes the change of the distribution function $f(u, \varphi, \tau)$ has the form

$$\left[\frac{\partial}{\partial\tau} + (u+\Delta)\frac{\partial}{\partial\varphi} + F(\varphi)\frac{\partial}{\partial u}\right] f(u, \varphi, \tau) = 0. \tag{1.3}$$

The quantity Δ can be related to the various characteristics of the beam as a function of the following (or tracking) system parameters: to the coordinates of its center of gravity, dimensions, etc. In the general case, if we denote by $K(u, \varphi, \omega)$ the reaction of the system with frequency ω to a shift of a point-like beam with respect to u, and φ, then in Fourier presentation the quantity $\Delta(\omega)$ can be described in the form of a linear function of the distribution function

$$\Delta(\omega) = \int\int K(u, \varphi, \omega) f(u, \varphi, \omega)\, du\, d\varphi. \tag{1.4}$$

Equations (1.3) and (1.4) represent a closed integral-differential system describing the behavior of the entire buildup of particles in an accelerator with self-regulation. We shall proceed further from the fact that this system permits a stationary (equilibrium) solution: $f_0(u, \varphi)$, $\Delta_0 = \text{const}$. We note that the constant component of the correction signal Δ_0, associated with the equilibrium distribution, can be set equal to zero without limiting the generality, since this leads simply to an insignificant indeterminacy of the equilibrium energy. It is not difficult to see that an extremely wide range of equilibrium distributions is possible, on which a unique requirement is imposed – the constancy of f_0 along the phase trajectory [see Eq. (3.2)]. In the general case, the center of the equilibrium phase φ_s as a consequence of the nonlinearity of the synchrotron oscillations, i.e., in conseque ce of the deviation of the potential well $-\int F d\varphi$ from parabolic. This shift is found to be greater, the larger the equilibrium phase of the beam. In accordance with the assumptions made above concerning the absence in the equilibrium state of a correction signal Δ_0, it should be assumed that the center of the equilibrium distribution with respect to energy coincides with E_S, i.e., $u_0 = 0$.

2. Method of Moments

First of all we shall consider the case of a beam of quite small dimensions, since by this example it is easier to trace the physical significance of the relationships obtained below. Multiplying the kinetic equation (1.3) by $(\varphi - \varphi_0)^j u^k$ and integrating with respect to the entire phase space, we obtain a system of equations for the set of distribution moments $M_{j,k} = \overline{(\varphi - \varphi_0)^j u^k}$ (the bar denotes the average):

$$\dot{M}_{j,k} - jM_{j-1,k+1} - j\Delta M_{j-1,k} - k\overline{F(\varphi)(\varphi - \varphi_0)^j u^{k-1}} = 0. \tag{2.1}$$

In accordance with the assumption made above concerning the smallness of the beam, the distribution moments should be reduced rapidly with increase of their number. Having expanded the quantity $F(\varphi)$ in a Taylor series around the point φ_0, Eq. (2.1) leads conveniently to the form

$$\dot{M}_{j,k} - jM_{j-1,k+1} - j\Delta(\tau) M_{j-1,k} - k\sum_{l=0}^{\infty} \frac{F^{(l)}(\varphi_0)}{l!} M_{j+l,k-1} = 0. \tag{2.2}$$

We note that the system of equations (2.2) is, generally speaking, nonlinear since the correction signal Δ is connected with the moments by the relationship (1.4). We now use the fact that the phase dimensions of the beam

$A \ll 1$ and that the moment $M_{j,k}(j, k \neq 0)$ has an order of smallness A^{j+k}. Since the equilibrium signal $\Delta_0 = 0$, then Eq. (2.2), to an accuracy up to terms in $\sim A^2$, gives

$$\varphi_0 \approx \varphi_s - \frac{\operatorname{ctg} \varphi_s}{2} M^0_{0,2}, \quad M^0_{0,2} \approx M^0_{2,0}, \tag{2.3}$$

and all the remaining equilibrium moments, which we shall denote by the superscript 0, are equal either to zero or have the highest order of smallness. It should be noted that the shift of the center of the beam from the equilibrium phase turns out to be of order A^2.

In order to find the natural frequencies of the system being investigated, it is necessary to linearize Eq. (2.2) around the equilibrium position, to apply to it a Fourier transform (to find the solution of $\sim \exp i\omega t$) and to use the relationship resulting from Eq. (1.4):

$$\Delta(\omega) = K_1(\omega) M_{0,1}(\omega) + K_2(\omega) M_{1,0}(\omega) + K_3(\omega) M_{2,0}(\omega) + \ldots, \tag{2.4}$$

where

$$K_1 = \frac{\partial K}{\partial u}\Big|_{\substack{u=0 \\ \varphi=\varphi_0}}, \quad K_2 = \frac{\partial K}{\partial \varphi}\Big|_{\substack{u=0 \\ \varphi=\varphi_0}}, \quad K_3 = \frac{1}{2} \cdot \frac{\partial^2 K}{\partial \varphi^2}\Big|_{\substack{u=0 \\ \varphi=\varphi_0}} \text{ etc.} \tag{2.5}$$

For simplicity, we shall limit ourselves only to the first two terms of the expansion (2.4), i.e., we shall assume the characteristics of the (following) tracking system $K(u, \varphi, \omega)$ to be linear with respect to u and φ. In other words, it is assumed that the correcting signal is developed with respect to data concerning the motion of the center of the beam φ and u, and is independent of its dimensions, shape, etc. No difficulties of principle arise in the calculation as a result of rejecting this limitation, but the calculations become too cumbersome.

If in Eq. (2.2) we are limited to terms in $\sim A^2$ inclusively, then only the first and second distribution moments enter into the considerations, forming two independent subsystems. Their partial frequencies in this approximation will be equal to

$$\omega = -i \frac{K_2}{2} \pm \left[1 + K_1 - \frac{K_2^2}{4}\right]^{\frac{1}{2}} \text{ for the first moments;} \tag{2.6}$$

$$\text{and } \omega = 0, \pm 2 \text{ for the second moments.} \tag{2.7}$$

Thus, we obtain the well-known result of [3]: by introducing a high degree of feedback ($|K_{1,2}| \gg 1$) the "rigidity" of the oscillations of the center of gravity of the beam can be increased strongly and even damping of them can be originated (for example, for $\operatorname{Re} K_2 < 0$). The natural oscillation frequency of the second moments, which in this approximation remain free, is equal to twice the frequency of the synchrotron oscillations in the absence of self-regulation.

By taking into account terms $\sim A^4$, the corrections to the natural frequency of the first two moments can be found (terms $\sim A^3$ make it possible to determine only the partial frequencies of the third moments, equal of course to ± 1 and ± 3). These calculations are quite cumbersome since they are associated with the calculation of a determinant of the 10th order. We shall mention only the most important result – the correction of the first approximation to the real partial frequency $\omega = 2$ of the second moments, since small corrections to the complex frequency (2.6) cannot change the nature of the motion qualitatively. If we assume that $\omega = 2 + \alpha (|\alpha| \ll 1)$, then

$$\alpha \approx \frac{\operatorname{ctg}^2 \varphi_s M^0_{2,0} [iK_2(\omega) - 2K_1(\omega)]}{6 [K_1(\omega) - 2iK_2(\omega) - 3]}\Big|_{\omega=2}. \tag{2.8}$$

Thus, damping ($\operatorname{Im} \alpha > 0$) and buildup ($\operatorname{Im} \alpha < 0$) of the oscillations are also possible at this frequency. The condition of stability for $|K_{1,2}| \gg 1$ is, obviously, the inequality

$$Re \frac{K_1}{K_2} < 0. \tag{2.9}$$

The rate of damping or buildup [for nonfulfillment of Eq. (2.9)] is proportional to the square of the equilibrium dimensions of the beam. We note that the correction to the frequency in Eq. (2.8) and to the criterion of stability in Eq. (2.9) are found to be somewhat different than in [4]. The range of applicability of the criterion obtained will be apparent from the more general considerations presented below.

3. Kinetic Equation Method

The method of moments discussed above is not completely valid and has certain obvious inadequacies. First of all it is difficult to show any normal physically valid method of closure of the system of equations (2.2). Although simply equating the highest moments to zero leads sometimes also as will be seen below, to a correct result, a number of other effects appear as a result of this method. For example, it is not possible by this method to obtain the corrections to the natural frequency because of nonlinearity of the synchrotron oscillations. Similarly, also with a hydrodynamic description of the plasma the method of moments does not take into account the effects of Landau type damping [5]. Finally, the applicability of the results obtained above is considerably limited by the assumption concerning the smallness of the beam.

In order to remove these limitations we shall investigate the beam stability by a more general method, arising directly from the kinetic equation (1.3). As before, we shall assume that there exists a certain equilibrium distribution in the phase space $f_0(u, \varphi)$ which is clearly independent of time and which does not give an error signal. The deviation from this equilibrium distribution function of $f(u, \varphi, \omega)$ and of the error signal $\Delta(\omega)$ we shall assume to be small and we shall carry out the linearization of the kinetic equation (1.3) with respect to these small perturbations:

$$\left[i\omega + u\frac{\partial}{\partial \varphi} + F(\varphi)\frac{\partial}{\partial u} \right] f(u, \varphi, \omega) = -\Delta(\omega)\frac{\partial f_0}{\partial \varphi}. \tag{3.1}$$

It is easy to show from the same equation that the equilibrium distribution function should be constant along the phase trajectory, i.e., $f_0 = f_0(\varepsilon)$, where

$$\varepsilon = \frac{u^2}{2} + U(\varphi) \quad \left(U = -\int_{\varphi_s}^{\varphi} F\, d\varphi \right) \tag{3.2}$$

is the Hamiltonian of the synchrotron oscillations in the absence of self-regulation. In connection with this, it is convenient to transfer from the variables u, φ to the new canonical conjugate variables ε, T, where

$$T = \int_{\varphi_1}^{\varphi} [2(\varepsilon - U)]^{-\frac{1}{2}} d\varphi \tag{3.3}$$

is a time characterizing the shift of a representative point along the phase trajectory. We denote by $\varphi_1(\varepsilon)$ and $\varphi_2(\varepsilon)$ respectively the left and right point of reversal of the phase oscillations, defined by the well-known condition

$$U(\varphi_1) = U(\varphi_2) = \varepsilon. \tag{3.4}$$

Thus, for $\varphi = \varphi_2$ the quantity T is equal to $T_0/2$ – the half period of the nonlinear synchrotron oscillations; for $u \gtrless 0$, corresponding $T \gtrless 0$.

In the new variables the kinetic equation assumes the form

$$\left[i\omega + \frac{\partial}{\partial T} \right] f(\varepsilon, T, \omega) = \Delta(\omega)\frac{df_0}{d\varepsilon} \cdot F \tag{3.5}$$

and has the solution

$$f(\varepsilon, T, \omega) = -i\Delta(\omega)\frac{df_0}{d\varepsilon}\sum_{k=-\infty}^{+\infty}\frac{F_k e^{-ik\Omega T}}{\omega - k\Omega}, \qquad \Omega \equiv \frac{2\pi}{T_0}, \tag{3.6}$$

where F_k are the coefficients of the expansion of F as a periodic function of the variable T in a Fourier series at the intercept $(-T_0/2, +T_0/2)$:

$$F_k = \frac{1}{T_0} \int_{-\frac{T_0}{2}}^{+\frac{T_0}{2}} F e^{ik\Omega T} dT. \tag{3.7}$$

We note that in accordance with the definition of T [see Eq. (3.3)]

$$\frac{d^2\varphi}{dT^2} = F(\varphi), \qquad F_k = -\Omega^2 k^2 \varphi_k, \qquad u_k = -ik\Omega\varphi_k. \tag{3.8}$$

Substituting the solution of equation (3.6) in formula (1.4), cancelling by $\Delta(\omega)$ and carrying out integration with respect to T, taking into account that $du\, d\varphi = d\varepsilon\, dT$, we obtain the characteristic equation for determining the spectrum of the natureal frequencies

$$1 = 2\pi i \int_0^\infty d\varepsilon \Omega \frac{df_0}{d\varepsilon} \sum_{-\infty}^{+\infty} \frac{K_{-k} k^2 \varphi_k}{\omega - k\Omega} \tag{3.9}$$

Equation (3.9) can be derived in a more convenient form if $K(u, \varphi, \omega)$ is divided into two parts:

$$K = K^+(\varphi, \omega) + K^-(u, \varphi, \omega) \tag{3.10}$$

and if K^- be extracted – the part which is linearly dependent on u. The importance of the notation we have introduced consists in that K^+ and K^- are respectively even and odd functions of T. Then Eq. (3.9) can be transcribed in the form

$$1 = 4\pi i \int_0^\infty d\varepsilon \Omega \frac{df_0}{d\varepsilon} \sum_{k=1}^{\infty} k^2 \varphi_k \frac{\omega K_k^+ - k\Omega K_k^-}{\omega^2 - k^2\Omega^2}. \tag{3.11}$$

We note that the Fourier transformation of $\Delta(\omega)$ is determined by formula (1.4) in the lower semiplane of the complex variable ω and is analytically extended to the upper semiplane, which corresponds to damped oscillations [5]. It is interesting that the possibility of such damping is associated in our case with nonlinearity of the synchrotron oscillations, which brings in the relationship $\Omega(\varepsilon)$.

4. Investigation of the Characteristic Equation

It can be seen from Eq. (3.1) or (3.6) that as a result of reducing the feedback to zero ($\Delta \to 0$ and $K \to 0$) the system has a continuous spectrum of natural oscillations which lie in bands close to the integral values corresponding to the various distribution moments. The width of these bands is determined by the spread of $\Omega(\varepsilon)$, i.e., by the nonlinearity of the oscillations. Thus, this case corresponds to general noncoherent synchrotron oscillations.

We shall consider the coherent effects associated with a self-regulating system in certain limiting cases.

For linear synchrotron oscillations, the phase φ depends harmonically on T, so that in the limiting case of a vanishingly small beam only the coefficient φ_1 differs from zero, and the characteristic equation has roots of the form of Eq. (2.6) and (2.7). If the finite (but small) amplitude of the oscillations be taken into account, the quantity φ depends on T, as is well known, in the following manner [6]:

$$\varphi(T) \approx \varphi_s - \sqrt{2\varepsilon} \cos \Omega T - \frac{\varepsilon}{2} \operatorname{ctg} \varphi_s + \frac{\varepsilon \operatorname{ctg} \varphi_s}{6} \cos 2\Omega T + \ldots, \tag{4.1}$$

where

$$\Omega \approx 1 - \frac{\varepsilon}{8}\left(1 + \frac{5}{3}\operatorname{ctg}^2 \varphi_s\right) + \ldots \tag{4.2}$$

If, as in Section 2, we limit ourselves to the case

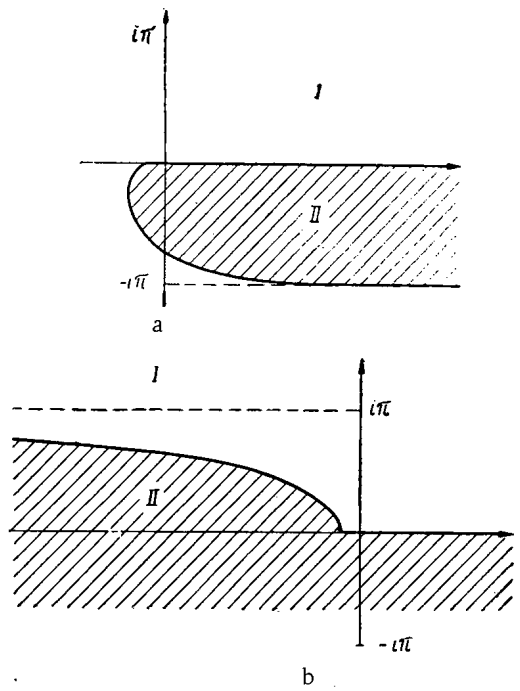

Fig. 1. Regions of stability (I) and instability (II) of a beam in the plane of the complex variable ξ: a) Linearly decreasing equilibrium distribution; b) linearly increasing equilibrium distribution.

$$K^+ = K_2(\omega)(\varphi - \varphi_0), \quad K^- = uK_1(\omega) \tag{4.3}$$

and find the small complex corrections to the natural frequency $\omega = 2$, then it is necessary to leave terms with k = 1 and k = 2 in the characteristic equation (3.11), so that for k = 1 it is possible to obtain at once $\omega = 2$ and $\Omega = 1$. Then, neglecting insignificantly small terms, we reduce the characteristic equation by means of Eq. (4.1) to the form

$$\xi = \pi J(\omega)\left(1 + \frac{5}{3}\operatorname{ctg}^2\varphi_s\right), \tag{4.4}$$

where

$$\xi = \frac{3[3 - K_1(\omega) + 2iK_2(\omega)]\left(1 + \frac{5}{3}\operatorname{ctg}^2\varphi_s\right)}{2\operatorname{ctg}^2\varphi_s[iK_2(\omega) - 2K_1(\omega)]}\Bigg|_{\omega=2},$$
$$J = \int_0^\infty \frac{df_0}{d\varepsilon}\cdot\frac{\varepsilon^2\, d\varepsilon}{\omega^2 - 4 + \varepsilon\left(1 + \frac{5}{3}\operatorname{ctg}^2\varphi_s\right)}, \tag{4.5}$$

and the integral J should be evaluated in accordance with the procedures mentioned above.

It can be seen from expressions (4.4) and (4.5) that the correction to the natural frequency depends significantly on the form of the equilibrium distribution function $f_0(\varepsilon)$, normalized such that

$$\int_0^\infty f_0(\varepsilon)\, T_0(\varepsilon)\, d\varepsilon = 1. \tag{4.6}$$

In particular, by choosing f_0 in the form

$$f_0 = \begin{cases} \text{const} & \varepsilon < \varepsilon_{\max} \\ 0 & \varepsilon > \varepsilon_{\max} \end{cases} \tag{4.7}$$

and assuming that

$$x = \frac{4 - \omega^2}{\varepsilon_{\max}\left(1 + \frac{5}{3}\operatorname{ctg}^2\varphi_s\right)}, \tag{4.8}$$

we obtain from expressions (4.4) and (4.5):

$$x = 1 + \frac{1}{2\xi} \tag{4.9}$$

or

$$\omega \approx 2 - \frac{\varepsilon_{\max}}{4}\left(1 + \frac{5}{3}\operatorname{ctg}^2\varphi_s\right) - \frac{\varepsilon_{\max}\operatorname{ctg}^2\varphi_s(iK_2 - 2K_1)}{12(3 + 2iK_2 - K_1)}\Bigg|_{\omega=2}. \tag{4.10}$$

It is not difficult to see that the second component in the right-hand side describes the frequency shift due to nonlinearity of the oscillations, and the third component is the same as in expression (2.8), obtained by the method of moments (we recall that $M_{2,0}^0 \approx \varepsilon_{\max}/2$). The stability condition has the simple form: Im ξ > 0.

In the example given here, in addition to the point $\varepsilon = \varepsilon_{\max}$, $df_0/d\varepsilon = 0$, so that natural damping does not occur. By way of a second example we shall consider a triangular distribution of the form

$$f_0 = \begin{cases} \text{const}\,(\varepsilon_{max} - \varepsilon) & \varepsilon < \varepsilon_{max}, \\ 0 & \varepsilon > \varepsilon_{max}, \end{cases} \tag{4.11}$$

which, together with Eq. (4.9) gives

$$\xi = -\frac{1}{2} - x - x^2 \ln\left(1 - \frac{1}{x}\right), \tag{4.12}$$

whereby the branch of the logarithm is chosen such that its value lies on the first folium for Im x > 0. In order to determine the limits of separation between the regions of stability (Im x < 0) and instability (Im x > 0) in the plane of the complex variable ξ, it is sufficient to put Im x = 0 in formula (4.12). Then, as a result of changes in the values of Re x along the real axis the value of the logarithm remains equal to $\ln|1 - 1/x| + i\pi$ for $0 < \text{Re}\,x < 1$ and $\ln|1 - 1/x|$ in other intervals. Figure a shows the stability region constructed on the plane of the complex variable ξ; the similar Fig. 1 shows the case of a linearly increasing distribution $f_0 = \text{const}\ \varepsilon$ ($\varepsilon < \varepsilon_{max}$). On the basis of these results, it can be concluded that the spread of particles with respect to synchrotron oscillation frequency exerts a stabilizing effect on the beam only in decreasing distribution of $f_0(\varepsilon)$ and in increasing distributions it leads to stability deterioration. Generally speaking, the region Re Im $\xi > 0$ is more favorable in the stability sense, because the choice of the parameters $K_1(2)$ and $K_2(2)$ do not, in this region, contradict the condition of stability of the oscillations of the beam center [see Eq. (2.6)].

Let us dwell further on the case $\omega \ll 1$, i.e., we shall investigate the stability of the beam relative to perturbations which are slow compared with the synchrotron oscillations. Expanding the right-hand side of Eq. (3.9) in powers of ω and having limited it to a linear term, we obtain a solution

$$\omega = i\,\frac{1 - 2\pi\int_0^\infty d\varepsilon\,\frac{df_0}{d\varepsilon}\,\widetilde{uK}}{2\pi\int_0^\infty \frac{d\varepsilon}{\Omega}\cdot\frac{df_0}{d\varepsilon}\,\widetilde{\varphi K}}, \tag{4.13}$$

which is valid in this case if the right hand side of this equation is small with respect to absolute magnitude. The wavy line in expression (4.13) denotes averaging with respect to T for constant values of ε, so that for a small beam and a control system of the form of Eq. (4.3) we find

$$\omega \approx -i\,\frac{1 + K_1(\omega)}{K_2(\omega)}, \quad |1 + K_1| \ll |K_2|. \tag{4.14}$$

Precisely the same expression for these same conditions is obtained from Eq. (2.6), which is quite natural, since for very low frequencies the beam oscillates as a single entity. Thus, the stability criterion of the beam center simultaneously ensures its stability at low frequencies.

In conclusion, we note that the characteristic equation (3.11) obtained is applicable not only to the simple case of Eq. (4.3) but also to more complex systems. Moreover, the proposed method of calculation, which is by no means limited to the condition $\varepsilon \ll 1$, permits the stability to be investigated of larger beams and also the effect of particles located outside the separatrix.

The authors express their appreciation to A. A. Kolomenskom for interest in the project.

LITERATURE CITED

1. É. L. Burstein, et al., Dokl. AN SSSR, 141, 590 (1961); Atomnaya énergiya, 12, 111 (1962).
2. W. Schnell, Proc. of Intern. Conf. on High Energy Accel. CERN (1959), p. 485; Yu. S. Ivanov and A. A. Kuz'min, Pribory i tekhnika éksperimenta, No. 4, 106 (1962).
3. É. L. Burstein, Yu. S. Ivanov, and A. A. Kuz'min, Pribory i tekhnika éksperimenta, No. 4, 102 (1962).
4. H. Hereward, Proc. of Intern. Conf. on High Energy Accel. Brookhaven (1961), p. 236.
5. L. D. Landau, ZhÉTF, 16, 574 (1946).
6. L. D. Landau and E. M. Lifshits, Mechanics [in Russian] (Moscow, Fizmatgiz, 1958), Section 29.

MEASUREMENT OF THE PHOTONEUTRON YIELD FROM THICK COPPER AND WATER TARGETS AND DETERMINATION OF THE EXCITATION FUNCTION OF THE (γ, n) REACTION FOR O^{16} AND Cu^{63} BY MEANS OF THE BELEN'KII-TAMM EQUILIBRIUM PHOTON SPECTRUM[1]

(UDC 539.172.3)

I. A. Grishaev, D. I. Sikora, V. A. Shkoda-Ul'yanov, and B. I. Shramenko

Translated from Atomnaya Énergiya, Vol. 18, No. 1, pp. 28-33, January, 1965
Original article submitted November 18, 1963

Experimental measurements were made of the photoneutron yields from practically infinite specimens of copper and water subjected to the action of electrons with energies of up to 66 MeV. On the basis of these data and the Belen'kii-Tamm theory, in accordance with [1, 2], the excitation functions of the (γ, n) reactions for O^{16} and Cu^{63} were calculated. The results were compared with the data obtained by other authors on thin specimens irradiated with bremsstrahlung gamma quanta.

If a monoenergetic beam of electrons impinges on a targe so thick that there is practically complete absorption of the photons capable of taking part in the (γ, n) reaction which are formed in the substance through the development of an avalanche, then, by experimentally measuring the photoneutron yield, one can compare it with the photoneutron yield calculated according to the avalanche theory using the known cross section of the (γ, n) reaction for the nucleus being investigated. The experimental value of the photoneutron yield can also be used for calculating the cross section of the (γ, n) reaction and comparing it with the cross sections obtained by other methods, where the results of the avalanche theory are not used. Thus, it is possible to judge whether the avalanche theory is suitable in some particular energy range for the solution of various types of problems, particularly for determining the excitation functions of photonuclear reactions. The nuclei selected for investigation in this study were O^{16} and Cu^{63}. The reason for this was that the initial data of the avalanche theory, specifically the probabilities of various processes involving gamma quanta and electrons when an avalanche is produced are better justified in the case of light elements. One should therefore expect that the results of the avalanche theory will also be more accurate in the case of light elements and possibly for intermediate values of Z.

In addition, the excitation function of the (γ, n) reaction for O^{16} and Cu^{63} nuclei in the giant-resonance region has been investigated by a number of authors, and no very great differences have been found between corresponding results – unlike the case of lead, for example.

Moreover in this case it is easy to measure the photoneutron yields by using the induced activity of the residual nuclei; this makes the method more convenient, since there is no need to take account of the energy dependence of the apparatus used for recording neutrons of different energies or of the angular anisotropy of the emitted photoneutrons which results from the finite dimensions of the avalanche in the specimen. This anisotropy is considerable in work using light-element targets, where targets of large dimensions are required for practically complete absorption of radiation which is effective for (γ, n) reactions. The longitudinal and transverse dimensions of the target were chosen on the basis of the data of [3, 4] regarding the dimensions of cascade showers and the data of special experiments carried out during the present.

[1]This work was done jointly by the Physics and Technology Institute of the Academy of Sciences of the USSR and the Uzhgorod State University.

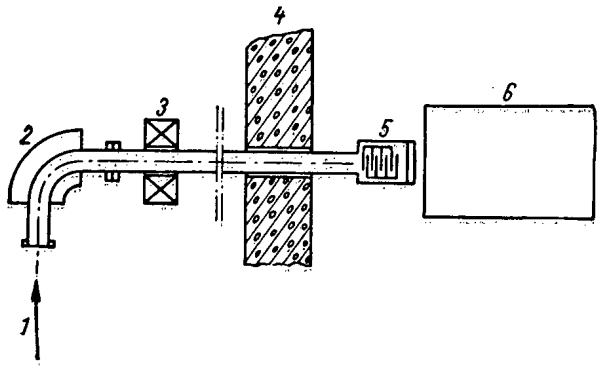

Fig. 1. Diagram of experimental measurement of photoneutron yields.

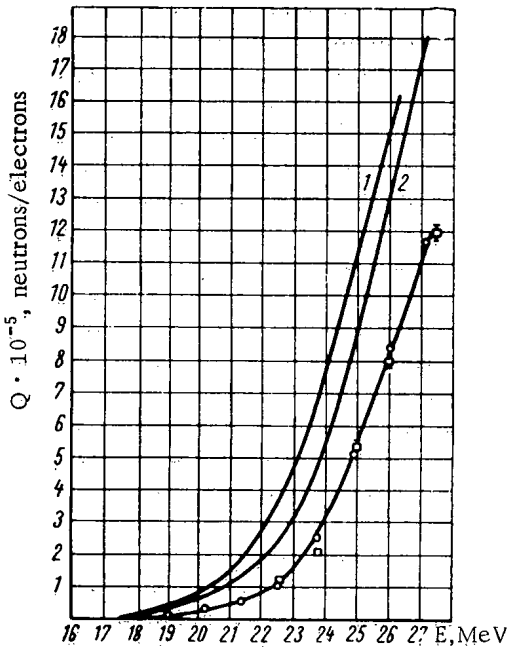

Fig. 2. Photoneutron yields from a thick water target [□) experimental points of the present study; ○) points obtained by using the cross sections of the (γ, n) reaction for O^{16} calculated by means of the Belen'kii-Tamm equilibrium spectrum and the experimental yield (this is the inverse problem, used for checking the calculations)]: 1) O^{16} yields calculated by means of the (γ, n) reaction cross section obtained in [18] and the Belen'kii-Tamm equilibrium photon spectrum; 2) O^{16} yields calculated by means of the (γ, n) reaction cross section obtained in [7] and the Belen'kii-Tamm equilibrium spectrum.

A diagram of the experimental measurement of the photoneutron yields is shown in Fig. 1.

The linear accelerator of the Physics and Technology Institute of the Academy of Sciences of the USSR was used as the source of monoenergetic electrons. The electron beam 1 passed through a magnetic analyzer 2 and was focused by the lenses 3; after passing through the secondary-emission monitor 5, it hit the target 6 under investigation. The concrete shield 4 was 1.75 m thick. The secondary-emission monitor consisted of two sets of aluminum foil sheets of equal thickness, with 10 sheets in each set. The sheets were 40 mm in diameter and had a thickness of 2.7 mg/cm^2. The sheets of one set were placed in the spaces between the sheets of the other set, like the arrangement of an air capacitor. A 200-V source was connected to the sheets of the emitter. The distance between the sheets was 2 mm.

The system had an energy resolution of 2%. The electron-beam monitor was combined with a current integrator of the type described in [5]. An RC circuit with a time constant equal to the lifetime of the radioactive isotope under investigation was connected to the input of the integrator; this automatically prevented any errors due to oscillations in the intensity of the electron beam [6].

Water (O^{16}). The target used for measuring the photoneutron yields from the $O^{16}(\gamma,n)O^{15}$ reaction was a tank 40 cm in diameter and 120 cm long, filled with distilled water. A specimen for the activity count was taken after the O^{15} solution had been thoroughly mixed so that it was homogeneous. The specific activity of the specimen was measured by means of an SI-2B end-window counter and an NS-9 cylindrical counter. The efficiency of the counter was determined by using a P^{32} solution of known concentration (±3%). Owing to the finite dimensions of the tank, part of the super-threshold gamma radiation left the tank from the transmission curves, this was found to be about 9%.

Figure 2 shows the photoneutron yields we obtained from water as a result of the (γ, n) reaction in O^{16} in the giant-resonance region; it also shows the calculated yields obtained by means of the Belen'kii-Tamm equilibrium spectrum and the cross sections published in [7, 8]. The critical energy value was taken to be 66.9 MeV. The relative error in the measurement of the photoneutron yields from O^{16} was ±2%, and we estimated the absolute errors at 7.5%. The erors in determination of the yields include the instability in the electron energy and the errors in the monitoring and recording of the induced activity. The energy of the electron beam was kept constant to within 0.02%, and the error in the monitoring of the electron beam was no more than 0.7%. The error in the recording of the induced activity was determined by the statistics of the count. The errors indicated are the same for O^{16} and Cu^{63}. Each point shown on the graphs represents the results of five to eight measurements. The data of Figs. 2 and 3 represent average results. Figure 4 shows all the hitherto published results of measurements of the

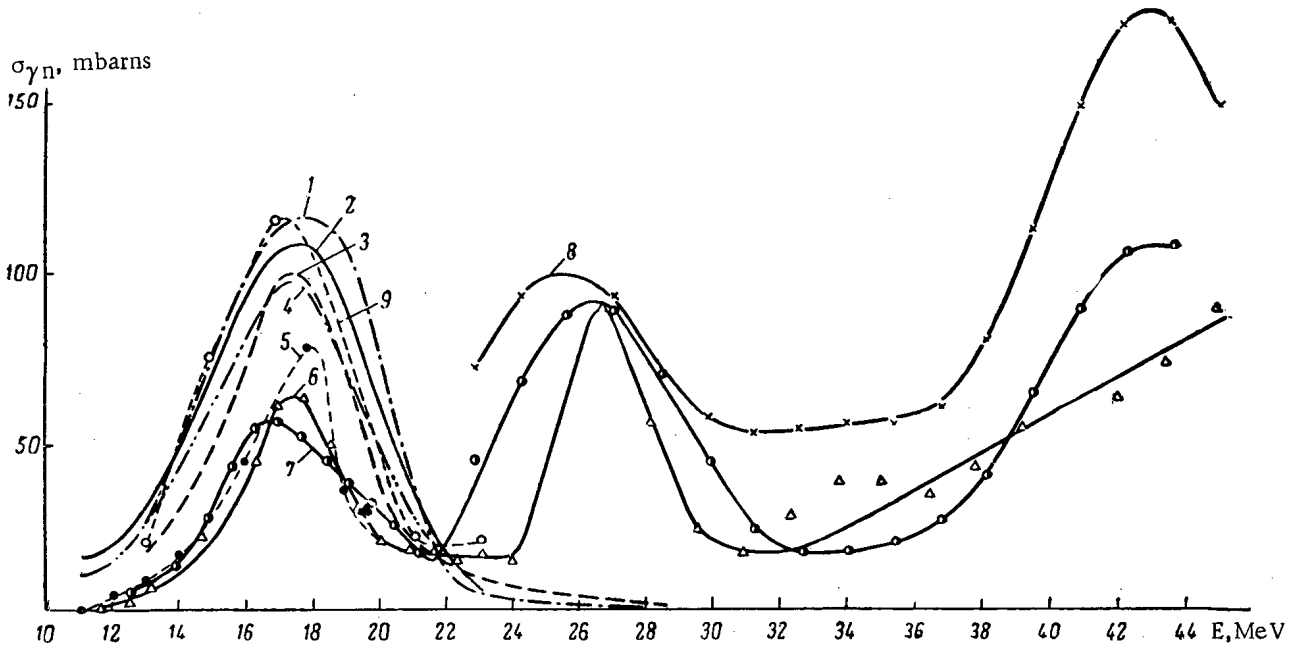

Fig. 3. Excitation function of the (γ, n) reaction for Cu^{63}: 1-4) Curves obtained with thin specimens and the Schiff spectrum by using the photon-difference method in [9-12]. The other curves are explained in the text.

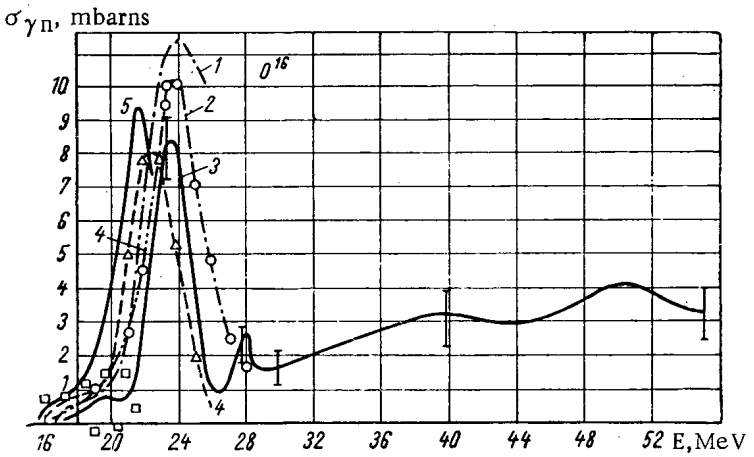

Fig. 4. Excitation function of the (γ,n) reaction for O^{16}: 1, 2, 4, 5) Curves obtained with thin specimens and the Schiff spectrum by using the photon-difference method, in [7, 8, 13, 14], respectively; 3) result of the present study.

excitation function of the (γ, n) reaction in O^{16}; curve 3 is the result derived from the data of the experiment described here, obtained by calculation using the Belen'kii-Tamm equilibrium photon spectrum. This curve represents the average of three independent calculations. The reduced errors result from the fact that the yield curve can be drawn in different ways within the limits of the experimental dispersion. In the high-energy range we first found the excitation function of the $O^{16}(\gamma, n)O^{15}$ reaction.

In order to check and compare the results, we also carried out the calculation by the photon-difference method extending over practically-infinite thick specimens. There was reasonably good agreement between the calculations done by the photon-difference method and those done by the method using the first and second derivatives of the yield with respect to energy [1, 15].

The photoneutron yields obtained from water in the range up to 66 MeV as the result of the (γ, n) reaction in O^{16} are shown in their entirety in Fig. 5. The data show that in the case of light elements, if we determine the ex-

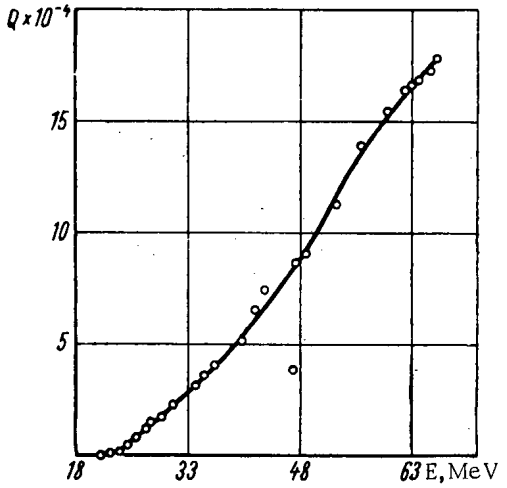

Fig. 5. Photoneutron yields (including the high-energy region) from water.

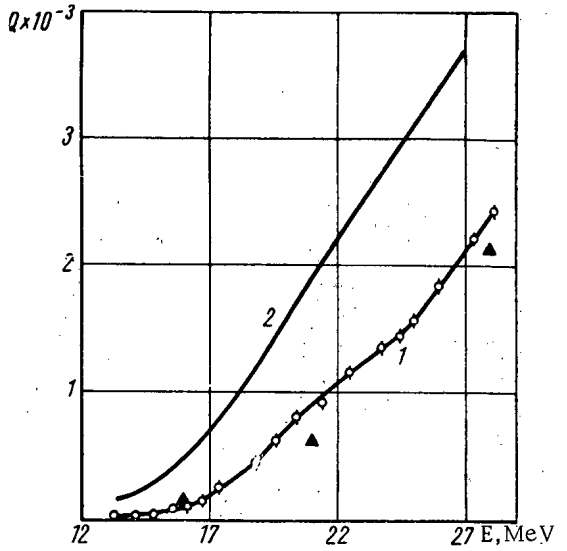

Fig. 6. Yield of photoneutron from Cu^{63}: 1) Experimental yields of the present study [▲) data of [17]]; 2) yield calculated from the cross section of the (γ, n) reaction for Cu^{63} [9] and the Belen'kii-Tamm equilibrium photon spectrum.

citation functions of photonuclear reactions by using the equilibrium spectrum of photons from the primary electrons, we obtain results lying (within the limits of dispersion) between the data obtained in the investigation of thin specimens with the Schiff spectrum and the photon-difference method. This dispersion is relatively small in the case of oxygen (see Fig. 4).

Copper (Cu^{63}). In this case the target for the measurement of the photoneutron yields was made of copper disks 120 mm in diameter and 2 mm, 5 mm, or 10 mm thick. The specimens for measurement, having the same diameter and 0.5 mm thick, were placed in the spaces between the disks. The total thickness of the target was 16 radiation lengths. The integral beta activity of the target was obtained by measuring the total activity of all the specimens by means of a special integrating instrument and an SI-2B end-window counter. The integrating instrument consisted of a rapidly rotating disk on which the specimens were placed. As the disk rotated, all the specimens passed under the counter, which measured their total beta activity. The rate of rotation of the disk was two revolutions per second. The efficiency of the end-window counter when used with a moving specimen was determined by using a beta-active $Sr^{90} + Y^{90}$ specimen. In determining the efficiency of the counter, we introduced corrections for the "dead time" of the counting instrument and for self-absorption and self-scattering in the specimens being measured. The method used to determine the correction for self-absorption and self-scattering in the measurement specimen was the displacement of an active layer along the thickness of the specimen. For this purpose, we used leaves of activated copper foil 30 mg/cm^2 thick and a set of copper foil leaves with a total thickness of 0.5 mm. The correction for self-scattering and self-absorption can be represented by the factor K = 1.13.

The measured yield of photoneutrons from Cu^{63} is shown in Fig. 6. The relative error of the measurement was 2.2%, and we estimated the absolute error at 7.5%.

Figure 6 also shows the photoneutron yield for Cu^{63} that was calculated by using the equilibrium photon spectrum and the cross section of the (γ, n) reaction in [9, 16]. It should be noted that the cross section obtained in [9] is the smallest among all those that have been published for Cu^{63} up to the present time.

In the 13-28 MeV electron energy range, the yields of photoneutrons from Cu^{63} were also measured by using a target as the collector of an electron beam, i.e., as a Faraday cylinder. By counting the activity of each individual specimen, we were able to plot the variation of the induced activity as a function of the target thickness (transmission curves). These curves are shown in Fig. 7. From the transmission curves we determined the total target dimensions required for complete absorption of the gamma quanta effective in the (γ, n) reaction, and we

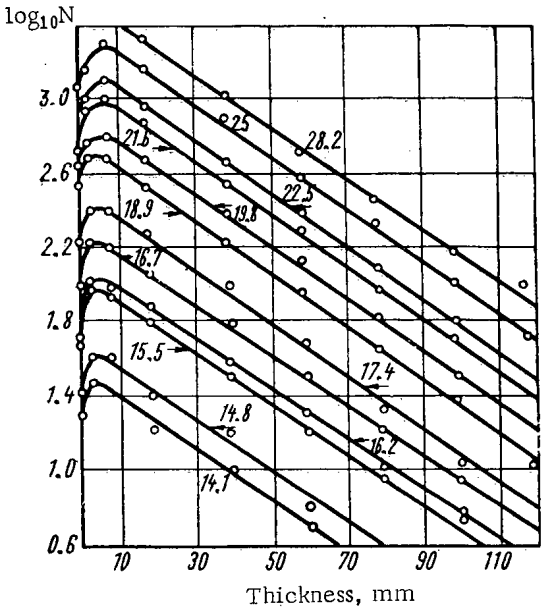

Fig. 7. Transmission curves for Cu^{63} (abscissa axis: thickness in mm; ordinate axis: logarithm of induced activity in relative units; the numbers next to the curves represent the electron energy in MeV).

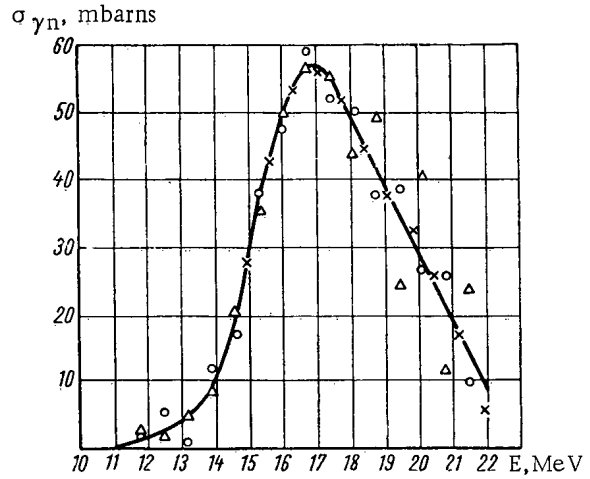

Fig. 8. Excitation function of the (γ, n) reaction in Cu^{63}, calculated by means of the Belen'kii-Tamm equilibrium photon spectrum and the experimental yields of the present study: ×) Method using first and second derivatives [1, 15]; ○) abbreviated photon difference method for thick specimens, proposed by D. I. Sikora; △) photon-difference method for thick specimens.

determined the total photoneutron yield from a target having a thickness of 12 avalanche units.

Figure 3 shows the excitation functions of the (γ, n) reaction in Cu^{63} in the energy range from the threshold to 45 MeV which were calculated by using the equilibrium photon spectrum in accordance with [1] and the experimental results of the present study (see Fig. 6); these functions were obtained by different computors within the dispersion limits of the data, i.e., by having each computor draw a curve of the yield within the limits of the experimental dispersion. Curve 5 in Fig. 3 was computed by M. P. Mazyukevich and I. L. Popshe using a photon-difference method extending over thick specimens; curves 6, 7, and 8 were calculated by means of photoneutron yields, in accordance with [1, 15], by D. I. Sikora, L. A. Shabalina, and Ya. E. Kost'y, respectively. A more complete understanding of the difference calculated excitation functions may be obtained from the data of Fig. 8 by using the first and second derivatives of the photoneutron yields with respect to energy in the first case and using the photon-difference method in the second case.

On the basis of the above data, we may draw the following conclusion. The excitation functions of the (γ, n) reactions in Cu^{63} which were obtained by different computors using different methods from the data on photoneutron yields obtained from thick specimens in the giant-resonance region are in reasonably good agreement with one another. When we compare the data so obtained with the excitation functions of (γ, n) reactions in Cu^{63} obtained by other authors (curves 1, 2, 3, and 4 of Fig. 3), we find that the cross section calculated for Cu^{63} by means of the Belen'kii-Tamm equilibrium photon spectrum and the data on photoneutron yields from specimens under conditions of practically complete absorption of the gamma radiation effective for the formation of neutrons is markedly lower even than the smallest cross section of the (γ, n) reaction for Cu^{63} obtained by using a thin specimen and the Schiff spectrum. At the maximum of the cross-section curve this difference can be represented by a factor of about 2.

In the giant-resonance energy region for checking purposes, the cross section of the (γ, n) reaction for Cu^{63} was found in the present study by using a thin target consisting of a first specimen 120 mm in diameter and 0.5 mm thick, by a beam of gamma quanta obtained from a thin radiator 0.1 mm thick. In this case the excitation-function calculations using the photon-difference method were carried out by D. I. Sikora; the data are reproduced in Fig. 3 (Curve 9), which indicates that they are in reasonably good agreement with the results obtained by other authors who also used the bremsstrahlung spectrum and thin specimens. The Wilson spectrum was used in the calculation. The (γ, n) reaction cross section shown in Fig. 3 was obtained by means of this spectrum.

The agreement between the results obtained by measurements made with thin specimens and the data of other authors indicates that the apparatus used for recording the electron beams and the induced activity had operated satisfactorily.

In conclusion, it should be noted that at the present time investigations are being carried on to explain the reasons for the large differences between the photoneutron yields determined experimentally and those calculated by means of the equilibrium photon spectrum from the primary electron when one uses the (γ, n) reaction excitation functions known today for heavy and intermediate elements.

The authors consider it their pleasant duty to thank all the staff members of the Physics and Technology Institute of the Academy of Sciences of the USSR and of the Department of Nuclear Physics of the Uzhgorod State University who took part in the preparation, setting up, and evaluation of the above-described experiments and in the calculation work; in particular, they wish to thank A. K. Walter, V. I. Gol'danskii, A. A. Krasnikov, V. V. Petrenko, G. L. Fursov, I. K. Nagy, L. A. Shabalina, Ya. E. Kost'yu, A. M. Pargal, M. P. Mazyukevich, M. P. Lorikyan, P. A. Medvedkov, and V. I. Startsev.

LITERATURE CITED

1. V. A. Shkoda-Ul'yanov, In the Collection: Some Problems of Modern Physics of the Nucleus and Elementary Particles [in Russian] (L'vov, L'vov State University Press, 1957), p. 89.
2. V. A. Shkoda-Ul'yanov, Ibid, p. 55.
3. Roberg, Nordheim, Phys. Rev., 75, 444 (1949).
4. Kantz, Hofstadter, Phys. Rev., 89, 607 (1953).
5. I. A. Grishaev, et al., Pribory i tekhnika éksperimenta, 6, 132 (1962).
6. Snowdon, Phys. Rev., 78, 299 (1950).
7. Carver, et al., Austral. J. Phys., 10, 312 (1957).
8. Ferguson, et al., Phys. Rev., 95, 77 (1954).
9. Berman, et al., Phys. Rev., 96, 83 (1954).
10. Katz, Canad. J. Phys., 29, 518 (1951).
11. Yohns, et al., Phys. Rev., 80, 1062 (1950).
12. Diven, et al., Phys. Rev., 80, 407 (1950).
13. Yohns, et al., Phys. Rev., 84, 856 (1951).
14. Montalbetti, et al., Phys. Rev., 91, 659 (1953).
15. V. A. Shkoda-Ul'yanov, In the Collection: Proceedings of the International Conference on Nuclear Reactions at Low and Intermediate Energies [in Russian] (Moscow, Izd-vo AN SSSR, 1958), p. 485.
16. Miller, Shuhl, and Tzara, Nucl. Phys., 32, 236 (1962).
17. Barber and George, Phys. Rev., 116, 1551 (1959).

TRANSIENT PROCESSES AND THE MEASUREMENT OF REACTIVITY OF A REACTOR CONTAINING BERYLLIUM

(UDC 621.039.51)

S. S. Lomakin and Yu. A. Nechaev

Translated from Atomnaya Énergiya, Vol. 18, No. 1,
pp. 33-40, January, 1965
Original article submitted January 24, 1964

The effect of the reactions $Be^9(n, 2n)Be^8$ and $Be^9(\gamma, n)Be^8$ on transient processes for a reactor containing beryllium nuclei is discussed. Calculations are presented and the deviation of the reactor period from asymptotic is measured; the efficiency of delayed neutrons and photoneutrons is determined experimentally. The reactor reactivity from photoneutrons is measured by an integral method.

It is well-known that the delayed fission neutrons determine the kinetics of a thermal reactor. At present there are completely reliable data concerning their yields and periods. The most complete data are given in [1-3], where the measured value of $\beta = 0.0064 \pm 0.0002$ is reported.

In reactions containing beryllium, photoneutrons are produced as a result of absorption of γ-radiation from long lived fission products and the reaction $Be^9(\gamma, n)Be^8$; these photoneutrons have a direct effect on the kinetics of such reactors by increasing the duration of transient processes. By the introduction of an insignificant contribution into the total neutron balance, the photoneutrons nevertheless exert a very considerable influence as a result of reactivity changes and if neglected they may lead to quite noticeable errors.

A number of authors [4-6] have determined experimentally the half lives and yields of beryllium photoneutrons on the basis of decay analysis of radioactive radiation in the reactor and directly in irradiated samples of uranium. An analysis is given in [3] of all the data, reduced to nine groups, with respect to the yields of photoneutrons and their periods. By taking into account these nine groups of photoneutrons together with the six groups of delayed neutrons, it was shown that a completely satisfactory description can be given of the existing experimental data concerning the measurement of the decay of neutron radiation in a reactor after shutdown.

By using these data (see Table 1), supplementary to calculations of the average energy of the delayed gamma rays and photoneutrons, the experimental results were processed of the measured reactivity, efficiency of delayed neutrons and photoneutrons and calculations are carried out of the errors in measuring the asymptotic period. In these measurements and calculations, the contribution by neutrons from the reaction $Be^9(n, 2n)Be^8$ and absorption of γ-rays by oxygen atoms in the case of beryllium oxide systems were taken into account.

Solution of the Kinetic Equations and Determination of the Error in Measuring the Asymptotic Period

The kinetic equations of a reactor in which delayed photoneutrons and prompt neutrons are formed from the reaction $Be^9(n, 2n)Be^8$ differ only insignificantly from the equations usually written for the reactor. However, the solutions may have considerable differences as a consequence of the conditions considered below.

For the systems being considered, the kinetic equations can be described in the form

$$\frac{dn}{dt} = \left(\frac{k_{\text{eff}} - 1}{l} - \frac{k\gamma\beta}{l}\right) n + \sum_i \gamma_i \lambda_i c_i, \qquad (1)$$

TABLE 1. Group Constants of Photoneutrons for Beryllium

Group number, i	γ-Emitter	Energy of γ-radiation, MeV	Lifetime	Decay constant, sec^{-1}	Yield β_i (10^{-5})
1	Kr^{90}, Se^{87}	1.78	0.51 min	$2.26 \cdot 10^{2}$	2.07
2	J^{136}, Br^{87}	2.49	1.3 min	$8.85 \cdot 10^{-3}$	3.66
3	Sb^{133}, Kr^{89}, Rb^{90}	2.66	3.2 min	$3.60 \cdot 10^{-3}$	1.85
4	Xe^{138}, Rb^{89}, Mo^{101}	2.5	15.5 min	$7.42 \cdot 10^{-4}$	3.68
5	Te^{134}, J^{134}, Br^{84}, Cs^{138}	2.42	43.2 min	$2.67 \cdot 10^{-4}$	0.36
6	J^{135}, La^{142}, Kr^{87}, Kr^{88}	2.15	3.11 h	$6.20 \cdot 10^{-5}$	3.20
7	Te^{131}	2.06	21.1 h	$1.59 \cdot 10^{-5}$	0.260
8	Te^{132}	2.02	77.7 h	$2.48 \cdot 10^{-6}$	0.038
9	La^{140}	2.51	12.8 days	$6.24 \cdot 10^{-7}$	0.057

$$\frac{dc_i}{dt} = \frac{k\beta_i}{l} n - \lambda_i c_i, \tag{2}$$

which are independent of the spatial coordinates and where k is the contribution to k_{eff} from fission and delayed neutrons, i.e., without neutrons from the reaction $Be^9(n, 2n)Be^8$; γ is the efficiency of the delayed neutrons; the remaining symbols are universal. By means of a Laplace transformation we obtain

$$pN - n_0 = \left(\frac{k_{eff} - 1}{l} - \frac{k\gamma\beta}{l}\right) N + \sum_i \gamma_i \lambda_i c_i, \tag{3}$$

$$pc_i - c_{i0} = -\lambda_i c_i + \frac{k\beta_i}{l} N, \tag{4}$$

where n_0 and c_{i0} are the value of n and c_i at the initial instant of time t_0, $N = \int_{t_0}^{\infty} e^{-p(t-t_0)} n(t)\, dt$. By solving Eqs. (3) and (4) relative to N we obtain

$$N = n_0 \frac{\frac{l}{k_{eff}} + \sum_i \frac{l\lambda_i c_{i0}}{k_{eff}\, \beta_i n_0} \cdot \frac{\gamma_i \beta_i}{p + \lambda_i}}{\frac{lp}{k_{eff}} - \frac{k_{eff} - 1}{k_{eff}} + \frac{k}{k_{eff}} \gamma\beta - \frac{k}{k_{eff}} \sum_i \frac{\gamma_i \lambda_i \beta}{p + \lambda_i}} \tag{5}$$

Inverse transformation gives

$$n(t) = n_0 \sum_i A j e^{p_j (t - t_0)}, \tag{6}$$

where

$$Aj = (1 - \varrho) \frac{\frac{l}{k_{eff}} + \sum_i \frac{l\lambda_i c_{i0}}{k_{eff}\, \beta_i n_0} \cdot \frac{\gamma_i \beta_i}{p_j + \lambda_i}}{(1 - \varrho)\frac{l}{k_{eff}} + \frac{k}{k_{eff}} \sum_i \frac{\gamma_i \beta_i \lambda_i}{(p_j + \lambda_i)^2}}, \tag{7}$$

and the values of p_j are the roots of the equation

$$\frac{lp_j}{k_{eff}} - \frac{k_{eff} - 1}{k_{eff}} + \gamma\beta \frac{k}{k_{eff}} - \frac{k}{k_{eff}} \sum_i \frac{\gamma_i \beta_i \lambda_i}{p_j + \lambda_i} = 0. \tag{8}$$

Equation (8) can be written in the form

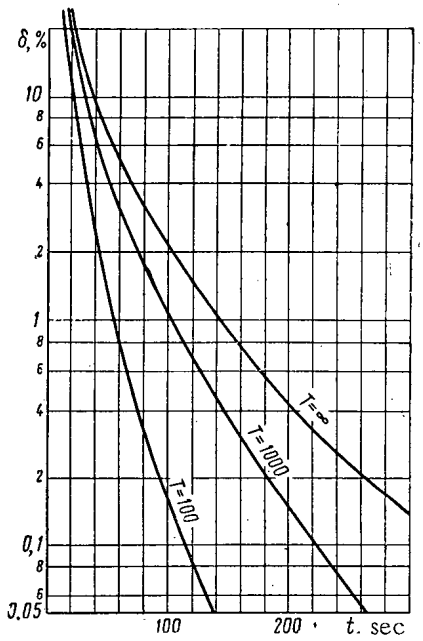

Fig. 1. Deviation of the measured period from asymptotic as a function of time after reactivity surge (reactivity $0.1 \cdot 10^{-2}$; T is the holding time at constant power level, sec; $l = 10^{-4}$ sec; beryllium moderator).

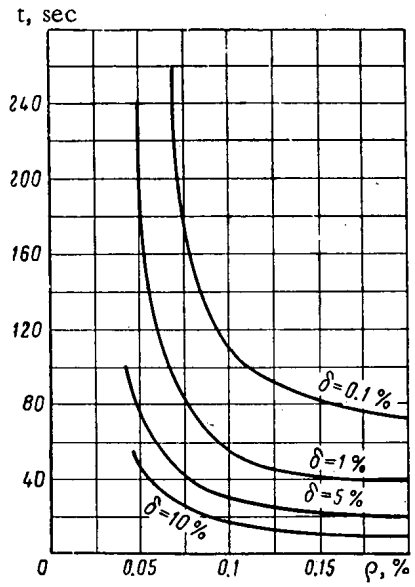

Fig. 2. Relationship between expected time after reactivity surge before measurement of the period and the magnitude of the reactivity for various values of δ (T = 1000 sec; $l = 10^{-4}$ sec; beryllium moderator).

$$\varrho = \frac{lp_0}{k_{\text{eff}}} + \frac{k}{k_{\text{eff}}} \sum_i \frac{\gamma_i \beta_i p_0}{p_0 + \lambda_i}, \tag{9}$$

where p_0 is the reciprocal of the asymptotic reactor period and ρ is the reactivity to be measured.

In order to calculate the value of A_j, and consequently also the value of n(t) for any instant of time, it is necessary to establish the relationship between n_0 and c_{i0} for the instant of time t_0. The connection between c_{i0} and n_0 is defined by the solution of equation (2), which, for constant values of n_0 and k and for c(0) = 0, has the form

$$c_i(T_{\text{hold}}) = \frac{n_0 \beta_i k}{l\lambda_i}(1 - e^{-\lambda_i T_{\text{hold}}}), \tag{10}$$

where $T_{\text{hold}} = t_0$ is the holding time of the reactor at constant power.

Thus, the function

$$n(t) = \sum_i A_j e^{p_j (t - t_0)},$$

which describes the transient process after a sudden surge of reactivity, depends on the A_j coefficients as determined from the expression

$$A_j = (1 - \varrho) \frac{\frac{l}{k_{\text{eff}}} + \frac{k}{k_{\text{eff}}} \sum_i \frac{\gamma_i \beta_i (1 - e^{-\lambda_i T_{\text{hold}}})}{p_j + \lambda_i}}{\frac{l(1-\varrho)}{k_{\text{eff}}} + \frac{k}{k_{\text{eff}}} \sum_i \frac{\gamma_i \beta_i \lambda_i}{(p_j + \lambda_i)^2}}. \tag{11}$$

The solution obtained for Eq. (1) and (2), taking into account photoneutrons, permits an analysis to be carried out of the transient processes in the case of change of magnitude of the reactor reactivity.

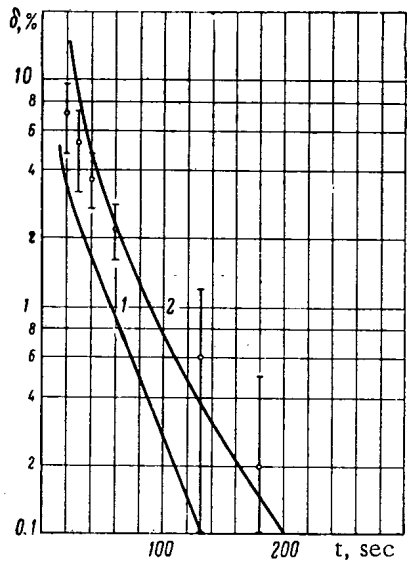

Fig. 3. Deviation of measured period from asymptotic for the assembly of beryllium oxide being investigated, as a function of time after reactivity surge for a holding time of 1000 sec at constant power (reactivity $0.1 \cdot 10^{-2}$, $l = 10^{-4}$ sec). ○) Experimental points; 1) calculated, without taking account of photoneutrons (six groups [3]); 2) calculated, taking into account photoneutrons (six and nine groups [3]).

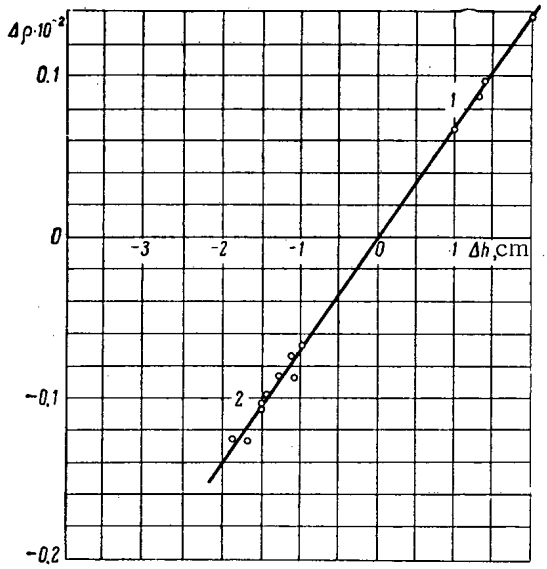

Fig. 4. Relationship between the system reactivity measured by two methods and the change of position of the control rods. 1) Method of positive period measurement (1 cm of rod equal to $0.0681 \cdot 10^{-2}$); 2) integral method (1 cm of rod equal to $0.0705 \cdot 10^{-2}$).

The presence of long lived photoneutron precursors, saturation of which takes place over an extremely long time, in measurements of reactivity leads to the fact that deviation from the asymptotic period of the reactivity being measured is found to be considerably greater than in the case when there are no photoneutrons. The magnitude of the deviation δ of the asymptotic period $1/p_0$ from the observed value $n(t)/\dot{n}(t)$

$$\delta = \frac{1/p_0 - n(t)/\dot{n}(t)}{1/p_0} \tag{12}$$

can be determined for different reactor holding times at constant power. Substituting the solution of equation (1) in expression (12), we obtain

$$\delta = \frac{(A_1/A_0)(p_1-p_0)e^{(p_1-p_0)t} + \ldots + (A_j/A_0)(p_j-p_0)e^{(p_j-p_0)t}}{p_0 + (A_1/A_0)p_1 e^{(p_1-p_0)t} + \ldots + (A_j/A_0)p_j e^{(p_j-p_0)t}}. \tag{13}$$

In order to select the cycle for the reactivity measurement with respect to the positive period, calculations were carried out of values of δ for various reactivities and holding times of the system at a constant power level. The results of the calculations are given in Figs. 1 and 2. The deviation of the measured period from asymptotic was determined experimentally for a reactivity of 0.1% in the critical beryllium oxide assembly being investigated. As the asymptotic period in these measurements, the steady state period was used as measured over 200 sec after a positive reactivity surge (for the stated time the value of δ, as shown by the calculations, does not exceed 0.1%). The results of the experiment and of the calculation are compared in Fig. 3.

Measurement of Reactivity

The calculated and experimental data obtained concerning the magnitude of the deviation of the measured period from asymptotic permits selection of the reactivity measurement cycle to be made.

In the experiments on the critical assembly, the results of which are given in the present paper, the holding time at constant power was taken equal to 1000 sec. A shorter holding time, although advantageous from the point of view of reducing δ, is inadvisable since prior to measurement of the positive period it is necessary to determine the critical state of the assembly.

The positive period was measured over 100-200 sec after the reactivity range. The measurement results were analyzed by the "inhour" equation. The cycle taken for the measurement of the period and the equipment used permitted the reactivity to be measured to an error not exceeding ± 1.5%. A section of the control rods was calibrated by the method mentioned. The data obtained are shown in Fig. 4.

In addition to the positive reactivities, the negative reactivities were measured by an integral method [7].

It has been shown that after a Laplace transform of Eq. (1) and (2) expression (5) is obtained which, for $l/k_{eff} \ll \sum_i l\lambda_i c_{i0}/k_{eff}\beta_i n_0$ and for p = 0 is transformed to the form

$$N(0) = \frac{n_0}{-\varrho} \sum_i \frac{l\lambda_i c_{i0}\gamma_i\beta_i}{k_{eff}\,\beta_i n_0 \lambda_i},$$

where

$$N(0) = \int_{t_0}^{\infty} n(t)\,dt,$$

whence

$$-\varrho = \frac{n_0}{N(0)} \sum_i \frac{l\lambda_i c_{i0}}{k_{eff}\,\beta_i n_0} \cdot \frac{\gamma_i\beta_i}{\lambda_i}. \tag{14}$$

If the reactor has previously operated for sufficiently long at stationary power, so that the condition $c_{i0}\lambda_i l/k\beta_i n_0 = 1$ is fulfilled for all the delayed neutron groups, then $-\rho$ is determined from the expression

$$-\varrho = \frac{n_0 k}{N(0)\,k_{eff}} \sum_i \frac{\gamma_i\beta_i}{\lambda_i}. \tag{14'}$$

In contrast from the "inhour" equation, Eq. (14) depends to a great extent on the quantity λ_i. The presence of photoneutrons in the system increases the significance of this fact. However, the difficulties can be overcome, to a considerable extent, if the photoneutron precursors do not reach saturation and if the quantity c_{i0} be determined, i.e., c_i at the instant of time t_0, when the source is eliminated from the solution of the equation

$$\frac{dc_i(t)}{dt} = \frac{k\beta_i}{l} n(t) - \lambda_i c_i(t). \tag{15}$$

For the case of constant value of k, the solution has the form

$$c_{i0}(t) = (k\beta_i/l)\, e^{-\lambda t_0} \int_0^{t_0} n(t)\, e^{\lambda t}\, dt. \tag{16}$$

After substituting Eq. (16) in Eq. (14), the equation for the reactivity being measured assumes the form

$$-\varrho = \frac{\frac{k}{k_{eff}} \sum_i \gamma_i\beta_i \int_0^{t_0} n(t)\, e^{-\lambda_i (t-t_0)}\, dt}{\int_{t_0}^{\infty} n(t)\, dt}. \tag{17}$$

The effect of long lived groups of photoneutrons on the magnitude of the reactivity can almost be eliminated by change of t_0, and the time of the experiment can be shortened significantly.

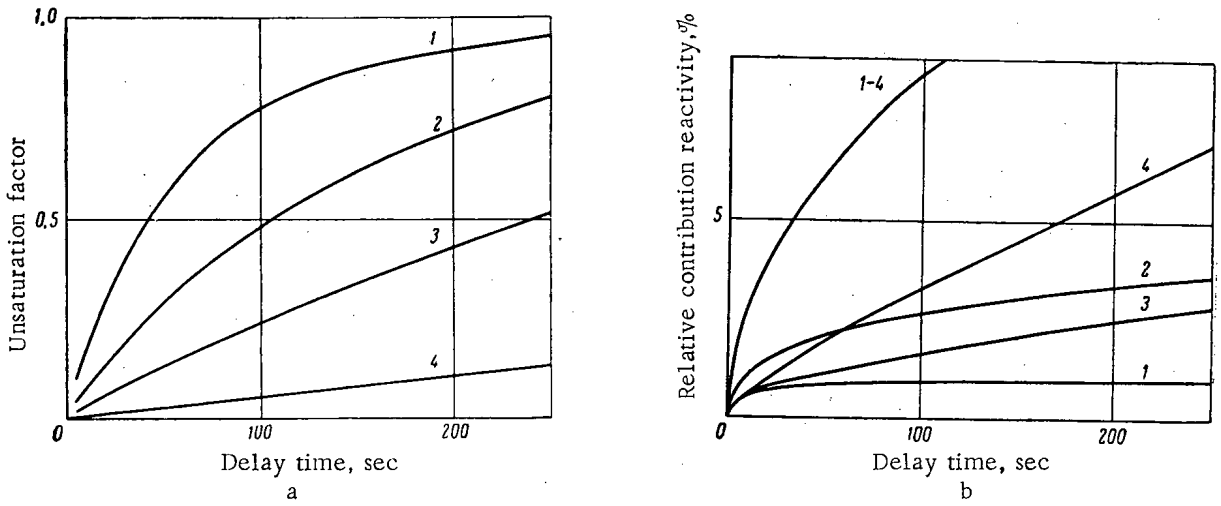

Fig. 5. Undersaturation factor of delayed photoneutron groups (a) and relative contribution to reactivity injected by the photoneutron groups (b) as a function of holding time of the neutron source in a subcritical assembly for $\rho = -1 \cdot 10^{-3}$ (figures near the curves are the number of groups).

Preliminary results of the use of the integral method in the absence of saturation of photoneutron precursors were obtained on an analog computer, by which the behavior of the reactor was reproduced with six delayed neutron groups and four photoneutron groups. By choice of scale factors it was presumed that as a result of saturation of the precursors $U_n = U_{c_n}$ and then

$$-\rho = \frac{n_0 k/k_{\text{eff}} \sum_i (\gamma_i \beta_i/\lambda_i)(U_{c_{i0}}/U_{n_0})}{\int_{t_0}^{\infty} n(t)\,dt}. \qquad (17')$$

The complex $\gamma_i \beta_i / \lambda_i$ of each group of delayed neutrons enters into this formula with its undersaturation factor $\Phi = U_{c_{i0}}/U_{n_0}$, depending on the holding time of the source in the recator.

The data obtained (Fig. 5a and 5b) permit conclusions to be drawn concerning the magnitudes of the undersaturation factor and the relative contribution to the reactivity of each photoneutron group as a function of the holding time of the source in the reactor, and to distinguish two possibilities for measuring the reactivity by the integral method: by using the undersaturation factor [Eq. (17)] or by choosing an operating cycle which will permit the photoneutron groups to be neglected, within the limits of the stated accuracy. We have used the first possibility.

A section of the control rod was calibrated by the integral method discussed in the critical assembly being investigated. The data obtained are given in Fig. 4, where both methods of reactivity measurement are compared.

Determination of the Efficiency of the Delayed Neutrons and Photoneutrons

In describing transient processes or in measuring reactivity, it is necessary to know the value of γ or $\beta_{\text{eff}} = \gamma\beta$, the effective fraction of delayed neutrons and photoneutrons.

For the critical assembly being investigated the quantity γ was measured by the method of substitution of fuel by absorber and by determining the change of reactivity originated by this substitution.

It follows from perturbation theory [8, 9] that the change of reactivity of the system as a result of changing the quantity of fuel and absorber is expressed as

$$\frac{\Delta k_{\text{eff}}}{k_{\text{eff}}} = \frac{1}{\int_V dv \left(\int_u \nu F^* F \Sigma_f \, du + \Sigma_{fT} \nu_T F_T F_T^* \right)} \int_V dv \left\{ \left[\int_u \nu F^* \delta\Sigma_f F \, du + \delta\Sigma_f F_T^* F_T \right] - \int_u \delta\Sigma_c F^* F \, du - \delta\Sigma_{cT} F_T F_T^* \right\}, \qquad (18)$$

where F is the neutron flux; F^* is an adjoint function; the suffix T denotes a thermal group.

If the absorption in the absorber inserted is equal to the absorption in the spent fuel at the site of location of the absorber, then $\delta\Sigma_c = 0$ and there will be no terms in expression (18) which will take absorption into account. If the system is divided into N parts and this substitution of fuel by absorber is performed in each part, then we can write

$$\sum_{l=1}^{N}\left(\frac{\Delta k_{\text{eff}}}{k_{\text{eff}}}\right)_l = \frac{\int_{V_1}\int_u \nu F^*\delta\Sigma_f F\,du\,dv + \ldots + \int_{v_N}\int_u \nu F^*\delta\Sigma_f F\,du\,dv}{\int_V\int_u \nu F^*\Sigma_f F\,du\,dv} = 1 \tag{19}$$

(for brevity of writing, the thermal group is included here under the integral sign).

The value of $\Delta k_{\text{eff}}/k_{\text{eff}} = k\gamma/k_{\text{eff}}\sum_i \beta_i p_0/(p_0 + \lambda_i)$ is determined in the experiments to measure the reactivity, if γ is assumed constant for all groups of delayed neutrons and photoneutrons. Then,

$$\gamma = \frac{1}{\sum_{l=1}^{N}\left(\frac{k}{k_{\text{eff}}}\sum_i \frac{\beta_i p_0}{p_0+\lambda_i}\right)_l}. \tag{20}$$

If the absorption cross section in the absorber inserted, Σ_c^a, does not match the absorption cross section of the fueld, Σ_c^f, than we obtain from Eq. (18)

$$\sum_{l=1}^{N}\left(\frac{\Delta k_{\text{eff}}}{k_{\text{eff}}}\right)_l = 1 + \frac{\int_v\int_u \left(\sum_c^f - \sum_c^a\right) F^*F\,du\,dv}{\int_v\int_u \nu F^*F\Sigma_f\,du\,dv} \tag{21}$$

and the correction to unity should be obtained by a numerical method. Expression (21) was used to determine the experimental error associated with the inaccuracy in Σ_c^f and Σ_c^a, since

$$\Delta\gamma = \frac{1}{\sum_{l=1}^{N}\frac{k}{k_{\text{eff}}}\sum_i \frac{\beta_i p_0}{p_0+\lambda_i}}\left[\frac{\int_v\int_u \left(\Delta\sum_c^f + \Delta\sum_c^a\right) F^*F\,du\,dv}{\int_v\int_u \nu F^*F\Sigma_f\,du\,dv}\right]. \tag{22}$$

Experiments to determine γ were carried out on a critical beryllium oxide assembly with fuel elements on a Teflon-4 base [10]. Specially prepared plates of Teflon-4 with a boron filler were used as the absorbing elements. The experiment consisted in the substitution of the fuel elements by absorbers and in measuring the change of reactivity caused by this substitution. Usually, one or two fuel elements were substituted during a single procedure. As a result of this, in order to reduce the number of substitution and measurements the symmetry used for the assembly was represented by a rectangular prism with square cross section. In order to ascertain the inaccuracy in the quantity γ, the same experiments were carried out for two cases when the absorption in the absorbing element was not equal to the absorption in the fuel element. It was found for the assembly being studied that $\gamma = 1.15$; the experimental error was 4%.

For comparison with the experiment, calculations were undertaken of the quantity γ. The difference between the prompt and delayed neutrons, as is well known, is due to their different initial energy. The energy of the delayed neutrons from U^{235} fission products was used in accordance with [2, 11, 12]. The energy of the photoneutrons was determined from consideration of the $Be^9(\gamma, n)Be^8$ reaction and from analysis of the γ-radiation which forms the photoneutrons (see table). In the formation of a Be^8, nucleus in the ground state as a result of the reaction $Be^9(\gamma, n)Be^8$, the energy of the photoneutron of the i-th group was determined from the expression

$$E_{n_i} = \bar{E}_{\gamma_i} - 1.67 \text{ MeV},$$

where E_{γ_i} is the average energy of the gamma radiation for the i-th photoneutron group; 1.67 MeV is the $Be^9(\gamma,n)Be^8$ reaction threshold. The average energy with which photoneutrons are formed was found to be 670 keV.

Since in the experiment carried out the value of γ obtained was relative to all groups of delayed neutrons and photoneutrons, the calculated value of γ was determined in accordance with [13] from the expression

$$\gamma = e^{x^2 \Delta \tau},$$

where $\Delta\tau$ is the difference between the increase of fission neutrons and delayed neutrons, and photoneutrons, whose spectrum was obtained. For the assembly investigated $x^2\Delta\tau = 0.13$ and $\gamma = 1.14$.

Thus, consideration of the effect of the $Be^9(\gamma, n)Be^8$ and $Be^9(n, 2n)Be^8$ reactions on the kinetics of systems containing beryllium has shown the necessity for taking these reactions into account for reactivity measurements and in choosing the measurement cycle. Analysis of the data obtained shows that by choosing the holding time of the reactor at a constant power level to be about 1000 sec, by measuring the period over 200 sec after the reactivity surge, the deviation from asymptotic of the period to be measured does not exceed 0.1% for periods within the interval 10-100 sec.

In measuring negative reactivities the taking into account, as suggested, of changing the amount of photoneutron precursors by the undersaturation factor makes it possible to use the integral method, which gives – as comparison with positive period measurements show – a satisfactory result.

Determination of the efficiency of the delayed neutrons and photoneutrons by the method of substituting fuel by absorber and comparison of the experimental and calculated data showed the good applicability of the numerical formula for the case with photoneutrons.

The special significance of the experiment in substituting fuel by absorber consists in the fact that it makes possible the determination of the constant in front of the summation in the expression $\gamma k / k_{eff} \sum_i \beta_i p_0 / (p_0 + \lambda_i)$ in the "inhour" formula, by eliminating the effect of existing inaccuracies in the delayed neutrons, photoneutron and neutron parameters of the $Be^9(n, 2n)Be^8$ on the result of the reactivity measurement. It is desirable always to carry out a normalized experiment of this nature prior to the precision experiments associated with reactivity measurements.

In conclusion, the authors tender sincere thanks to N. N. Ponomarev-Stepnoi for valuable advice and interest in the work, and to Ya. V. Shevlov for discussion of the results.

LITERATURE CITED

1. G. Keepin, et al., Phys. Rev., 101, 1044 (1957).
2. G. Keepin, et al., J. Nucl. Energy, 6, No. 1/2 (1957).
3. G. Keepin, Nucleonics, 2, 151 (1962).
4. A. K. Krasin, et al., In the Book: Proceedings of the Second International Conference on the Peaceful Uses of Atomic Energy, Geneva, 1958 [in Russian] (Moscow, Atomizdat, 1959), Vol. 2, p. 39.
5. P. Benoist, et al., Proceeding of the 2nd Intern. Conf, United Nations, Geneva (1958), Vol. 12, p. 89.
6. S. Bernstein, et al., J. Appl. Phys., 27, 18 (1956).
7. U. Hojgn, Nucl. Sci. and Engng., 8, 518 (1960).
8. L. N. Usachev, Reactor Construction and the Theory of Reactors. Report of the Soviet Delegation at the International Conference on the Peaceful Uses of Atomic Energy [in Russian] (Moscow, Izd-vo AN SSSR, 1955), p. 251.
9. G. I. Marchuk, Numerical Methods of Assessing Nuclear Reactors [in Russian] (Moscow, Atomizdat, 1958), p. 205.
10. N. N. Ponomarev-Stepnoi, S. S. Lomakin, and Yu. G. Degal'tsev, Atomnaya énergiya, 15, 259 (1963).
11. R. Batchelor and H. McHuder, J. Nucl. Energy, 3, 7 (1956).
12. D. Hughes, et al., Phys. Rev., 73, 111 (1948).
13. E. Cross and J. Marable, Nucl. Sci. and Engng., 7, 281 (1960).

THE CRYSTAL HYDRATE $UF_4 \cdot {}^4/_3\, H_2O$

(UDC 546.791.4)

Yu. V. Gagarinskii, E. I. Khanaev, N. P. Galkin,
L. A. Anan'eva, and S. P. Gabuda

Translated from Atomnaya Énergiya, Vol. 18, No. 1,
pp. 40-45, January, 1965
Original article submitted July 24, 1964

X-ray diffraction, refractometry, infrared spectroscopy, nuclear magnetic resonance and thermography are used to study a new hydrated form of uranium tetrafluoride, $UF_4 \cdot {}^4/_3 H_2O$, and its dehydration products. This is a hitherto unknown monoclinic crystal hydrate of UF_4. Its water of crystallization is attached by a hydrogen bond to the fluorine. The water molecules can be divided into three groups of different bond strength, corresponding to three peaks in the absorption bands of the valence and deformation vibrations of the O—H bonds. The substance dehydrates in two stages. Its crystalline class is retained down to the composition $UF_4 \cdot H_2O$. On further dehydration down to $0.5\, H_2O$ it undergoes a phase transformation accompanied by change of structure. The crystalline lattice thus formed is very close to that of the cubic hydrate.

[1] and [2] describe two crystal hydrates of uranium tetrafluoride: $UF_4 \cdot 2.5\, H_2O$, which is orthorhombic, and $UF_4 \cdot nH_2O$ $(0.5 < n < 2)$, which is cubic. We have found another, previously unknown, hydrate, whose properties are described below. It is a bright grass-green, contrasting with the deep green cubic and pale green orthorhombic hydrates. Its water content, after washing with alcohol and ether and drying in air, corresponds approximately to the composition $UF_4 \cdot 1.4H_2O$. By the calorimetric method [3] it was established that the formula is $UF_4 \cdot {}^4/_3 H_2O$.

We investigated this hydrate by x-ray diffraction, optical methods (refractometry and infrared spectroscopy), thermography and nuclear magnetic resonance (NMR). Under the microscope it appears as long thin greenish crystals with spherical concretions. It is homogeneous: the crystals are optically anisotropic and have normal and oblique extinctions, showing that they belong to the monoclinic system. Table 1 gives the refractive indices n of a specimen of composition $UF_4 \cdot 1.4H_2O$ (measured by immersion, error of order ± 0.005), and the density (determined by pycnometry in toluene with error ± 0.01 g/cm^3). For comparison, the same data, taken from [4], are given for the cubic and orthorhombic hydrates and the monoclinic anhydrous form of UF_4.

Table 1 shows that the new crystal hydrate differs markedly in crystallographic properties from the cubic and orthorhombic hydrates. The refractive indices are close to those of anhydrous UF_4 (only n_{min} differs appreciably). These optical data show clearly that this actually is a new crystal hydrate of uranium tetrafluoride.

X-ray diffraction photographs of the substance were taken with a URS-50I apparatus in filtered Cu radiation. For comparison, photographs were also taken for the stable monoclinic form of anhydrous UF_4, the higher, orthorhombic, crystal hydrate $UF_4 \cdot 2.5\, H_2O$ and the lower, cubic, hydrate $UF_4 \cdot 1.5\, H_2O$. They show that the substance under investigation does not resemble any of the previously known forms of UF_4 and is not a mixture of them. This confirms the conclusion, drawn from the optical data, that it is a new substance. The x-ray diffraction spectra are shown in Fig. 1a.

To determine the nature of the water bonds in the new hydrate, we investigated its infrared absorption spectra and nuclear proton magnetic resonance spectra. The method of measuring the former spectrum is given in [4], that for the latter in [5]. The infrared absorption spectrum of monoclinic $UF_4 \cdot 1.4H_2O$ is given in Fig. 2 (curve 1), the positions of the absorption maxima in Table 2. The absorption band corresponding to valence vibration of the O—H bond has three maxima at 2950, 3365 and 3480 cm^{-1}, that corresponding to deformation vibration of the O—H bond has less clearly visible maxima at 1565, 1625, and 1645 cm^{-1}. The presence of absorption in this region shows that the compound is of the crystal hydrate type, the water being present as molecules. The absorption band corre-

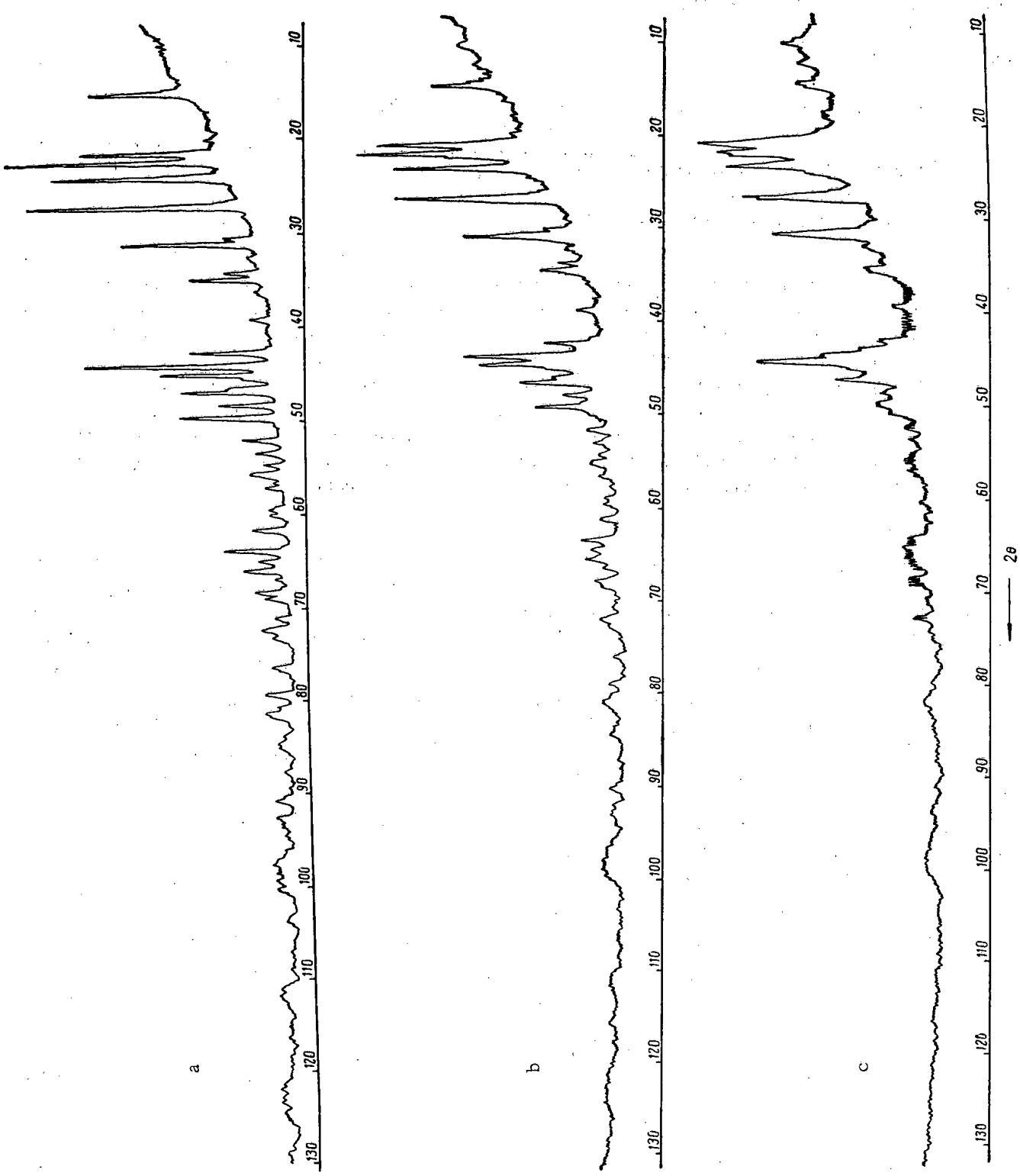

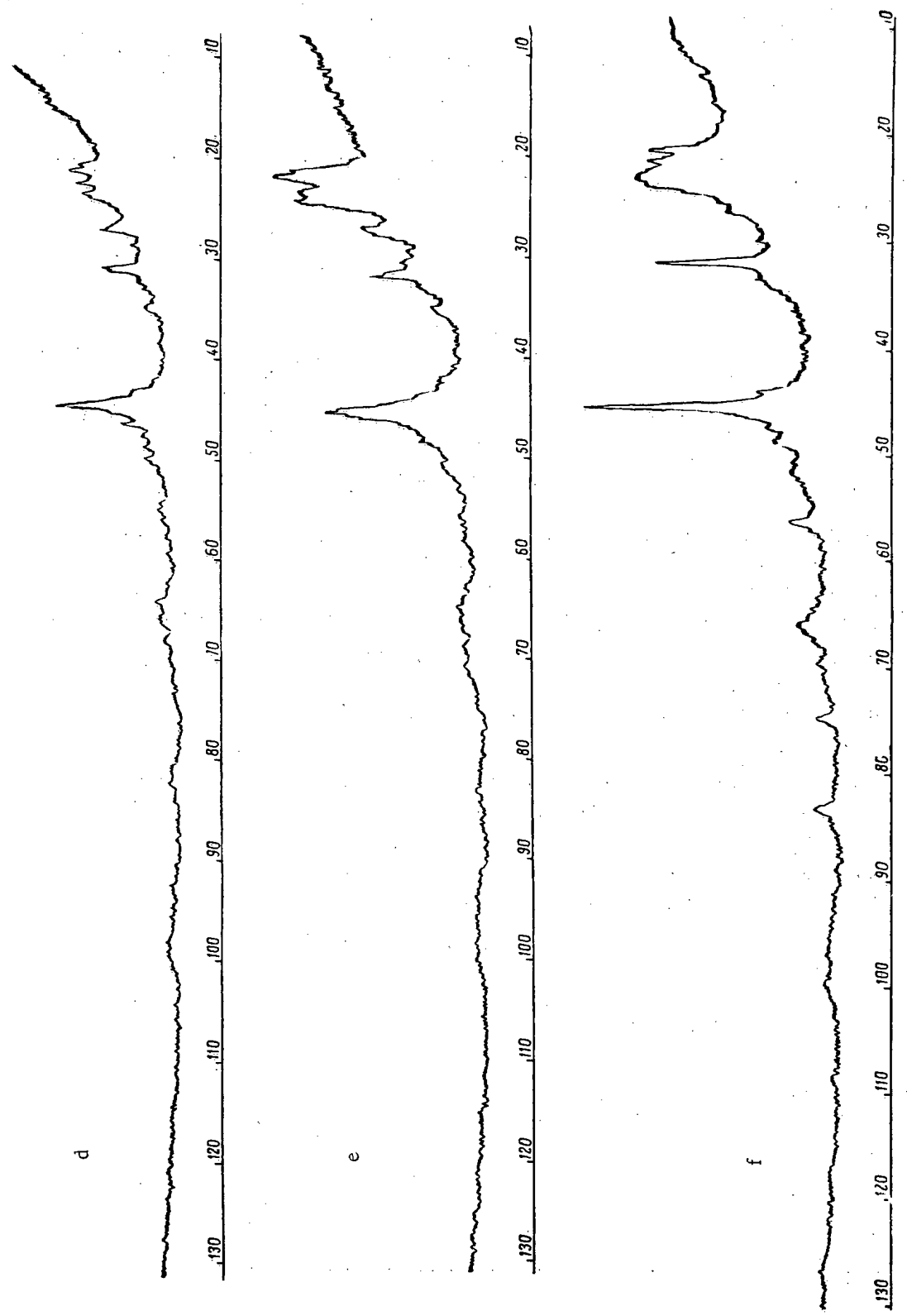

Fig. 1. X-ray diffraction spectra of $UF_4 \cdot {}^4/_3H_2O$, and the products of its dehydration and subsequent rehydration. a) Original crystal hydrate; b) $UF_4 \cdot H_2O$; c) $UF_4 \cdot 0.70H_2O$; d) $UF_4 \cdot 0.45H_2O$; e) $UF_4 \cdot 0.20\,H_2O$; f) $UF_4 \cdot 1.40H_2O$, obtained by hydrating specimen of composition $UF_4 \cdot 0.20H_2O$.

TABLE 1. Refraction Constants of the Various Forms of Uranium Tetrafluoride

Composition	Crystal class	n_{max}	n_{med}	n_{min}	$\bar{n}$	d_4^{25}, g/cm^3	Ω_D, cm^3
$UF_4 \cdot 1.4H_2O$	Monoclinic	1.596	1.586	1.567	1.582	5.79	19.77
$UF_4 \cdot 1.5H_2O$	Cubic	—	1.523	—	1.523	5.08	20.51
$UF_4 \cdot 2.5H_2O$	Orthorhombic. . .	1.545	1.537	1.529	1.537	4.70	23.86
UF_4	Monoclinic	1.594	1.584	1.549	1.576	6.68	15.58

TABLE 2. Maxima of Absorption Bands (in cm^{-1}) in Infrared Spectra of Specimens Obtained by Dehydrating Crystal Hydrates of Monoclinic Uranium Tetrafluoride

Curve No. in Fig. 2	Composition	Dehydration temperature, °K	Deformation vibrations of O—H bond, cm^{-1}	Valence vibrations of O—H bond, cm^{-1}
1	$UF_4 \cdot 1.40H_2O$		1565; 1625; 1645	2950; 3365; 3480
2	$UF_4 \cdot 1.00H_2O$	150	1590; 1645; 1675	2935; 3365; 3480
3	$UF_4 \cdot 0.30H_2O$	200	1615; 1640; 1675	3465
4	$UF_4 \cdot 0.10H_2O$	250	1650	3470
5	$UF_4 \cdot 1.40H_2O$	Obtained by hydrating $UF_4 \cdot 0.10H_2O$	1680	3400

sponding to valence vibration of the water molecule is markedly broadened and displaced towards longer wavelengths. It follows that in the new hydrate the water is also attached by a hydrogen bond. The presence of three maxima in the absorption bands corresponding to valence and deformation vibration of the O—H bond leads to the supposition that in $UF_4 \cdot 1.4H_2O$ the water molecules can be subdivided into three groups according to bond strength.

Figure 3 shows the NMR spectrum of the crystal hydrate, taken at 290°K, and the derivative spectra at 90 and 290°K. The second moment of the NMR lines is 27.5 ± 0.3 Oe^2 at 90°K and 23.6 ± 0.9 Oe^2 at 290°K. At 290° the relative intensity of the central peak, which determines the fraction of mobile water molecules, is about 5%.

The shape at 90° of the new hydrate's NMR spectrum can be explained by the presence of a hydrogen bond between the water molecules and a fluorine atom, OH—F. In this case we should have a three-spin system whose spectrum should be a triplet (or unresolved triplet degenerating into a singlet).

At 90°K the second moment of the NMR spectrum is less for the monoclinic hydrate than for the other hydrates [6]. This means that, provided the distance between the protons in the water molecules remains constant, the mean H—F distance in this hydrate is relatively greater than in the other hydrates of UF_4.

Figure 4 shows the thermogram for dehydration of the new hydrate in a vacuum, recorded by means of an PFK-59 Kurnakov pyrometer. The graph shows that the dehydration takes place in two stages. As in the cases of the other two hydrates, an unstable form of anhydrous UF_4 is produced and on further heating this undergoes an irreversible transformation to the stable form. This process is accompanied by heat evolution, as shown by the exothermic peak at 330°K.

X-ray and optical investigations were made of the products formed by dehydrating $UF_4 \cdot 1.4H_2O$ in a vacuum at various temperatures. The results are given in Tables 2 and 3. As seen from Table 3, during vacuum dehydration the crystal class of the original substance remains unchanged at least until the composition $UF_4 \cdot H_2O$ is reached; only its refractive index changes slightly. The x-ray diffraction spectra show that the structure remains unchanged. On reaching the composition $UF_4 \cdot 0.45H_2O$ and after further dehydration, the optical properties and x-ray diffraction patterns change appreciably. If a specimen of composition $UF_4 \cdot 0.20H_2O$ is washed with alcohol and ether, dried in air for 24 h and then rehydrated, the resulting substance has a very slight anisotropy; all the strong and medium lines in its x-ray diffraction spectrum correspond to those for the cubic hydrate. Additional, very weak lines betray the presence of a small quantity of another phase (which apparently causes the slight anisotropy).

Figure 2 gives the infrared absorption spectra of similar specimens obtained by dehydrating the monoclinic hydrate in various degrees. The positions of the absorption maxima are given in Table 2. This table shows that,

TABLE 3. Optical Properties of Substances Obtained by Dehyrating Monoclinic Crystal Hydrate of UF_4

Composition	Dehydration temperature, °K	N	Remarks
$UF_4 \cdot 1.40H_2O$		1.582	Anisotropic spherulites
$UF_4 \cdot 1.00H_2O$	150	1.570±0.008	The same
$UF_4 \cdot 0.45H_2O$	175	1.52±0.01	Almost isotropic
$UF_4 \cdot 0.20H_2O$	250	1.504±0.006	Weakly anisotropic
$UF_4 \cdot 1.10H_2O$	Obtained by hydrating $UF_4 \cdot 0.20H_2O$	1.545±0.003	Weakly anisotropic

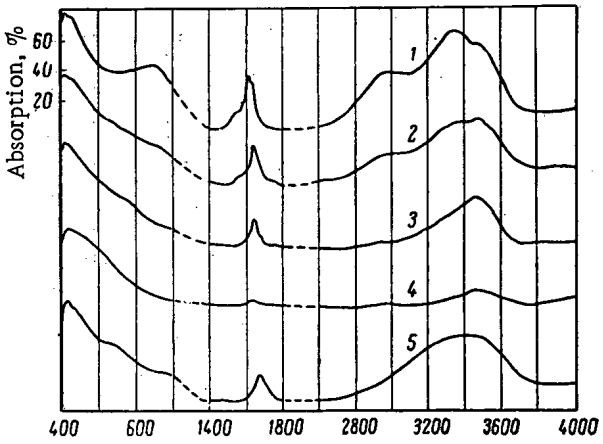

Fig. 2. Infrared spectra of monoclinic lower crystal hydrate of uranium tetrafluoride and of specimens obtained by dehydrating it. 1-5) Specimen numbers in Table 2.

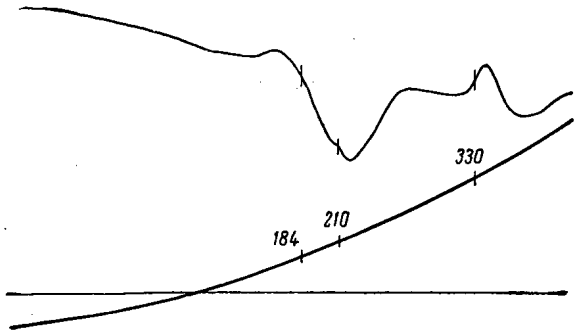

Fig. 4. Thermogram for dehydration of monoclinic lower hydrate $UF_4 \cdot 1.40H_2O$. Heating rate 4 deg/min.

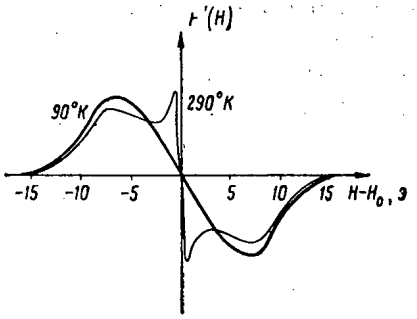

a

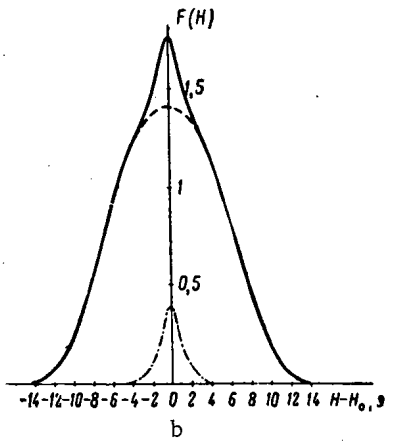

b

Fig. 3. a) Derivative NMR spectra of monoclinic crystal hydrate of uranium tetrafluoride of composition $UF_4 \cdot 1.40H_2O$ at 90 and 290°K; b) [integrated] spectrum at 290°K. ——) spectrum at 290°K; – – – –) broad component; - . - . - . -.) narrow component corresponding to highly mobile water. Vertical scale chosen so that total area is equal to unity.

in the frequency region of valence deformation vibrations of the O–H bond, the absorption bands of the specimen of composition $UF_4 \cdot 1.00H_2O$ retain the structures of the corresponding bands for the original crystal hydrate. On transition to composition $UF_4 \cdot 0.30H_2O$ the spectrum of valence vibrations of O–H becomes simpler. The maxima at the long-wave end disappear, the spectrum being left with one band at 3470 cm^{-1}, very similar to the absorption band for valence vibrations of O–H for the cubic hydrate of identical composition [4].

$UF_4 \cdot 1.40H_2O$ obtained by hydrating $UF_4 \cdot 0.10H_2O$ has an absorption even more like that of the cubic hydrate of identical composition. The maxima of its infrared absorption spectra are at the same positions as those of the cubic hydrate.

The above results thus show that the original hydrate undergoes a phase transition between the composition $UF_4 \cdot 1.00H_2O$ and $UF_4 \cdot 0.5H_2O$, accompanied by a structural change; dehydration products containing less than $0.5H_2O$ per UF_4 molecule cannot be rehydrated to the original $UF_4 \cdot {}^4/_3H_2O$.

In conclusion, the authors would like to thank S. S. Batsanov for the refractometric work, recording the infrared spectra and discussing the results, and L. A. Khripin for recording the thermograms.

LITERATURE CITED

1. W. Zachariasen, Acta crystallogr., 2, 388 (1949).
2. J. Dawson, R. D'Eye, and A. Truswell, J. Chem. Soc., November 3922 (1954).
3. Yu. V. Gagarinskii and V. P. Mashireev, Zh. neorgan. khim., 4, 1246 (1959).
4. S. S. Batsanov and Yu. V. Gagarinskii, Zh. struktur. khim., 4, 387 (1963).
5. S. P. Gabuda, et al., Zh. struktur. khim., 5, 303 (1964).
6. Yu. V. Gagarinskii, S. P. Gabuda, and G. M. Mikhailov, ibid., p. 383.

THE RELATIVE VOLATILITY OF SOLUTIONS OF HTO IN H_2O

(UDC 546.23:536.432.1)

Ya. D. Zel'venskii, V. A. Shalygin, V. S. Tatarinskii, and D. A. Nikolaev

Translated from Atomnaya Énergiya, Vol. 18, No. 1, pp. 46-48, January, 1965
Original article submitted January 27, 1964

A method of simple distillation, with calculations performed according to Rayleigh's equation, was used to determine the separation factor α of solutions of HTO in H_2O in the 38-100°C temperature range. The results obtained are expressed by the equation $\log_{10}\alpha = 38.80/T - 0.0935$. The data of our study are close to the separation factor values calculated on the basis of earlier measurements of the vapor pressure of T_2O (see Atomnaya Énergiya, Vol. 8, No. 5, p. 420, 1960).

The data available in the literature regarding the values of the relative volatility (separation factor) α of solutions of tritium water are unreliable and contradictory. In [1] it was stated that the boiling point of hydrogen-tritium water, HTO, is lower than that of ordinary water, H_2O, i.e., that the former is more volatile. This conclusion was contradicted by the data obtained by Price [2], who used the ratio of the activities of the liquid and gaseous phases to determine the separation factor of HTO and H_2O solutions in the 25-80°C temperature range. According to Price, for example, at 55°C the separation factor of the HTO-H_2O system is 1.13.

Considerably lower values of α were found in [3] by a method using a fractionating column: $\alpha = 1.051$-1.053 at 70°C and $\alpha = 1.036$ at 100°C. At the two temperatures investigated, according to [3], $(\alpha_T - 1)/(\alpha_D - 1) = 1.37 \pm 0.02$, where α_D is the separation factor of the HDO $-$ H_2O system. Theoretically, the ratio of the enrichment factors, $(\alpha_T - 1)/(\alpha_D - 1)$ should be $\frac{4}{3}$ [4].

In 1960 M. Popov and F. Tazetdinov published the results of their measurements of the vapor pressure of tritium water, T_2O, in the 12-95°C temperature range [5]. Using water specimens with concentrations of 83.4% and 98.12% T_2O, the authors of [5] conducted their measurements by a static method. The resulting values of vapor pressure, converted to the values for 100% T_2O, are expressed by the generalized equation

$$\lg p = 7.9957 - \frac{1654.9}{t - 222}.$$

Popov and Tazetdinov computed the vapor pressure of HTO on the assumption that it is equal to the geometric mean of the vapor pressures of T_2O and H_2O. At 25°C, according to [5], $\alpha = p_{H_2O}/p_{HTO} = 1.097$, instead of the value of 1.295 found in [2]. There is less disagreement between the data of [5] and [3].

In order to check and improve the accuracy of such very divergent data on the value of the separation factors of solutions of tritium water, the study described below was carried out.

Experimental Procedure

In order to determine the separation factor, we used the method of simple distillation, with calculations performed according to Rayleigh's equation. This method is relatively simple and, at the same time, sufficiently rigorous and free from unverified assumptions, which makes it possible to obtain accurate results [6]. The experimental technique consists in evaporating a large amount of the initial solution, under isobaric equilibrium conditions, until a small residual amount is left.

For dilute solutions of the less volatile component, the separation factor is calculated by means of the equation [6]:

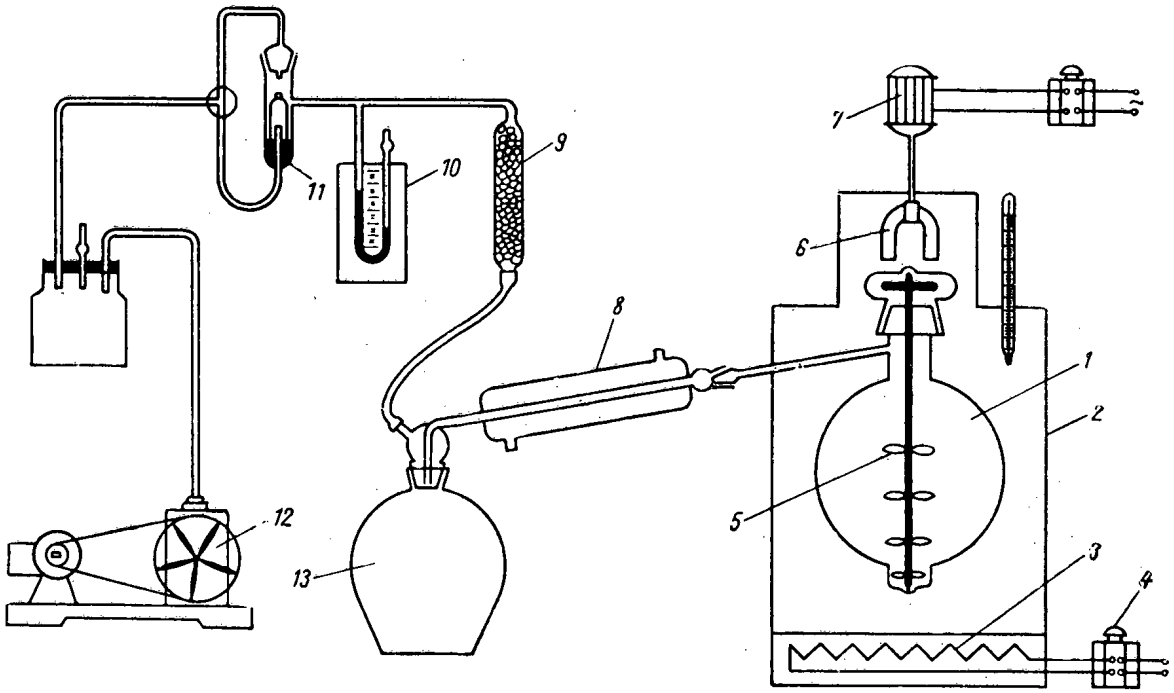

Fig. 1. Schematic of equipment used for determining separation factor: 1) Still; 2) shell of air thermostat; 3) heater; 4) autotransformer; 5) stirrer; 6) magnet; 7) motor; 8) water condenser; 9) drying column with zeolite; 10) manometer; 11) manostat; 12) vacuum pump; 13) condensate collector.

$$\alpha = \frac{\lg (W_0/W_к)}{\lg (W_0/W_к) + \lg (A_0/A_к)}, \quad (1)$$

where W_0/W_f is the ratio of the amount of the initial solution to the amount of the final solution, and A_0/A_f is the ratio of specific activities.

A schematic of the equipment used for the distillation is shown in Fig. 1. The still 1 was placed in an air thermostat 2, whose temperature was kept 10-20°C higher than the boiling point of water in order to prevent condensation of vapor on the walls of the still. The still was equipped with a magnetically driven stirrer. In accordance with the results of the preliminary tests, the rotation rate was kept between 80 and 100 rpm. The steam, being liquefied in he condenser 8, flowed into the collector 9. A predetermined constant pressure was maintained in the apparatus by means of a vacuum pump 12 and an automatic manostat 11. The distillation was carried out at a slow rate, in order not to disturb the vapor-liquid equilibrium.

For a separation factor α which is close to unity, it is desirable to increase the ratio W_0/W_f if we wish to improve the accuracy of the results. However, if the volume of the still is made excessively large, this will upset the conditions on which Eq. (1) is based (according to our data, the residual liquid at the end of the distillation should be not less than 1% of the original amount). We therefore carried out the distillation in two stages, with a volume reduction factor of W_0/W_f = 50-60 in each stage. To achieve this, after the first stage all of the residual liquid was poured into a smaller still, in which the second stage of the distillation was carried out.

The amount of water before and after the distillation was determined by weighing. The activity of the tritium water before and after the distillation was measured by a scintillation method. The scintillator used was a solution of paraterphenyl in dioxane containing an admixture of the preparation POPOP (5 g of paraterphenyl and 0.1 g of POPOP per liter of dioxane). To make the measurements, on the basis of preliminary tests, we mixed 0.1 ml of the water to be analyzed w th 9.9 ml of a scintillating solution of the indicated composition.

The resulting solution was poured into a glass cuvette sealed with Canada balsam to the face of the FÉU-19M photomultiplier. The latter was combined with a "Volna" instrument complex. When we measured the background, we poured a mixture consisting of 9.9 ml of the scintillating solution and 0.1 ml of ordinary distilled water into the same cuvette. The activity was measured with an accuracy of 1%. The specific activity of the tritium water used was about 0.5 mCi/ml.

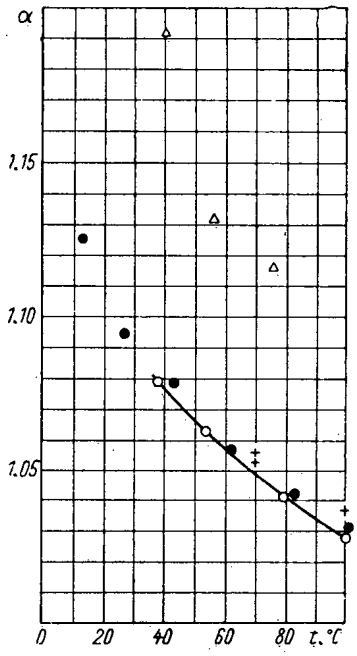

Fig. 2. Comparison of separation factors according to the data of various studies: ○) Present study; △) [2]; +) [3]; ●) [5].

Results of the Measurements

The separation factor of dilute solutions of tritium water was determined at pressures of 50-750 mm Hg, which corresponds to varying the boiling point from 38 to 100°C. The results obtained are given below.

Pressure, mm Hg	50	100	300	750
Boiling point, °C	38.1	52.0	76.8	100.0
Volume reduction in first stage of distillation, W_0/W_I	61.0	59.2	56.4	62.2
Volume reduction in second stage of distillation, W_I/W_f	52.8	61.6	52.3	52.5
Total volume reduction, W_0/W_f	3220	3646	2940	3260
Activity, A_0, of original water, pulses per 100 sec	58,600	58,720	58,740	58,790
Activity, A_f, of remainder after distillation	95,400	105,330	80,670	72,760
Separation factor α calculated according to Eq. (1)	1079	1064	1041	1027
Separation factor α_{calc} calculated according to Eq. (2).	1080	1065	1041	1027

The variation of the separation factor as function of temperature can be represented by the equation $\log_{10} \alpha = A/T - B$. Accordingly, the resulting experimental data can be expressed by the general equation

$$\lg \alpha = \frac{38.80}{T} - 0.0935. \qquad (2)$$

As can be seen from the tables, the deviation of α_{calc} from the experimental values of α is no more than 0.01.

Figure 2 shows the values of the separation factors in comparison with the data obtained in other studies. As can be seen from the figure, the results of the present study are in satisfactory agreement with the data of [5], which were obtained by a different method. There is also comparatively little difference between the two values of α obtained in [3] by a third method. Price's data [2] are considerably higher and must be considered erroneous. The assertion of Libby and Cornog [1] that the vapor pressure of HTO is higher than that of H_2O is also incorrect.

LITERATURE CITED

1. W. Libby and R. Cornog, Phys. Review, 60, 171 (1941).
2. A. Price, Nature, 181, 262 (1958).
3. P. Avinur and A. Nir, Nature, 188, 652 (1960).
4. I. Bigeleisen, Tritium in the Physical and Biological Sciences, Vienna, IAEA (1962), Vol. 1, p. 161.
5. M. M. Popov and F. M. Tazetdinov, Atomnaya Énergiya, 8, 420 (1960).
6. Ya. D. Zel'venskii and V. A. Shalygin, Zh. prikl. khimii, 31, 1501 (1957).

DETERMINATION OF γ-RAY AND NEUTRON ABSORBED DOSE IN POLYMERS

(UDC 639.121.7)

F. A. Makhlis and I. M. Kolpakov

Translated from Atomnaya Énergiya, Vol. 18, No. 1,
pp. 48-52, January, 1965
Original article submitted January 9, 1964

Together with results, a method is given for calculating the γ-ray and neutron absorbed dose in several polymers which is based on the elemental composition of the materials and the energy of the radiation.

In radiochemical studies and in the radiation treatment of various materials and biological subjects, the basic physical problem is the determination of the amount of energy which is absorbed by the irradiated medium, i.e., the determination of absorbed dose. Strictly speaking, this criterion, although it is fundamental, need not be unique. Clearly, radiochemistry lacks a concept resembling the coefficient of relative biological effectiveness (RBE) in radiation biology. Actually, for the same absorbed energy, the changes in the properties of a polymer under neutron irradiation can differ from the corresponding changes under γ-irradiation [1]. However, the required quantitative data are lacking, and we are forced to proceed solely on the basis of the magnitude of the absorbed energy, on which the final effect of the irradiation process depends to a considerable extent, other conditions being equal.

Gamma Irradiation

With the exception of calorimetry, there are no known experimental methods by which one might determine the magnitude of the absorbed dose for each specific material under γ irradiation. However, the use of the calorimetric method is made difficult by the complex configuration of the absorbed dose field which is produced by actual irradiation equipment. Consequently, one ordinarily resorts to indirect methods for determining the absorbed dose, using various liquid dosimetric systems of air ionization. A number of important considerations connected with the determination of absorbed dose from the results of radiation dose measurements were discussed in [2].

Knowing the magnitude of the absorbed dose D_1 in a definite volume occupied by one material, one can obtain the corresponding magnitude of the absorbed dose D_2 for another material, other conditions being equal, from the relation

$$D_1 = \frac{(\mu_a/\varrho)_1}{(\mu_a/\varrho)_2} D_2, \tag{1}$$

where $(\mu_a/\rho)_1$ and $(\mu_a/\rho)_2$ are the true mass absorption coefficients for γ radiation in the first and second materials. If the radiation dose in air is known, then the conversion to absorbed dose in the irradiated material is accomplished on the basis of formula (1). Indeed, if it is assumed that the energy needed for the formation of an ion pair in air is 34 eV, the energy equivalent of the roentgen in air with fulfillment of electron equilibrium is 87.7 erg/g. From that, we obtain

$$D_M = 0.877 \frac{(\mu_a/\varrho)_M}{(\mu_a/\varrho)_{air}} \text{ [rad/R]}, \tag{2}$$

where the subscript "M" indicates the irradiated material. The true mass absorption coefficient for a multicomponent system $(\mu_a/\rho)_{syst}$ consisting of n elements is defined as

$$(\mu_a/\varrho)_{syst} = \sum_1^n g_j (\mu_a/\varrho)_j, \tag{3}$$

where g_j is the fractional weight of the j-th element in the system.

TABLE 1. Values of D_M for Different Elements, rad/r

Element	γ-Energy, MeV						
	0.1	0.2	0.5	1.0	2.0	5.0	10.0
H	1.54	1.73	1.74	1.74	1.74	1.60	1.36
C	0.811	0.870	0.877	0.877	0.877	0.864	0.834
N	0.844	0.873	0.877	0.877	0.877	0.876	0.866
O	0.877	0.883	0.877	0.877	0.877	0.880	0.894
F	0.905	0.845	0.832	0.830	0.835	0.850	0.880
Na	1.072	0.870	0.837	0.840	0.843	0.877	0.832
Mg	1.255	0.912	0.864	0.852	0.870	0.910	0.990
Al	1.395	0.899	0.845	0.842	0.852	0.900	0.991
Si	1.70	0.96	0.875	0.867	0.876	0.945	1.06
S	2.28	1.01	0.884	0.870	0.877	0.968	1.100
Cl	2.55	1.02	0.850	0.832	0.840	0.940	1.11
K	3.37	1.11	0.864	0.850	0.859	0.970	1.55
Ca	4.13	1.20	0.894	0.870	0.877	1.01	1.213
Fe	8.34	1.60	0.864	0.819	0.820	1.0	1.261

In order to simplify the computations, values of D_M are given in Table 1 for elements frequently encountered in radiochemistry and radiobiology. These values were obtained by using the values of μ_a/ρ in [3]. Table 2 gives values of D_M for water and a number of polymers.

Neutron Irradiation

For reasons which are given in [4], radiation treatment of materials with neutrons is possible under very limited conditions, but the calculation of absorbed dose is necessary in order to estimate the radiation resistance of materials intended for operation in nuclear reactors. In the calculations given below for the absorbed dose in polymer irradiation with thermal and fast neutrons, the assumption was made that the neutrons undergo only one collision during penetration of the irradiated material.

The validity of such an assumption is verified by the following considerations.

1. The thickness of polymer products (for example, rubber products) which are irradiated usually does not exceed the neutron mean free path. Thus, the thermal neutron ranges in water and polyethylene are 0.28 and 0.24 cm, respectively; for 1 MeV neutrons, they are 2.45 and 2.3 cm, and 11.0 and 7.7 cm for 10 MeV neutrons.

2. The value of the absorbed energy we obtained was close to the maximum absorbed energy for the thickness of the irradiated object. This followed from a comparison of the experimentally determined distribution of neutron absorbed depth dose in a paraffin phantom [5] with computed values which were obtained with the "first collision" approximation. The deviation between the corresponding values did not exceed 4% for neutron energies of 0.24-1.0 MeV.

Thermal Neutron Irradiation

For the elements which are present in a majority of the materials used in radiochemistry, the following basic reactions are characteristic of interactions with thermal neutrons:

$$N^{14}(n, p)C^{14},\ \sigma = 1.76 \text{ barn},\quad Q = 0.623 \text{ MeV},\quad K = 0.996,$$

$$O^{17}(n, \alpha)C^{14},\ \sigma = 0.5 \text{ barn},\quad Q = 1.72 \text{ MeV},\quad K = 0.00039,$$

$$Cl^{35}(n, p)S^{35},\ \sigma = 0.17 \text{ barn},\quad Q = 0.62 \text{ MeV},\quad K = 0.7543.$$

Here, σ is the cross section for the respective reaction, cm^2; Q is the energy of the emitted particles, MeV; K is the isotopic fraction in a natural mixture of isotopes. The contribution from the $O^{17}(n, \alpha)C^{14}$ reaction is negligibly small, because of the insignificant amount of O^{17} in a natural mixture of isotopes. One can assume that the energy transferred by the products of the other two reactions is absorbed in the immediate vicinity of the location of the neutron-nucleus interaction. Then the absorbed dose, normalized to unit neutron flux, is

$$D_{ij} = 1.6 \cdot 10^{-8} N_j K_j Q_{ij} \sigma_{ij} \ [\text{rad}/(\text{neut} \cdot \text{cm}^{-2})]. \quad (4)$$

Here, N_j is the number of atoms of element j per cm^3; the subscript i identifies the reaction under consideration, and the subscript j, the material under consideration. For the $N^{14}(n, p)C^{14}$ reaction, D_{ij} is $7.5 \cdot 10^{-10}$ rad/neut-cm^{-2}, and for the $Cl^{35}(n, p)S^{35}$ reaction, it is $0.239 \cdot 10^{-10}$ rad/neut-cm^{-2}. In the emission of protons or α-particles, one can neglect the energy of recoil nuclei.

TABLE 2. Values of D_M for Water and Several Polymers, rad/R

Polymer	γ-Energy, MeV							
	0.1	0.5	0.8	1	1.5	2	5	10
Polyethylene, SKEP, butyl rubber	0.91	1.0	1.00	1.0	1.0	1.0	0.97	0.91
Natural rubber	0.90	0.99	0.98	0.98	0.99	0.99	0.96	0.90
SKS, SKB	0.89	0.97	0.97	0.97	0.97	0.97	0.94	0.90
Nitrile rubber	0.88	0.96	0.96	0.96	0.96	0.96	0.93	0.88
Silicone rubber	1.2	0.95	0.94	0.94	0.94	0.94	0.95	0.97
Fluoresin, "Viton" type	0.89	0.86	0.76	0.76	0.76	0.86	0.87	0.87
Hypalon	1.38	0.95	0.95	0.94	0.94	0.94	0.95	0.96
Teflon	0.88	0.84	0.84	0.84	0.84	0.84	0.85	0.86
Water	0.96	0.97	0.97	0.97	0.97	0.97	0.96	0.94

TABLE 3. Values of the Absorbed Dose, Normalized to Unit Neutron Flux, for Water and Several Polymers, rad/neut-cm^{-2} · 10^{-10}

Material	Neutron energy, MeV							
	thermal	0.1	0.5	0.8	1	2	5	10
Polyethylene, SKEP, butyl rubber	0.155	9.0	21.9	28.5	31.6	42.7	61.2	75.5
Natural rubber	0.136	8.1	20.6	25.8	28.6	38.8	55.5	69.0
Nitrile rubber	0.67	6.74	17.2	21.5	23.9	32.5	46.7	58.7
Silicon rubber	0.124	5.15	13.3	16.6	19.1	24.9	35.8	44.4
Fluoresin, "Viton" type	0.091	2.19	4.35	5.5	6.0	8.8	12.9	18.0
Fluoresin, Kel-F type	6.10	0.77	2.67	3.43	3.74	6.04	8.53	12.6
Hypalon	4.05	5.9	15.0	18.8	20.9	28.2	40.8	50.7
Teflon	0.019	1.03	1.39	1.84	1.93	7.3	5.1	9.0
Water	0.139	6.8	17.8	21.6	27.0	32.4	45.5	56.8

TABLE 4. Values of D_{ij} Normalized to Unit Fast Neutron Flux, rad/neut-cm^{-2} · 10^{-10}

Element	Neutron energy, MeV						
	0.1	0.2	0.5	1.0	2.0	5.0	10.0
H	60.5	92	148	205	278	390	455
C	0.512	0.96	1.94	2.93	3.95	7.41	13.1
N	—	0.64	1.03	2.00	2.86	6,42	12.0,
O	0.23	0.47	1.67	5.0	2.07	4.33	8.15
F	1.07	0.39	0.65	1.09	3.10	4.46	7.72
Na	0.11	0.49	0.35	1.20	2.01	3.77	7.55
Mg	0.25	0.35	0.77	0.83	1.91	3.24	1.86
Al	0.15	0.22	0.43	0.64	1.67	2,71	4.19
Si	0.023	0.50	0.35	1.04	1.08	2,75	4.12
S	0.13	0.18	1.19	0.47	1.04	2.07	1.6
Cl	0.025	0.064	0.16	0.33	0.90	1.99	3.05
Ca	0.005	0.022	0.11	0.23	0.46	1.15	2.30
Fe	0.23	0.05	0.09	0.13	0.28	0.70	1.01

The energy released in radiative capture can also be found with formula (4), the only difference being that Q_{ij} is understood to be the binding energy released with the addition of a neutron to the nucleus [6]. Then the γ-ray energy which is absorbed by a thin layer of irradiated material of thickness r can be approximated by the relation

$$D_{ij} = D_{ij}\mu_a r, \tag{5}$$

where μ_a is the γ-quantum linear absorption coefficient for the material under consideration.

If a single γ-quantum is emitted in neutron capture by the hydrogen nucleus and, with some approximation, by the carbon nucleus, then one can assume with a reasonable amount of accuracy that three γ-quanta with energies $Q_{ij}/3$ each are emitted in the case of the materials of interest to us.

The contribution of nuclear recoil energy and induced activity to the absorbed dose is negligibly small in this case [7].

Results from a computation of the magnitude of the absorbed dose, normalized to unit thermal neutron flux, are given in Table 3 for water and several polymers.

Fast Neutron Irradiation

The energy which is transferred to a polymer as the result of elastic scattering of fast neutrons is determined from the relation

$$D_{ij} = 1.94 \cdot 10^{16} E \sum \frac{\sigma_{ij} g_j}{(A_j+1)^2} \text{ [rad/neut-cm}^{-2}\text{]}, \tag{6}$$

where σ_{ij} is the neutron elastic scattering cross section for nuclei of element j, cm^2; g_j is the proportion of element j in the mixture; A_j is the atomic weight of element j; E is the neutron energy, MeV.

In hydrogenous materials, the principal process which is responsible for the transfer of energy to matter is scattering by hydrogen. The fraction of the energy which is transferred by this process is 85-90% of the total absorbed dose [8]. To facilitate computations using formula (6), values of D_{ij} (rad/neut-cm^{-2}) are given in Table 4 for elements often encountered in radiochemistry (only elastic scattering of neutrons was considered in the calculations).

The relative role of inelastic neutron scattering as compared with elastic scattering increases with increasing energy and with the atomic number of the irradiated material. Of the light elements which make up polymers, only fluorine has an inelastic scattering cross section of 1.25-0.5 barns for neutron energies of 0.5-1.0 MeV; furthermore, γ-quanta with energies of 0.109 and 0.197 MeV are emitted. At neutron energies exceeding 1 MeV, inelastic scattering is also possible in aluminum, magnesium, iron, and other metals found in resins. The energy of the accompanying γ-quanta is approximately 1 MeV. Therefore, the contribution of γ-radiation from inelastic scattering to the absorbed dose can compete with the contribution from elastic scattering only for neutron energies above 0.5 MeV and only if the proportion of metal in the composition of the irradiated material is sufficiently great.

The fast neutron radiative capture cross section is hundreds of times smaller than the scattering cross section, and only a small fraction of the energy released is absorbed in light elements in the case of thin, irradiated objects; consequently, one can neglect the contribution to the absorbed dose from γ-rays in (n, γ) reactions. A similar conclusion is reached with regard to secondary charged particles, recoil nuclei, and induced activity.

The results of absorbed dose calculations, normalized to unit fast neutron flux, are given in Table 3 for water and several polymers.

With reactor irradiation, the contributions of fast and thermal neutrons to the total absorbed dose depends on the composition of the polymer. For the majority of polymers, the absorbed dose from fast neutrons exceeds by far the corresponding value for thermal neutrons. Polymers which contain a considerable quantity of fluorine are an exception. Calculations which were carried out for the irradiation of polyethylene and Kel-F in the core of the VVR-M thermal reactor [9] showed that the thermal neutron absorbed dose in polyethylene did not exceed 1%, and for Kel-F was 50%, of the fast and intermediate neutron absorbed dose. For irradiation in the vicinity of the beryllium reflector, the analogous values were 3% for polyethylene and 100% for Kel-F.

In conclusion, we wish to thank E. N. Smagin for valuable discussions.

LITERATURE CITED

1. A. Charlesby, Nuclear Radiations and Polymers [Russian translation] (Moscow, Izd-vo inostr. lit., 1962).
2. Yu. V. Sivintsev, Atomnaya énergiya, 9, 39 (1960).

3. R. Berger, Rad. Res., 15, 1 (1961).
4. F. A. Makhlis and A. Kh. Breger, Kauchuk i resina, No. 8, 18 (1964).
5. A. M. Kogan, et al., Atomnaya énergiya, 7, 351 (1959).
6. B. Price, C. Horton, and K. Spinney, Nuclear Radiation Shielding [Russian translation] (Moscow, Izd-vo inostr. lit., 1959).
7. M. I. Shal'nov, Neutron Tissue Dose [in Russian] (Moscow, Atomizdat, 1960).
8. R. Eger, Dosimetry and Radiation Shielding [in Russian] (Moscow, Gosatomizdat, 1961).
9. V. V. Goncharov, et al., Proceedings of the Second International Conference on the Peaceful Use of Atomic Energy [in Russian] (Dokl. sov. uchenykh, Moscow, Atomizdat, 1959), Vol. 2, p. 293.

INCREASING THE DEPTH OF PROSPECTING FOR CONCEALED URANIUM ORE BODIES BY MEANS OF THE PRIMARY AUREOLE

(UDC 550.8/546.791)

S. V. Grigoryan

Translated from Atomnaya Énergiya, Vol. 18, No. 1,
pp. 52-57, January, 1965
Original article submitted February 14, 1964

A study of the primary uranium aureoles in one hydrothermal deposit showed that, by using systematic chemical analysis (sampling analysis of the mobile uranium content), the primary aureole can be more fully revealed, and the depth of aureole prospecting for hidden uranium ores thus increased. It is shown that this method of analysis is most effective for elements whose aureoles are of small extent and intensity, owing to high background content in the country rocks, low ore content, etc.

Recent investigations have shown that uranium ores of hydrothermal origin are surrounded by aureoles of uranium and other elements; these can be used in prospecting for concealed uranium ore bodies [1, 2]. The main elements used as indicators of uranium ores are those forming the most extensive aureoles.

A study of the distribution characteristics of elements in a number of hydrothermal uranium deposits showed that, in any cross section, as one moves laterally away from the ore, the concentrations of uranium and its accessory minerals decrease in geometric progression [2, 3]. The distribution of any element around the ore can thus be represented by a graph (Fig. 1). Since the concentration decreases in geometric progression, the distribution is represented by a straight line in semilog coordinates.

In practice, aureoles are mapped with respect to the least anomalous content of an element, just as in prospecting for deposits the limits of commerical ores are determined from the boundary content of the required component [2]. In Fig. 1 the half-width of the aureole corresponds to the intercept cut off by the distribution graph on the horizontal line representing the least anomalous content. In actual fact the aureole will be considerably wider: with increasing distance from the ore body, the element concentrations introduced during ore formation decrease, not down to the least anomalous content, but to the content in the interstitial solutions which saturated the rocks when the ore and aureole were formed. This is due to the fact that, when the primary aureoles were formed, the element contents were equalized between the ore-bearing solutions and the interstitial solutions saturating the country rock. The aureoles formed by this equalization will also have the maximum possible size. Let us call them "true," and those mapped from the least anomalous content "apparent." The difference between these aureoles will increase with the least anomalous content of any element.

The vertical extent of the apparent aureoles is much less than that of the true ones. The relation between the dimensions of the apparent and true aureoles was studied in detail on one hydrothermal uranium deposit occurring in granites.

The deposit appeared as numerous fine tarry fluorite veinlets, forming stockwork ore bodies of various sizes, elongated in a northwesterly direction. The dip of the ore bodies is steep. The boundaries of the commerical ores are known from the results of assays.

In mapping the aureoles of the elements, the least anomalous uranium content was determined from the geochemical background value and standard deviation in the rocks [4]. The method of mapping is given in more detail in [2].

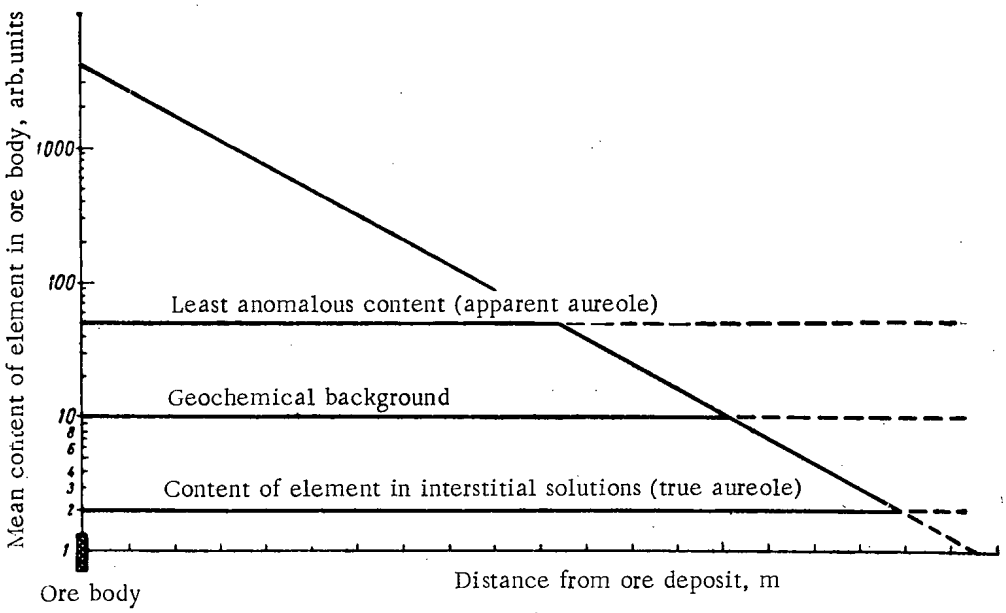

Fig. 1. Distribution of a chemical element around an ore deposit.

To determine the vertical extents of the apparent and true aureoles, we drew graphs of the linear productivity[1] of the uranium aureoles in a vertical cross section through the ore body (Fig. 2). The linear productivity of the aureole at a given horizon was found by multiplying the mean uranium content by the width of the aureole. The abscissae in Fig. 2 represent the linear productivity calculated from the aureole of mobile uranium [2, 4]. The ordinates represent the distance of the sampling horizons from the ore body, plotted on a linear scale. It is seen that the linear productivity of the uranium aureole is represented by a nearly straight line. To determine the vertical extent of the uranium aureole above the ore body, this line must be produced to meet the line corresponding to the least anomalous linear productivity. (This productivity corresponds to the aureole of minimum breadth and with mean content equal to the least anomalous content.) The apparent minimum breadth is equal to the sampling interval (5 m). However, we took it as 10 m, since the aureole must be mapped by at least two samplings. Conversely, samples in which the high concentration of elements is caused by random factors (e.g., background variation) may be mistaken for an aureole. For the ore deposit described, the least anomalous uranium content was taken as 0.0016%, which exceeds the geochemical background (GB) of the surrounding granites, 0.0007%, by twice the standard deviation (GB + 2σ). The minimum anomalous productivity will thus be $0.0016 \cdot 10 = 0.016$ m %.

The extent of the uranium aureole above the ore body was found by extrapolation to be 180 m (Fig. 2). That of the true aureole above the same ore body was determined in a similar manner. It is equal to the distance from the ore body to the point of intersection of the straight line representing the productivity with a vertical line corresponding to the linear productivity (given by the product of the uranium content in the interstitial solutions and the minimum aureole breadth, 10 m). Graphical determination shows that, in this cross section, the true aureole extends about 500 m above the ore body, i.e., more than 2.5 times the extent of the apparent aureole.

From the above it is clear that the depth of an aureole survey can be increased by decreasing the least anomalous productivity of the aureole (preferably by reducing the least anomalous content, since decreasing the sampling interval leads to a considerable rise in working expenses).

To choose an appropriate method of systematic sample analysis (the essential point of the problem), we studied the forms of uranium occurrence within the aureole.

The uranium content of an aureole accumulates from the primary distribution in the country rock (the Clarke content) and from uranium introduced by the hydrothermal solutions and forming the aureole.

Many investigators, having studied the occurrence of primary uranium in magmatic rocks, remark that part of the uranium can be extracted from the rocks by relatively weak solvents, but the whole is extracted only by breaking down the crystalline structures of the rock-forming and accesory minerals. Tauson [6] distinguishes between two main forms of uranium in granitoids: non-isomorphic and isomorphic. He assigns the name "non-iso-

[1]The idea of linear productivity of a diffuse aureole is due to A. P. Solovov [5].

TABLE 1. Degree of Uranium Extraction by Na_2CO_3 from Pitchblende and Sooty Uraninite

Sample No.	Uranium mineral	Total U content, %	Extraction into solution, %
A-3	Pitchblende	$3.6 \cdot 10^{-4}$	75
A-12	»	$9 \cdot 10^{-4}$	89
A-5	»	$8 \cdot 10^{-4}$	75
C-89	»	0.2	90
C-1	»	0.31	74
A-9	Uraninites	$3.6 \cdot 10^{-4}$	100

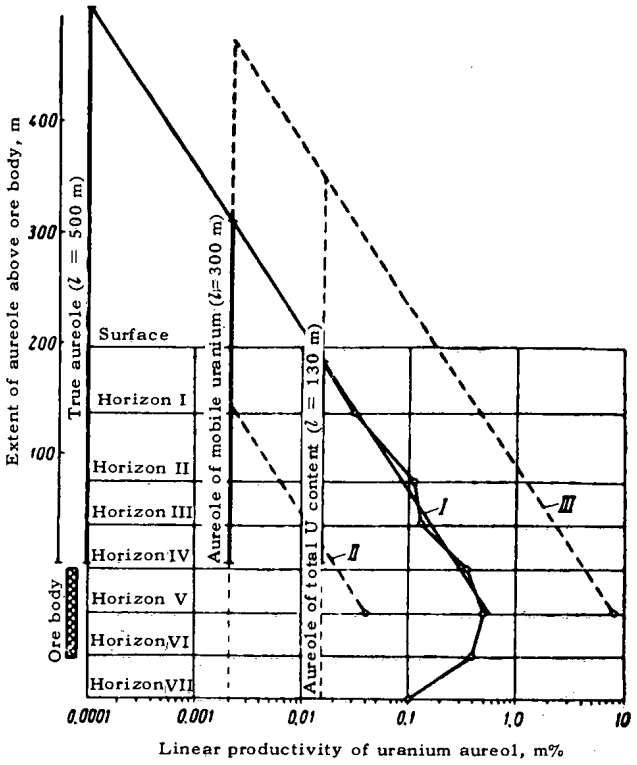

Fig. 2. Extent of uranium aureoles above an ore body. I, II, III) Linearized changes of productivity of uranium aureole in a vertical direction.

morphic" to that part of the uranium which can be extracted by boiling with 5% ammonium carbonate solution containing hydrogen peroxide. In these conditions the crystalline lattice of the rock-forming and accessory minerals is practically undisturbed. Tauson considers that, with this method of analysis, the uranium from separate minerals (such as oxides) also passes into solution. Experiments have shown that granitoid rocks have a negligible content of non-isomorphic uranium.

Our investigations showed that uranium, introduced into the country rocks during the formation of an ore body, occurs mainly as the individual minerals pitchblende and the sooty uraninite group of oxides [2]. In order to bring the latter into solution without destroying the crystal lattices of the rock-forming and accessory minerals, weighed samples were boiled for 30 min with 2% soda solution containing hydrogen peroxide as oxidizer.

To determine the degree of uranium extraction from pitchblende and oxides, an artificial mixture of these minerals with pure quartz sand was treated as described. The total uranium content of the samples was determined by melting weighed portions with soda. The results showed that pitchblende and uraninite are satisfactorily dissolved by soda solution (see Table 1).

It should be noted that Na_2CO_3 solution extracts only a tiny part of the primary, so-called mobile uranium from the country granites outside the limits of the aureole [6-8]. The least anomalous content of mobile uranium for the granites of the deposit described is equal to $2 \cdot 10^{-4}$%, which also exceeds the geochemical background (0.00004%) by twice the standard deviation (GB + 2σ). The (linear) least anomalous productivity for mobile uranium is 0.002 m %. As shown by the graphical determinations, the extent of the mobile uranium aureole above the ore body is more than 1½ times that revealed by measuring the total U content (see Fig. 2). In other words, the above method of systematic sample analysis considerably increases the effective depth of prospecting for concealed ore bodies by means of uranium aureoles.

This conclusion, based on graphical construction, is confirmed by mapping the aureoles in a vertical cross section through the ore body. Figure 3 shows the uranium aureoles around a concealed ore body. The graph of the linear productivity in this cross section is given in Fig. 2. The aureole is mapped twice, according to sample assays of mobile uranium and of total U content. To reduce the number of analyses, the total U content was determined only for the samples taken at the surface and first horizon (see Fig. 3).

The mobile uranium aureole is the wider and longer of the two. The mobile U content of all the surface samples was anomalous, whereas that of total U in the same samples was less than the minimum anomalous value – i.e., no total-U aureole is observed at the surface of this cross section. At the first horizon the width of the U aureole is small. It follows from Fig. 3 that, if the total U aureole were used in prospecting for this ore body, it would not be located.

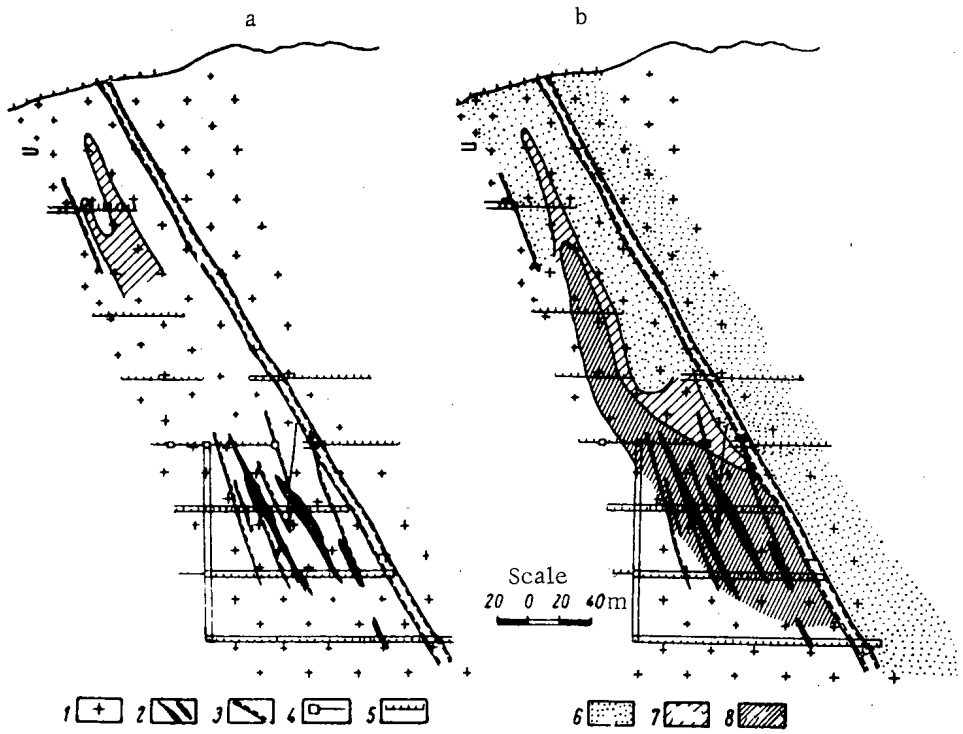

Fig. 3. Primary uranium aureoles: a) Aureole of total U content; b) aureole of mobile uranium. 1) Granites; 2) ore body; 3) faults; 4) workings and boreholes; 5) sampling intervals. Uranium contents, %: 6) 0.002-0.0015; 7) 0.0015-0.005; 8) > 0.005.

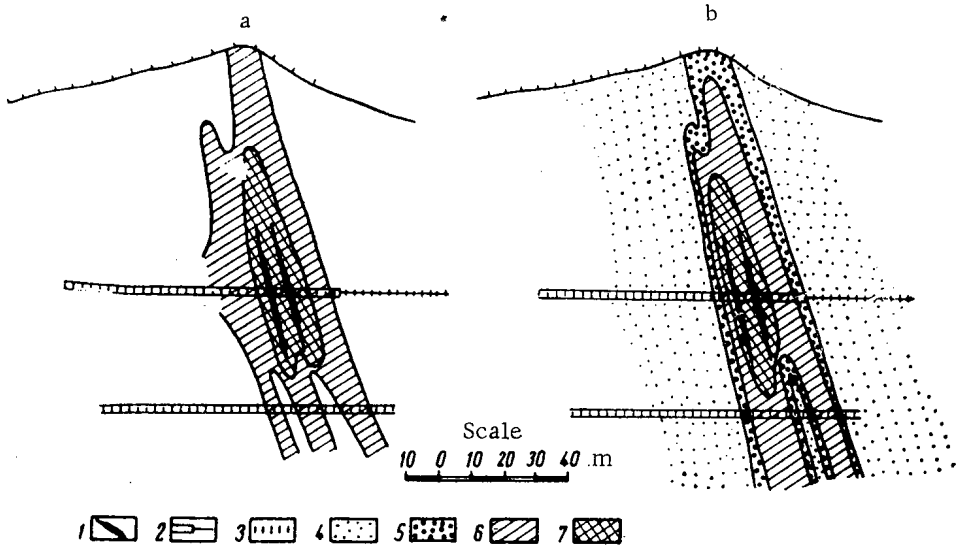

Fig. 4. Primary uranium aureoles: a) Of total U content; b) of mobile U. 1) Ore body; 2) working and boreholes; 3) sampling intervals. Uranium contents, %: 4) 0.0002-0.0005; 5) 0.0005-0.0015; 6) 0.0015-0.005; 7) > 0.005.

Figure 4 shows the uranium aureoles around two contiguous concealed uranium ore bodies. The latter are revealed at the surface by only two samples, if the least anomalous total U contents are used. For mobile U, however, all the surface samples fall within the aureole. Furthermore, at the surface directly above the ore bodies an anomalous field of mobile uranium is found, its width exceeding that of the aureole of total U content (see Fig. 4).

The method of analysis for mobile uranium is easier than that for the total content. It facilitates the bulk sample analysis which is so necessary in geochemical prospecting. We can expect this systematic analysis method to be most effective for elements with small apparent aureoles of low intensity. Figure 2 shows that the use of systematic analysis increases the extension of the apparent maximum-productivity aureole of uranium by a factor of 1.2 (curve III), while the extension of the aureole with minimum productivity is increased nearly ten times (curve II).

The following conclusions may be drawn.

1. The use of systematic chemical analysis (determination of the mobile uranium content) permits fuller exposure of primary uranium aureoles and increased depth of prospecting for concealed uranium ores by means of primary aureoles.

2. The use of systematic chemical analysis will be most effective for elements with apparent aureoles which are, owing to high background concentration in the country rocks, low concentration in the ores, etc., of small dimensions and intensities.

3. By means of systematic chemical analysis it will be possible to find primary aureoles for a number of new elements which cannot be discovered by total content determinations, as their background levels are high and, consequently, so are their least anomalous contents.

LITERATURE CITED

1. A D. Kablukov and G. I. Vertepov, Geologiya rudnykh mestorozhdenii, No. 2, 20 (1960).
2. E. M. Yanishevskii, et al., Endogenous Diffusion Aureoles of Certain Hydrothermal Deposits [in Russian] (Moscow, Gosgeoltekhizdat, 1963).
3. H. Morris and T. Lovoring, Econ. Geol., 47, 7, 685 (1952).
4. S. V. Grigoryan, Razvedka i okhrana nedr, No. 2, 26 (1964).
5. A. P. Solovov, Razvedka i okhrana nedr, No. 4, 48 (1952).
6. L. V. Tauson, Geokhimiya, No. 3, 9 (1956).
7. L. S. Evseeva and A. I. Perel'man, Geochemistry of Uranium in the Supergene Zone [in Russian] (Moscow, Gosatomizdat, 1962).
8. A. S. Saukov, Radioactive Elements of the Earth [in Russian] (Moscow, Gosatomizdat, 1961).

LETTERS TO THE EDITOR

PHASE STABILITY OF PARTICLE BLOBS IN ACCELERATORS WITH AUTOMATIC CONTROL

(UDC 621.384.60)

É. A. Zhil'kov

Translated from Atomnaya Énergiya, Vol. 18, No. 1,
pp. 58-59, January, 1965
Original article submitted May 8, 1964

The characteristic equation for a system of particles performing nonlinear synchrotron oscillations in an accelerator with automatic correction of the accelerating field's frequency $\omega_0 = q\omega_s$ with respect to the beam was derived in [1]:

$$1 = 2\pi i \int d\varepsilon \frac{df_0}{d\varepsilon} \Omega(\varepsilon) \sum_{-\infty}^{+\infty} \frac{K_{-k} k^2 \varphi_k}{\omega - k\Omega(\varepsilon)} . \quad (1)$$

Here, ω is the natural oscillation frequency in $\Omega(0)$ units, where $\Omega(o)$ is the frequency of linear synchrotron oscillations; ε and $\Omega(\varepsilon)$ are the energy and the frequency of nonlinear synchrotron oscillations; $f_0(\varepsilon)$ is the equilibrium distribution function of the blob; $K(\omega)$ is the system's reaction to the shift of the point blob with respect to u and φ at the frequency ω; φ_k and K_{-k} are the coefficients of the expansions of $\varphi(\varepsilon, T)$ and $K(\varepsilon, T)$ as periodic functions of the variable $T = \int_{\varphi_1}^{\varphi} \frac{d\xi}{u(\varepsilon, \xi)}$ in Fourier series at the section $\left(-\frac{\pi}{\Omega(\varepsilon)}; \frac{\pi}{\Omega(\varepsilon)}\right)$, $u = \frac{2\pi\Omega(0)}{eV_0 \sin\varphi_s} \int_E^{E_s} \frac{dE}{\omega_s(E)}$

Certain general stability criteria for small-size blobs were found in [1] under the assumption that the automatic control system corrected the position of the blob's center of gravity.

Here, we shall investigate the stability of small blobs in the presence of a system of automatic control with respect to second moments and also the stability of higher moments.

Consider the stability of a small blob [1] in the case where feedback with respect to the blob dimensions is provided [2], i.e., when not only the center of gravity, but also deviations of the blob dimensions with respect to their equilibrium values $\Psi^0 = V^0 = \varepsilon$; $W^0 = 0$ are corrected. The automatic control system is described by the equation

$$K(\omega) = K_1(\omega) u + K_2(\omega) \varphi + K_3(\omega)(\Psi - \Psi^0) + K_4(\omega)(V - V^0) + K_5(\omega) W, \quad (2)$$

where $K_i(\omega)$ are the transfer constants of the feedback circuits with respect to the corresponding blob characteristics, and $\Psi = (\varphi - \varphi_0)^2$, $V = u^2$ and $W = (\varphi - \varphi_0)u$ are the characteristics of the blob dimensions.

By substituting Eq. (2) in (1) and using the dependence of the phase φ on the time T [3]

$$\varphi(T) \approx \varphi_s - \sqrt{2\varepsilon} \cos\Omega T - \frac{\operatorname{ctg}\varphi_s}{2}\varepsilon + \varepsilon \frac{\operatorname{ctg}\varphi_s}{6} \cos 2\Omega T - \frac{\varepsilon\sqrt{2\varepsilon}}{96}(1 + \operatorname{ctg}^2\varphi_s) \cos 3\Omega T + \ldots, \quad (3)$$

where

$$\Omega \approx 1 - \frac{1}{8}\varepsilon\left(1 + \frac{5}{3}\operatorname{ctg}^2\varphi_s\right),$$

we find the characteristic equation for determining the natural oscillation frequency of the blob:

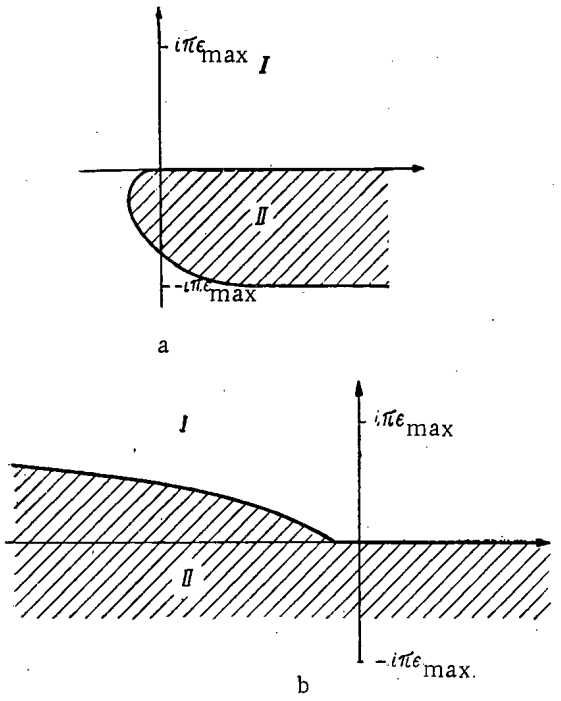

Fig. 1. Regions of stability (I) and instability (II) of a blob in the plane of the convex variable ξ_1. a) Linearly falling equilibrium distribution; b) linearly rising equilibrium distribution.

$$\xi=\pi J\left(1+\frac{5}{3}\operatorname{ctg}^2\varphi_s\right), \tag{4}$$

while

$$\xi=\left.\frac{\left(1+\frac{5}{3}\operatorname{ctg}^2\varphi_s\right)(3+2iK_2-K_1)}{4i\operatorname{ctg}\varphi_s\left[\frac{\operatorname{ctg}\varphi_s}{6}(K_2+2iK_1)-K_4+K_3-iK_5\right]}\right|_{\omega=2}, \tag{5}$$

$$J=\int\frac{df_0}{d\varepsilon}\cdot\frac{\varepsilon^2\,d\varepsilon}{\omega^2-4+\varepsilon\left(1+\frac{5}{3}\operatorname{ctg}\varphi_s\right)}. \tag{6}$$

If we consider that the distribution is uniform [1], we obtain the solution of (4) in the following form:

$$\omega=2-\frac{\varepsilon}{2}\left(1+\frac{5}{3}\operatorname{ctg}^2\varphi_s\right)-\left.\frac{i\operatorname{ctg}\varphi_s\bar{\varepsilon}\left[\frac{\operatorname{ctg}\varphi_s}{6}(K_2+2iK_1)-K_4+K_3-iK_5\right]}{3+2iK_2-K_1}\right|_{\omega=2}, \tag{7}$$

where $\bar{\varepsilon}=\frac{\varepsilon_{max}}{2}$.

The results obtained in [1], where the parameter ξ denotes the expression defined by (5), remain valid for a triangular distribution. Consequently, the introduction of feedback with respect to the blob dimensions produces the same effect as the consideration of a slight nonlinearity in correcting the center of gravity. This makes it possible to secure the blob's stability throughout the entire acceleration cycle by choosing suitable transfer constants K_3, K_4, and K_5.

We shall analyze the stability of a blob described by the three first distribution moments. In this approximation

$$\xi_1=\left.\frac{\left(1+\frac{5}{3}\operatorname{ctg}^2\varphi_s\right)\{8+3iK_2-K_1-i\bar{\varepsilon}[K_2(0.94+0.12\operatorname{ctg}^2\varphi_s)+iK_1(0.8+0.1\operatorname{ctg}^2\varphi_s)-3.2\operatorname{ctg}\varphi_s(K_3-K_4-1.5iK_5)]\}}{\frac{3}{16}i(1+\operatorname{ctg}^2\varphi_s)\left[\frac{1}{8}(1+\operatorname{ctg}^2\varphi_s)(K_2+3iK_1)-\operatorname{ctg}\varphi_s(2K_4-K_3+1.5iK_5)\right]}\right|_{\omega=3}. \tag{8}$$

For a uniform distribution, we find from expression (1)

$$\omega=3-\frac{3\bar{\varepsilon}}{4}\left(1+\frac{5}{3}\operatorname{ctg}^2\varphi_s\right)-\frac{i\bar{\varepsilon}^2}{8}(1+\operatorname{ctg}^2\varphi_s)\left.\frac{\left[\frac{1}{8}(1+\operatorname{ctg}^2\varphi_s)(K_2+3iK_1)+\operatorname{ctg}\varphi_s(K_3-2K_4-1.5iK_5)\right]}{8+3iK_2-K_1}\right|_{\omega=3}. \tag{9}$$

If we use a triangular distribution, the characteristic equation assumes the following form:

$$\xi_1=-\varepsilon_{max}\left[\frac{1}{3}+\frac{y}{2}+y^2+y^3\ln\left(1-\frac{1}{y}\right)\right],$$
$$y=\frac{4(9-\omega^2)}{9\varepsilon_{max}\left(1+\frac{5}{3}\operatorname{ctg}^2\varphi_s\right)}. \tag{10}$$

The logarithm branch is chosen in such a manner that the logarithm value for Im y > 0 lies on the first sheet. The figure shows the stability region for the blob, plotted in the plane of the convex variable ξ_1 for the linearly falling (a) and the linearly rising (b) distributions.

The stability criteria for blobs characterized by higher moments are established in a similar manner. It should be mentioned that it is rather difficult to consider the stability of higher moments by using the method of moments [1]. We shall formulate a general statement concerning the stability of higher moments for a small blob. The characteristic equation for the k-th moment is given by

$$\xi_{k-2}=\pi J_k\left(1+\frac{5}{3}\operatorname{ctg}\varphi_s\right), \tag{11}$$

where ξ_{k-2} is a $(k-2)$-power polynomial with respect to ε_{max}, and

$$J_k=\int\frac{df_0}{d\varepsilon}\cdot\frac{\varepsilon^k\,d\varepsilon}{\varepsilon-x}, \qquad x=\frac{4\,(k^2-\omega^2)}{k^2\varepsilon_{max}\left(1+\frac{5}{3}\operatorname{ctg}^2\varphi_s\right)}. \tag{12}$$

For a uniform distribution (natural damping is absent), the correction for the frequency of the k-th moment α_k that is secured by the automatic control system is proportional to the $(k-1)$th moment of the equilibrium distribution function $\left[\alpha_k\approx\varepsilon_{max}^{k-1}=\varepsilon^{\overline{k-1}}=\int\varepsilon^{k-1}f_0(\varepsilon)\,d\varepsilon\right]$. By calculating J_k for any other equilibrium distribution function, we readily see that the order of natural damping for the k-th moment is ε_{max}^{k-2}. Therefore, the effect connected only with the automatic control system, which is a small quantity of a higher order with respect to ε_{max}, is less important. Thus, the stability of higher moments is basically determined by natural damping, i.e., by the form of the blob's equilibrium distribution function. For small blobs, the moments rapidly decrease with an increase in their numbers. The stability (instability) regions of higher moments given by Eq. (11) became narrower. In practice, the stability criterion for small blobs depends on the first, the second, and, perhaps, the third, moments. Higher moments apparently have no significance. At high frequencies $\omega \gg 1$, the stability of small blobs is determined by the criterion for the stability of the center of gravity. The above results naturally cannot be applied to blobs whose dimensions cannot be considered as being small, since expansions of the type (3) cannot be used in this case.

The author acknowledges his deep gratitude to A. N. Lebedev for his guidance in the work and to A. A. Kolomenskii for the discussion.

LITERATURE CITED

1. É. A. Zhil'kov and A. N. Lebedev, Present issue, p. 22.
2. H. G. Hereward, Proc. of Intern. Conf. on High Energy Accel. Brookhaven (1961), p. 236.
3. L. D. Landau and E. M. Lifshits, Mechanics [in Russian] (Moscow, Fizmatgiz, 1958), Paragraph 29.
4. É. A. Zhil'kov, Pribory i tekhnika éksperimenta, No. 1 (1965).

SIMPLE METHOD FOR MEASURING THE FREQUENCY OF FREE TRANSVERSE OSCILLATIONS IN CYCLOTRONS

(UDC 621.384.612)

S. A. Kheifets and S. K. Esin

Translated from Atomnaya Énergiya, Vol. 18, No. 1,
p. 60, January, 1965
Original article submitted January 29, 1964

The usual method for measuring the frequency of transverse oscillations of particles in cyclotrons consists in exciting coherent betatron oscillations and measuring the frequency of the voltage induced at the signal electrodes [1, 2]. The energy scattering of particles in the circulating beam leads to a rapid disappearance of the coherent part of oscillations. If it is necessary to measure the frequency fairly often (in comparison with the damping time), repeated pulse excitations of oscillations may result in a considerable increase in the beam's aperture. We shall demonstrate that the frequencies of transverse oscillations can also be measured by introducing local perturbations of the equilibrium orbit which are constant in time. We shall assume that a certain perturbation exists at the azimuth s_0. In this case, the right-hand side appears in the equation describing transverse oscillations:

$$\frac{d^2x}{ds^2}+\omega^2(s)\,x=\Pi_{s_0}(s), \tag{1}$$

where

$$\Pi_{s_0}(s)=\begin{cases}0, & 0\leqslant s<s_0-a,\\ \Pi_0, & s_0-a\leqslant s\leqslant s_0+a,\\ 0, & s_0+a<s\leqslant L\end{cases} \tag{2}$$

where L is the orbit length.

The forced solution of equation (1), which describes a new equilibrium orbit with respect to which free oscillations take place, is given by

$$x(s)=\frac{\Pi_0}{2\sin\pi Q}\,\xi\,|\varphi(s)|\cos[\tau(s)-\eta+\pi Q\varepsilon]. \tag{3}$$

It should be noted that this equation describes the equilibrium orbit only outside the perturbed section. In this equation, $\varphi(s) = |\varphi(s)|\exp i\tau(s)$ is the Floquet function, normalized by the condition $\varphi(d\varphi^*/ds) - \varphi^*(d\varphi/ds) = -2i$; Q is the number of betatron oscillations per revolution, and

$$\varepsilon=\begin{cases}+1, & 0\leqslant s<s_0-a,\\ -1, & s_0+a<s\leqslant L.\end{cases} \tag{4}$$

The modulus and the phase of the integral $\int_{s_0-a}^{s_0+a}\varphi ds$ are denoted by ξ and η, respectively.

We shall now assume that the azimuthal length of the perturbation is $2a \ll L/Q$. In this case,

$$\xi=\int_{s_0-a}^{s_0+a}|\varphi(s)|\,ds=2a\,|\bar{\varphi}|_{s_0};$$
$$\eta=\tau(s_0). \tag{5}$$

It is readily seen that the shift of the equilibrium orbit at the azimuth $s_0 + L/2$ is

$$x\left(s_0+\frac{L}{2}\right)=\frac{\Pi_0 a}{\sin \pi Q}|\varphi(s_0)|\cdot|\bar{\varphi}|_{s_0}. \tag{6}$$

This follows from the fact that

$$\tau(s)=\frac{2\pi Q}{L}s+\chi(s), \tag{7}$$

where $\chi(s)$ is a periodic function whose period is equal to the period of the function $\omega^2(s)$ in Eq. (1). Hence it follows that, after measuring the difference between the equilibrium orbit positions at the azimuth diametrically opposite to the local perturbation for the cases of applied and removed perturbation, relationship (6) can be used for determining the difference between Q and the nearest integer.

The change in the modulus of the Floquet function that enters expression (6) is quadratic with respect to $\Delta\omega^2$ [3] for distortions which preserve the periodicity of the magnetic structure. In the general case, gradient distortions can be represented as a sum of two parts, one of which has the same period as the basic structure, while the other, which is nonperiodic, alters $|\varphi|^2$ in the first order. Due to this, the frequency correction which appears due to the second part cannot be rigorously determined by means of a single local perturbation. Nevertheless, the frequency value can be obtained with a sufficiently high accuracy by averaging the measurement results for several locations of perturbation.

If we neglect the second term in relationship (7), an approximate equation for the equilibrium orbit outside the perturbed section can be obtained from Eq. (3):

$$x(s)=\frac{\Pi_0|\bar{\varphi}|_{s_0}a}{\sin \pi Q}|\varphi(s)|\cos 2\pi Q\left(\frac{s-s_0}{L}+\frac{\varepsilon}{2}\right). \tag{8}$$

This expression indicates that, in the presence of local perturbation, the spatial frequency of orbit distortions is equal to the number of betatron oscillations under the above assumptions. The change in the phase of the cosine curve in Eq. (8) that occurs at the perturbed section [see Eq. (4)] secures the closure of the orbit regardless of the fact that the number of oscillations Q is not an integer.

LITERATURE CITED

1. A. A. Vasil'ev, A. A. Kuz'min, and V. A. Uvarov, Pribory i tekhnika éksperimenta, No. 4, 134 (1962).
2. V. V. Vladimirskii, et al., Pribory i tekhnika éksperimenta, No. 4, 245 (1962).
3. Yu. F. Orlov and S. A. Kheifets, Electron Accelerators. Transactions of the Third Intercollegiate Conference [in Russian] (Izd. Tomskogo Universiteta, 1961).

NOMOGRAMS FOR DETERMINING THE POTENTIAL BARRIER'S HEIGHT AND FOR THE BREIT-WIGNER FORMULA

(UDC 539.170.13)

G. N. Potetyunko

Translated from Atomnaya Énergiya, Vol. 18, No. 1,
pp. 61-62, January, 1965
Original article submitted January 9, 1964

The equations of the elements (scales and binary fields) of two nomograms for determining the potential barrier's height and for the Breit-Wigner formula are derived in the present article. The method of equalized points was used for plotting the first nomogram [1], and the method of oriented transparencies was used for plotting the other nomogram [2].

The potential barrier's height is determined by the equation

$$V=\left[1.4399\frac{Z_1Z_2}{a}+20.906\frac{l(l+1)}{Ma^2}\right] \tag{1}$$

where Z_1 and Z_2 are the charges of colliding particles, M is their reduced mass, and a is the channel radius [3].

Let us introduce new independent variables: $Z = Z_1Z_2$ and $L = 20{,}906,\ l(l+1)$. Then, expression (1) is reduced to the Cauchy form with a binary field:

$$Va^2-\alpha Za-\frac{L}{M}=0, \qquad \alpha=1.4399. \tag{2}$$

The equations of the nomogram scales are given by

$$\left.\begin{aligned} &x_1=0,\quad y_1=\mu_1V,\quad x_2=d,\quad y_2=h+\mu_2\alpha Z,\\ &x_3=\frac{d}{1-\mu a},\quad y_3=\left(h-\mu_2\frac{L}{M'}\right)\frac{x_3}{d}. \end{aligned}\right\} \tag{3}$$

Here, μ_1 and μ_2 are the moduli of the V and Z scales, $\mu = \mu_2/\mu_1$; d is the distance between these scales, h is the difference between the ordinates of the Z = 0 and V = 0 points, and M' = Ma.

The V and Z scales are drawn on parallel straight lines. The binary field (a; M') constitutes the totality of two families of straight lines. The straight lines which depend on a are parallel to the V and Z scales; the straight lines which depend on M' constitute a pencil of lines with the center at the point x = 0 and y = 0. The slope of the pencil depends not only on M', but also on l. Therefore, a separate nomogram must be drawn for each l value. The simple nomogram plot and the rules for utilizing it are shown in Fig. 1.

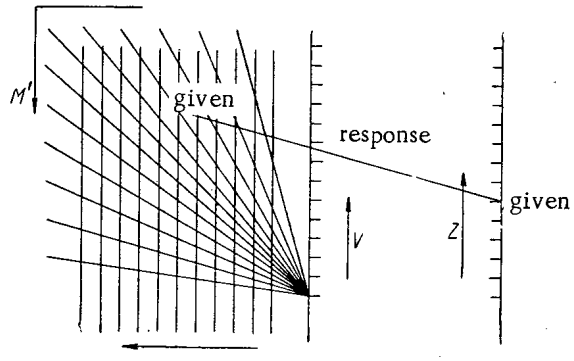

Fig. 1. Diagram of the nomogram for determining the potential barrier's height.

Let us consider in greater detail the case where $l = 0$; in this case, the pencil of straight lines in nomogram (3) degenerates into the straight line that carries the a scale. However, for $l = 0$, besides this nomogram, it is possible to draw another nomogram, which is more convenient for large Z_i values than the one obtained above. Actually, for $l = 0$, Eq. (1) assumes the following form:

$$V=1.4399\frac{Z_1Z_2}{a}. \tag{4}$$

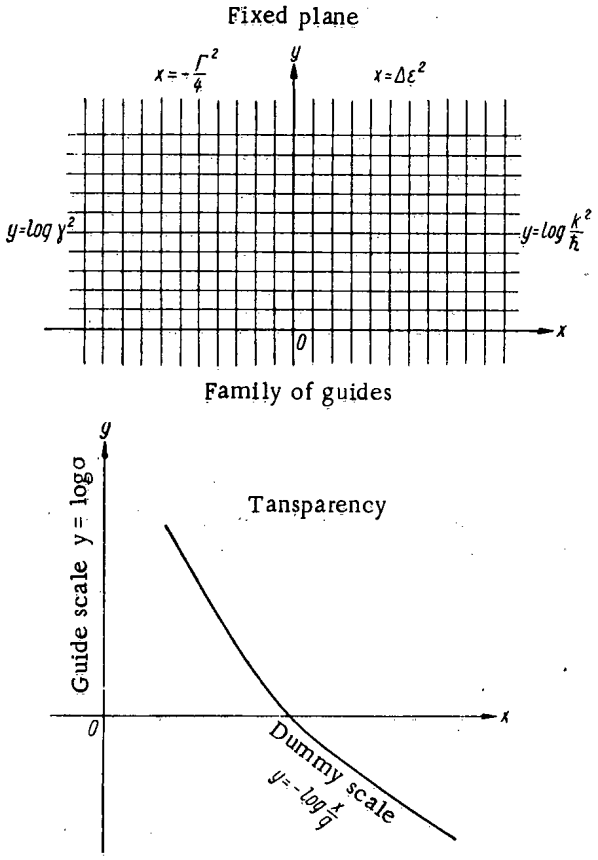

Fig. 2. Diagram of the nomogram for the Breit-Wigner formula.

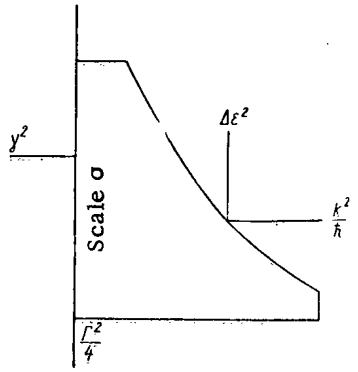

Fig. 3. Scheme for utilizing the nomogram for the Breit-Wigner formula.

For Eq. (4), a composite nomogram with parallel logarithmic scales can be drawn by using the ordinary method [1] without introducing the auxiliary Z.

We shall now plot the nomogram for the Breit-Wigner formula:

$$\sigma_r = g\frac{\hbar}{k^2}\cdot\frac{\gamma_1\gamma_2}{(\varepsilon-\varepsilon_r)^2+\frac{\Gamma^2}{4}}, \qquad (5)$$

$$\sigma_e = g\frac{\hbar}{k^2}\cdot\frac{\gamma_0^2}{(\varepsilon-\varepsilon_r)^2+\frac{\Gamma^2}{4}}. \qquad (6)$$

We shall introduce the new variables $\Delta\varepsilon \equiv \varepsilon - \varepsilon_r$ and $\gamma^2 = \gamma_1\gamma_2$ in Eq. (5). The replacement of the product of the partial widths γ_1 and γ_2 by the square of a certain different width (which will be referred to as the nomographic width) makes it possible to use a single nomogram for both Eqs. (5) and (6). In order to find γ with respect to the assigned γ_1 and γ_2 values, we can plot a nomogram consisting of equalized points on parallel logarithmic scales.

We shall now write (5) in the form of the system of equations

$$\frac{\hbar\gamma^2}{\sigma k^2} = \lambda, \quad \frac{\Delta\varepsilon^2+\frac{\Gamma^2}{4}}{g} = \lambda. \qquad (7)$$

We shall draw a nomogram for this system by using the method of oriented transparencies [2]. For this, we shall reduce (7) to the basic canonic form:

$$\Delta\varepsilon^2 - \lambda g = -\frac{\Gamma^2}{4} - 0, \quad \lg\frac{k^2}{\hbar} + \lg\lambda = \lg\gamma^2 - \lg\sigma.$$

The very simple equations of the nomogram have the following form:

Fixed plane

Field $(\Delta\varepsilon, k)$: $x = \Delta\varepsilon^2$; $y = \log k^2/\pi$.
Field (Γ, γ): $x = -\frac{1}{4}\Gamma^2$; $y = \log\gamma^2$.

Transparency

Dummy scale: $x = g\lambda$; $y = -\log\lambda$.
Scale σ: $x = 0$; $y = \log\sigma$.

It is obvious that the fixed plane contains two binary fields, which constitute the totality of straight lines that are parallel to the coordinate axes. In this case, the $(\Delta\varepsilon, k)$ field is located in the right-hand half-plane, while the (Γ, γ) field is located in the left-hand half-plane. The transparency has the $y = \log\sigma$ scale and the dummy scale of the auxiliary variable λ, whose equation is $y = -\log x/g$. The type of the dummy scale depends on the value of the statistical factor g. Therefore, a separate transparency is necessary for each g value. It is, of course, possible to use only a single transparency and draw the dummy scales for all g value on a single sheet of paper. However, one must use such a nomogram not according to the rules given below, but according to the rules proposed in [4].

When superimposing the transparency on the fixed plane, the dummy scale of the transparency is brought into contact with the point of the binary field ($\Delta\varepsilon$, k), while the σ scale is brought into contact with the point of the binary field (Γ; γ). The transparency is oriented by means of the straight-line guide of the transparency (scale σ), which must be parallel to the family of guides of the fixed plane (vertical straight lines).

The simple nomogram is shown in Fig. 2, while the scheme for using it is given in Fig. 3.

LITERATURE CITED

1. M. V. Pentkovskii, Nomography [in Russian] (Moscow, Gostkhteoretizdat, 1949).
2. G. S. Khovanskii, Nomograms with Oriented Transparencies [in Russian] (Moscow, Gostekhteoretizdat, 1957).
3. Nuclear Physics Manual [Russian translation from the English], Edited by L. A. Artsimovich (Moscow, Fizmatigiz, 1963).
4. B. A. Sirenko, Collection of Articles on Nomography No. 1 [in Russian] (Moscow, Izd. Vychislitel'nogo, Tsentra AN SSSR, 1963), p. 92.

SIMPLE UNSTEADY-STATE KINETIC EQUATION

(UDC 539.121.7)

V. G. Morozov and S. A. Kholin

Translated from Atomnaya Énergiya, Vol. 18, No. 1,
pp. 62-63, January, 1965
Original article submitted January 31, 1964

We have found the solution, integrated with respect to the angle of the one-velocity kinetic equation for an infinite homogeneous medium with isotropic plane or a point source. The scattering is considered as isotropic in the laboratory system.

The kinetic equation for the distribution density of particles in the case of a plane isotropic source is given by

$$\frac{\partial\psi}{\partial t}+v\mu\frac{\partial\psi}{\partial x}+\beta\psi=\frac{h}{2}\int\limits_{-1}^{1}\psi\,d\mu+\frac{1}{2}\,\delta(x)\,\delta(t), \tag{1}$$

where $\beta = 1/l_{tot}$ is the reciprocal of the total range, $h = 1/l_s$ is the reciprocal of the scattering range, v is the velocity of particles, and x is the distance from the radiating plane.

The solution, integrated with respect to the angle, of the problem (1) for an isotropic point source $[\psi_{sp}(r, t)]$ is related to the corresponding solution of Eq. (1) for a plane source $[\psi_{pl}(x, t)]$:

$$\psi_{sp}(r,\ t)=-\frac{1}{2\pi x}\cdot\frac{d}{dx}\psi_{pl}\ (x,\ t)\Big|_{x=r}, \tag{2}$$

where r is the distance from the point source. The solution of equation (1) was obtained by using two methods: the method of the double Laplace transform and Monin's corrected method. The solution is expressed by the integral along the contour l (Fig. 1) in the complex z plane:

$$\psi_{pl}(x,\ t)=\frac{e^{-\beta vt}}{2vt}\left\{\theta\left(1-\left|\frac{x}{vt}\right|\right)+\frac{hvt}{\pi i}\int\limits_{l}\left(\frac{1}{2}\ln\frac{z+1}{z-1}\right)^{2}\exp\left[\frac{hvt}{2}\left(z+\frac{x}{vt}\right)\ln\frac{z+1}{z-1}\right]dz\right\}. \tag{3}$$

The solution for the point source is obtained by simply differentiating (2); it is given by

$$\begin{aligned}\psi_{sp}(r,\ t)&=\frac{e^{-\beta vt}}{4\pi r^{2}}\left\{\delta(r-vt)+h\frac{r}{vt}\ln\frac{vt+r}{vt-r}-\frac{h}{\pi i}(hr)\int\limits_{l}\left(\frac{1}{2}\ln\frac{z+1}{z-1}\right)^{3}\exp\left[\frac{hvt}{2}\left(z+\frac{z}{vt}\right)\ln\frac{z+1}{z-1}\right]dz\right\}\\&=\frac{e^{-\beta vt}}{4\pi r^{2}}\left[\delta(r-vt)+h\Phi\left(hr,\ \frac{r}{vt}\right)\right].\end{aligned} \tag{4}$$

Decomposition with respect to powers of h constitutes decomposition with respect to collisions. In actual calculations, it is better to transform the above contour into the contour L (see Fig. 1). The $\exp(-\beta vt)\Phi(hr, r/vt)$ function was calculated for several distance values equivalent to two, three, four, and six ranges without absorption ($\beta = h$) (Fig. 2). It is seen that a diffusion maximum appears at $hr = 3$. The asymptotic form of solution (4) for $vt \to \infty$ implies diffusion behavior:

$$\psi_{sp}(r\ ,\ t)\cong\frac{e^{-\beta vt}}{4\pi r^{2}}\ \frac{2h}{\pi}\,hr\int\limits_{0}^{\pi/2}\frac{\psi\sin hr\psi}{\sin^{2}\psi}\,e^{hvt\psi\operatorname{ctg}\psi}\,d\psi\to\frac{1}{8}\left(\frac{1}{\pi Dt}\right)^{3/2},$$

where $D = l_s v/3$ is the diffusion factor; $vt \gg r$.

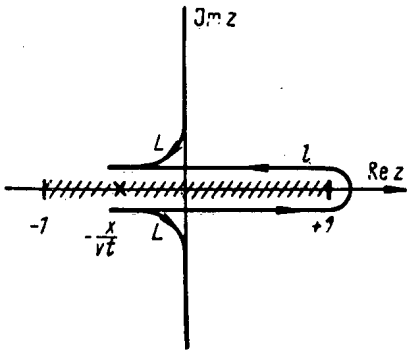

Fig. 1. Integration contour.

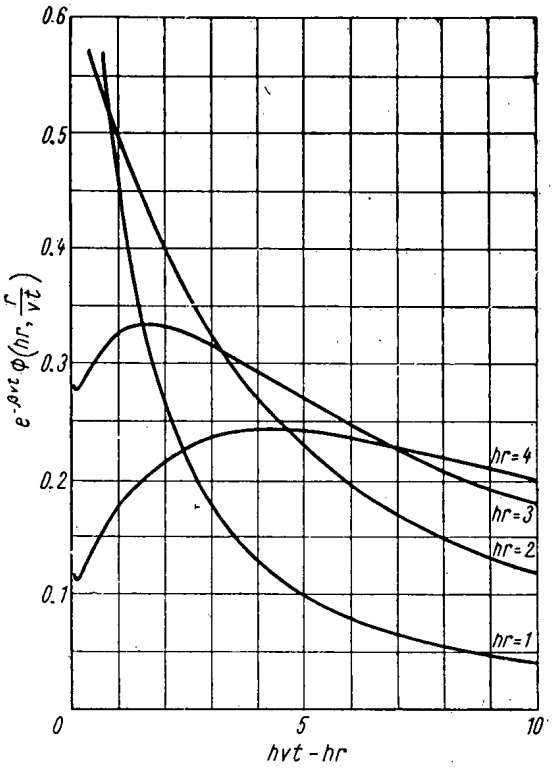

Fig. 2. The $e^{-hvt}\,\Phi(hr, \frac{r}{vt})$ function for distances equivalent to 2, 3, 4, and 6 ranges without absorption (β = h).

Monin attempted to solve this problem [1], but his solution contained an error which prevented him from finding the correct answer. In solving the singular equations

$$\frac{\partial^n}{\partial\eta^n} F_n^{\pm}(\eta, \mu) = \frac{n}{2}\left[P\frac{1}{\mu-\eta} \pm i\pi\delta(\mu-\eta)\right]\frac{\partial^{n-1}}{\partial\eta^{n-1}}\int_{-1}^{1} F_{n-1}^{\pm}(\eta, \mu)\,d\mu,$$

where $-1 \leq \mu \leq 1$; $-1 < \eta \leq 1$, he erroneously omitted the δ-function.

LITERATURE CITED

1. A. S. Monin, Teoriya Veroyatnosti i Ee Primenenie, 1, 328 (1956).

ANGULAR DISTRIBUTION OF γ-QUANTA IN U^{233}, U^{235}, AND Pu^{239} FISSION ON THERMAL NEUTRONS

(UDC 539.17.015:539.173.4)

G. A. Petrov, D. M. Kaminker, G. V. Val'skii, and L. A. Popeko

Translated from Atomnaya Énergiya, Vol. 18, No. 1, pp. 64-65, January, 1965
Original article submitted February 26, 1964

Anisotropy in the emission of γ-quanta in U^{233}, U^{239}, and Pu^{239} fission on thermal neutrons was noted in [1-4]; however, the data obtained there are highly contradictory.

The aim of the experiments described here was to measure the angular correlation of the fragments and γ-rays produced in the fission of U^{233}, U^{235}, Pu^{239} on thermal neutrons in order to find the dependence of the degree of anisotropy on the nature of the target nucleus and the energy of γ-quanta.

In designing the experimental device, we took into account the possibility of measuring the dependence of anisotropy on the mass ratio of fission fragments. Therefore, n-p semiconductor detectors with operating areas of 0.25, 0.5, and 1 cm^2 were used for the recording the spectrometric measurements of fission fragments. FÉU-13 and FÉU-33 photomultipliers with NaI(Tl) crystals, whose height and diameter were equal to 60 mm, were used for the recording of γ-quanta. Special attention was paid to strict symmetry of the system and reliable separation from prompt fission neutrons, which, in a laboratory system, are emitted basically in the direction of fission.

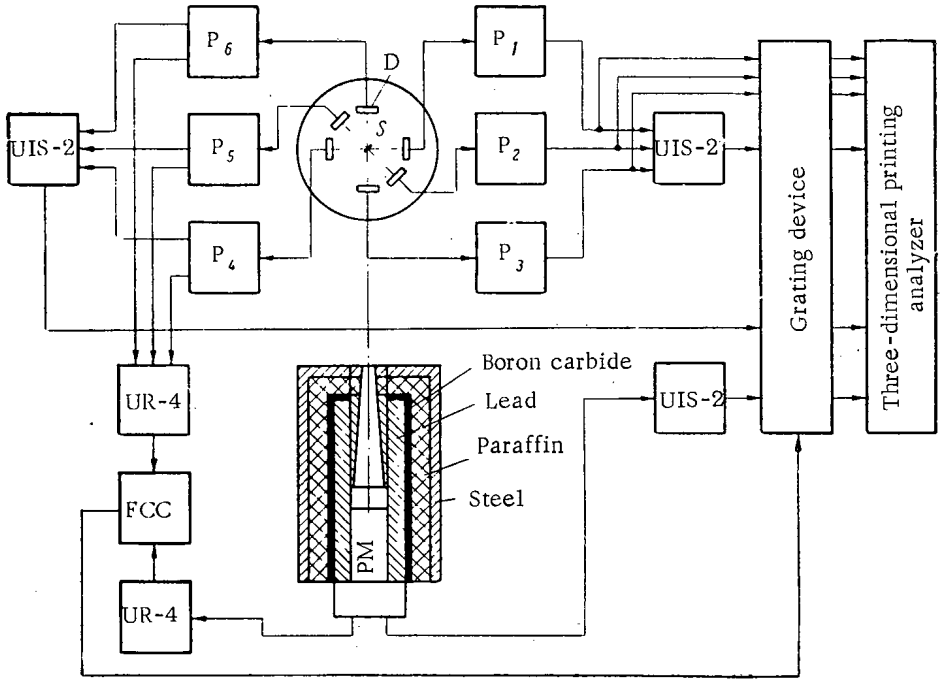

Fig. 1. Block diagram of the experimental setup. S) Fission source; D) semiconductor detectors; P) low-noise preamplifiers; UIS-2) linear amplifiers; UR-4) fast amplifiers; FCC) fast coincidence circuit.

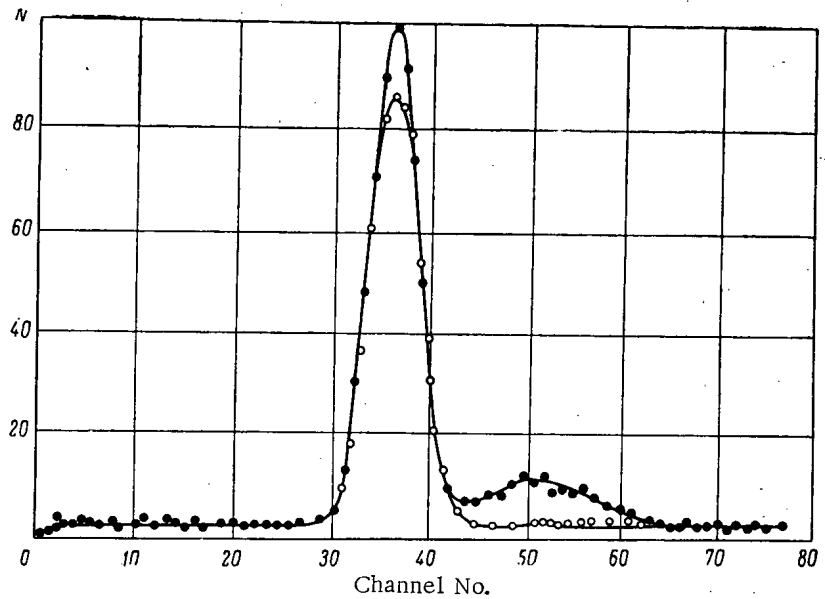

Fig. 2. Distribution of converter amplitudes for a 1.1 nsec with of the analyzer channel. ●) 0°; ○) 90°.

TABLE 1. Angular Distribution of Fission γ-Quanta

Target nucleus	No. of fissions, 10^6			Degree of anisotropy, %		Threshold of γ-quanta
	0°	45°	90°	0°	45°	
U^{233}	34	10	43	13±2	11±3	100 keV
	35.5	—	30.5	12±2	—	480 keV
	23.5	—	22	9±3	—	100 keV 1 cm Pb
Pu^{239}	39	20	40	14±2	10±3	100 keV
	54	—	54.8	16±2	—	100 keV 1 cm Pb

A multichannel experimental device with a fast-slow coincidence circuit [$\tau = (1\text{-}2) \cdot 10^{-8}$ sec] was used in the first experiments on measuring the correlation between γ-rays and fragments in U^{235} fission. The number of fast coincidences of pulses produced by γ-quanta with energies above 100 keV and the pulses produced by fission fragments were measured simultaneously for three angles. The amplitudes of pulses from paired fragments and γ-quanta and the angle between the directions of emergence of fragments and γ-quanta were recorded on the strip chart of a three-dimensional analyzer (the block diagram of the experimental setup is shown in Fig. 1).

The semiconductor detectors and the fissionable material (0.1 mg/cm^2), which was deposited on a Teflon film (20 μg/cm^2), were placed in a cylindrical thin-walled aluminum vacuum chamber. The beam of thermal neutrons from the reactor's horizontal channel was directed along the axis of the chamber. The photomultiplier was placed in a combined shield consisting of lead, paraffin, and iron at a distance of 50-70 cm from the chamber's axis. Experiments have shown that the probability of the emission of γ-quanta under an angle of 0°, with respect to the direction of fission is somewhat higher than the probability of emission under an angle of 90° with an anisotropy of (12 ± 2)%. This is in good agreement with the results obtained in [4], while it contradicts the data from [1-3].

The angular distribution of γ-radiation in the fission of U^{233} and Pu^{239} and the dependence of anisotropy on the energy of γ-quanta were measured by means of a single-channel experimental device. In this device, the fast coincidence circuit was replaced by a converter for transforming time into amplitude, which provided reliable control of the separation of fast neutrons. The resolving time was 5-8 nsec.

The experimental geometry was the same as in the first experiments, with the difference, however, that only a single semiconductor detector was used. One of the patterns obtained in the 100-channel Raduga amplitude analyzer is shown in Fig. 2. The left-hand peak pertains to γ-rays, while the right-hand peak pertains to fission neutrons. The background of random coincidences was determined separately for each pattern and subtracted from the area under the peak due to γ-rays. In these experiments, we used U^{235}, U^{233}, Pu^{239} sources with a thickness of 1 mg/cm^2 and a spot diameter of $\sim$ 8 mm, which were deposited on an aluminum foil with a thickness of 5 μ. In order to prevent the recording of pulses due to α-particles, the discrimination threshold was set at a level exceeding the amplitude of these pulses by a factor of 2-3, in which approximately 80% of fission fragments that reached the detector were recorded. At the beginning and at the end of measurements, the system's symmetry was checked by means of Hf^{181}, Cs^{137}, and Co^{60} sources, which were placed in the chamber instead of the target. The absence of asymmetry was checked with an accuracy to 1% for γ-quanta whose energies exceeded 50 keV.

The resolution of the γ-spectrometer for the Cs^{137} line was 15%. The discrimination threshold for pulses due to γ-quanta varied from 100 to 480 keV. Several series of measurements were performed using a 100-keV dicrimination threshold and a lead filter (thickness: 1 cm) in the path of γ-quanta. The measurement results are given in the table; the statistical errors are indicated. The correction for the finite solid angles of the detectors produced an average increase of 0.5% in the anisotropy.

These results make it possible to draw the following conclusions. The anisotropy values are close to each other for U^{233}, U^{235}, and Pu^{239}. As was mentioned in [5], the spins of the basic states of target nuclei may cause a certain disorientation of the angular momentum arising as a result of noncentral breakup of the neck in fission. If such an effect takes place, the maximum difference between anisotropies should be expected for U^{235} (7/2) and Pu^{239} (1/2).

Our results yield somewhat larger values of the anisotropy of γ-quanta in the case of Pu^{239}. However, the measurement accuracy must be higher if a more definite conclusion is to be reached. Within the limits of measurement errors, the anisotropy value does not change in the range of γ-quantum energies from 100 to 500 keV. This result can be checked by directly comparing the spectra of γ-quanta in fission at the angles of 0 and 90°.

The experiments were performed by using the VVRM reactor of the Leningrad Institute of Physics and Technology. The authors take this opportunity to express their gratitude to the personnel servicing the reactor.

LITERATURE CITED

1. W. Whitehouse, Progr. Nucl. Phys., 2, 150 (1952).
2. R. Leachman, Proc. of the Second Intern. Conf. on the Peaceful Uses of Atomic Energy, Geneva, U. N. (1958), Vol. 15, P/665.
3. M. Hoffman, Bull. Amer. Phys. Soc., Ser. 2, 3, 1 (1958).
4. M. V. Blinov, et al., ZhETF, 43, 1644 (1962).
5. V. M. Strutinskii, ZhETF, 37, 861 (1959).

DETERMINATION OF THE ABSOLUTE YIELD OF THE 74-keV U^{239} AND 87-keV Th^{233} γ-LINES

(UDC 539.166)

L. N. Yurova and A. V. Bushuev

Translated from Atomnaya Énergiya, Vol. 18, No. 1,
pp. 65-67, January, 1965
Original article submitted June 24, 1964

Certain parameters of physical processes that occur in nuclear reactors containing U^{238} or thorium, such as conversion ratio, the effective resonance integral, the probability of the avoidance of resonance capture, and cadmium ratios, can be investigated by recording the γ-radiation of U^{239} or Th^{233}. In order to estimate the efficiency of these methods, it is necessary to know the absolute yields of these radiations (the number of γ-quanta per decay). The absolute yield of the U^{239} line with E_γ = 74 keV is not known at the present time [1, 2], while the only source of data on the most intensive Th^{233} line with E_γ = 87 keV is the private communication mentioned in [2]. The absolute yields of the above lines were measured with respect to the x-ray Au^{198} line with an energy of 72 keV, the absolute yield of which is known with a high degree of accuracy; it is equal to 2.57 ± 0.07% [3]. The measurements method consisted in the following: specimens of Au^{197} and U^{238} or Au^{197} and Th^{232} were simultaneously irradiated in the graphite prism of a thermal reactor. The γ-radiation spectra of the irradiated specimens were investigated by means of a scintillation spectrometer with a NaI(Tl) crystal and a 100-channel amplitude analyzer. The figure shows the measured spectra of U^{239}, Th^{233}, and Au^{198}. The areas under the photopeaks of the lines under investigation were determined with respect to these spectra. As is known [4, 5], the areas under the photopeaks of γ-lines serve as the measure of their intensity in the low-energy range. Six to eight repeated measurements were performed on each of the specimens. The results of these measurements were used for plotting the decay curves and determining the intensity of the corresponding lines at the instant when the irradiation was terminated. The measured intensity J of a line is related to its absolute yield α by the following expression:

$$J = n\bar{v}N\sigma_{th}\left(1-\frac{1}{R}\right)(1-e^{-\lambda t})\,\alpha\omega p\mu_{\text{ph}}g,$$

where nv is the neutron flux in which the specimen was irradiated, t is the irradiation time, N is the number of nuclei of the isotope to be investigated in the specimen, λ is the radioactive decay constant of the isotope under investigation, σ_{th} is the cross section of thermal neutron capture by nuclei of the isotope under investigation, ω is the share of the γ-quanta emitted by the specimen that have reached the spectrometer's crystal, p is the probability of absorption of the γ-quantum under investigation in the crystal, μ_{ph} is the relative probability of the photoeffect for the γ-quantum under investigation, g is a coefficient which takes into account self-absorption of the radiation under investigation in the specimen, and R is the cadmium ratio for the isotope under investigation at the irradiation point.

Specimens of U^{238} and gold (or Th^{232} and gold) were irradiated in the same neutron flux over the same period of time. The dimensions of all specimens and the measurement geometry were identical. The measurements were performed by means of a 40 × 40 mm NaI(Tl) crystal, which secured a 100% efficiency in recording all the γ-radiation under investigation.

The energies of all the γ-lines mentioned are so low that practically all their interactions with matter in the crystal can be reduced to the photoeffect, i. e., $\mu_{ph} = 1$. Considering what has been said above, the intensities of any two of the lines under investigation can be expressed in the following manner:

$$\frac{J_1}{J_2} = B\frac{N_1\left(1-\frac{1}{R_1}\right)\alpha_1 g_1}{N_2\left(1-\frac{1}{R_2}\right)\alpha_2 g_2},$$

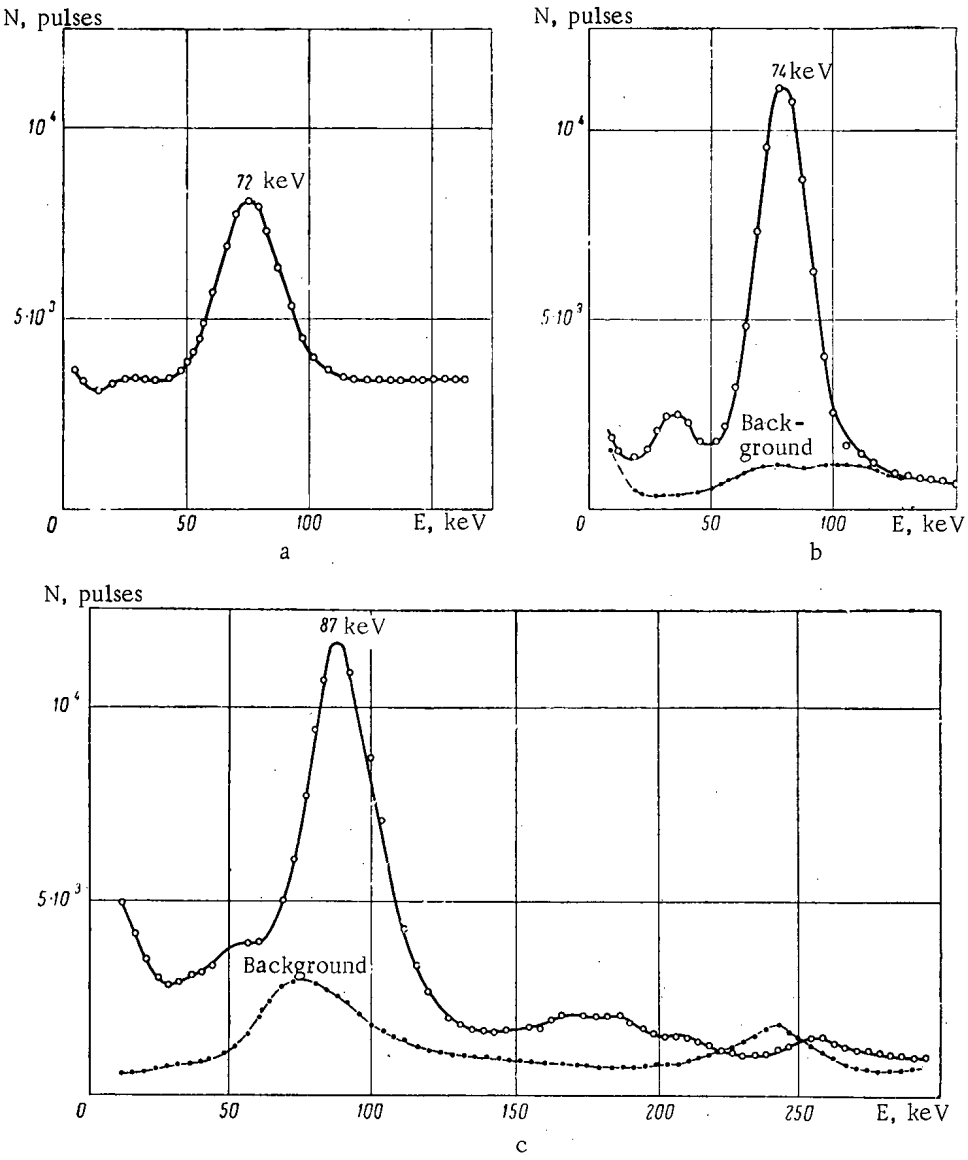

Fig. 1. Measured γ-spectra of Au^{198} (a), U^{239} (b), and Th^{233} (c).

where

$$B=\frac{\sigma_{th_1}(1-e^{-\lambda_1 t})}{\sigma_{th_2}(1-e^{-\lambda_2 t})}.$$

The σ_{th} values were borrowed from [6], while the λ values were taken from [1]. The chemical composition of the specimens was investigated by means of chemical and spectral analysis. The impurities detected in analysis could not produce a noticeable background, which was confirmed by the measurement results; extraneous γ-radiations that would vary in time were not detected in the experiments. The concentration of U^{235} in uranium specimens amounted to 1/230 of the concentration in a natural mixture of isotopes, so that the background of fission fragments was absent in measurements.

Knowing the exact weight of specimens and their chemical compositions and isotope concentrations, we determined N—the number of atoms of the isotope under investigation in the specimen. The cadmium ratios R were determined experimentally.

The self-absorption values for thorium, gold, and uranium specimens differed from each other due to the difference between the atomic numbers of the elements and the energies of the radiations under investigation. Therefore, the J_1/J_2 ratio was determined for infinitely thin specimens, for which the measurements were performed with

sets of specimens with different thicknesses. The thus measured ratios of intensities of the 74-keV U^{239} and the 72-keV Au^{198} lines and also of the 87-keV Th^{233} and the 72-keV Au^{198} lines made it possible to determine the ratios of absolute yields of these uranium and thorium lines.

If the absolute yield of the 72-keV Au^{198} line is known, then, by using the ratios measured, one can determine the absolute yield of the 74-keV U^{239} line, which is equal to 43.5 ± 3.0%, and the absolute yield of the 87-keV Th^{233} line, which is equal to 2.9 ± 0.2%. The latter value agrees with data in the private communication mentioned in [2], according to which the absolute yield of the 87-keV Th^{233} line is 2.7%.

In conclusion, we hereby extend our thanks to E. Efimov, who prepared the specimens, and to B. Zhuravlev for his help in the measurements.

LITERATURE CITED

1. B. S. Dzhelepov, et al., Decay Schemes of Radioactive Nuclei [in Russian] (Moscow–Leningrad, Izd. AN SSSR, 1963).
2. D. Strominger, J. Hollander, and G. Seaborg, Rev. Mod. Phys., 30, 2 (1958).
3. G. Nijgh, et al., Nuclear Spectroscopy Tables, North-Holland Publishing Company, Amsterdam (1959).
4. V. O. Vyazemskii, et al., Scintillation Method in Radiometry [in Russian] (Moscow, Gosatomizdat, 1961).
5. Beta- and Gamma-Spectroscopy [in Russian], Edited by K. Zigban (Moscow, Fizmatgiz, 1959).
6. D. Hughes and R. Schwartz, Neutron Cross Sections, BNL (New York, 1959).

SPATIAL DISTRIBUTION OF NEUTRONS WITH ENERGIES OF 3 AND 15 MeV IN BERYLLIUM

(UDC 539.125.52)

S. P. Belov, V. A. Dulin, Yu. A. Kazanskii, and S. G. Tsypin

Translated from Atomnaya Énergiya, Vol. 18, No. 1,
pp. 67-68, January, 1965
Original article submitted January 2, 1964

Reactor reflectors constitute important shielding elements, since they exert a strong influence on the formation of the spectrum of neutrons that enter the shield. Beryllium, which has good moderating power and a small neutron absorption cross section is often used as the reflector material. The mechanical and thermodynamic properties of beryllium also satisfy the requirements imposed on reflectors.

Measurements of the spatial distribution of neutrons with initial energies of 3 and 15 MeV were performed for the purpose of investigating the shielding properties of beryllium. The $H^2(H^2, n)He^3$ and $H^3(H^2, n)He^4$ reactions were used as the neutron sources. The electrostatic generator's target was introduced into an 80 × 88 × 112-cm prism, made of metallic beryllium cubes on a 4-cm side, to a depth of 30 cm from the front end of the prism. The overall weight of the prism was 1358 kg, while the mean density was 1.72 ± 0.02 g/cm^3. Fission chambers with U^{235} and Th^{232} were used in measurements with 3-MeV neutrons; for neutrons with an energy of 15 MeV, besides the chambers, we also used threshold indicators, the energy thresholds of which are given below:

Indicator	$P^{31}(n, p)$	$Al^{27}(n, p)$	$Si^{28}(n, p)$	$Al^{27}(n, \alpha)$
Effective energy threshold, MeV	3	5	5	~7

The threshold indicators were placed in cadmium casings, which had a thickness of 0.8 mm. Since Th^{232} contained a certain amount of U^{235} impurity, while the spectrum of neutrons in beryllium contained many soft neutrons, especially at large distances, the count of the chamber with Th^{232} in the cadmium casing was multiplied by

$$A = \frac{R_{Cd}^5 - R_{Cd}^2}{R_{Cd}^5 - 1},$$

where R_{Cd}^5 and R_{Cd}^2 are the cadmium ratios for chambers with U^{235} and Th^{232}, respectively. The cadmium ratios for the fission chamber with U^{235} are given in Fig. 1. The A value was determined experimentally for all distances;

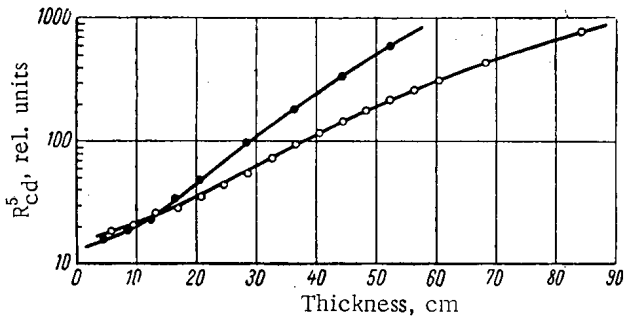

Fig. 1. Cadmium ratio in beryllium for the fission chamber with U^{235} for the following neutron energies: ●) 3 MeV; ○) 15 MeV.

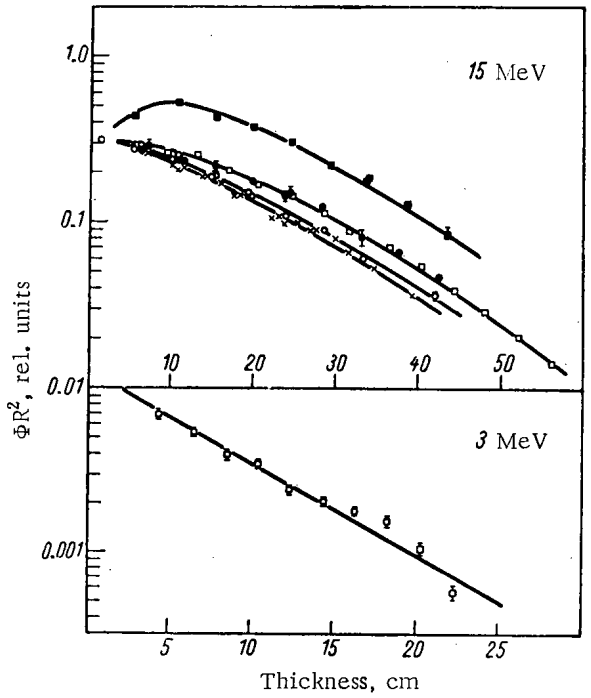

Fig. 2. Spatial distribution of 3- and 15-MeV neutrons in beryllium, measured by means of different detectors. □) $P^{31}(n, p)Si^{31}$; ●) $Al^{27}(n, p)Mg^{27}$; ○) $Al^{27}(n, \alpha)Na^{24}$; ×) $Si^{28}(n, p)Al^{28}$; □) fission chamber with Th^{232}.

for the neutron energy of 3 MeV and a distance of 20 cm, it was equal to 0.73.

The neutron attenuation curves are given in Fig. 2. From the attenuation curves for 15-MeV neutrons, it is seen that the accumulation of scattered neutrons (the rise of the attenuation curve for small thicknesses) decreases with an increase in the detector's threshold energy.

According to measurements by means of the fission chamber with Th^{232} for thicknesses over 40 cm, the relaxation length is equal to 11 cm and close to the transport length (λ_{tr} = 10.6 ± 0.5 cm) calculated with respect to data from [1]. According to measurements where the fission chamber with Th^{232} was used, the relaxation length of 3-MeV neutrons was equal to 8 cm for thicknesses of 5-20 cm. For these thicknesses, the behavior of the attenuation curve agrees well with the dosimetric curve of fission spectrum attenuation calculated in [2] (see the solid curve at the bottom of Fig. 2). It should be mentioned that the relaxation length determined with respect to the same attenuation curve [2] is equal to 7.3-7.4 cm for thicknesses over 50 cm.

Data from [3] and our data indicate that the relaxation length values calculated with respect to attenuation curves for monoenergetic neutrons for the threshold reactions are close to the λ_{tr} values for the initial neutron energy. It is interesting to note that the relaxation length of neutrons with an energy of 3 MeV, calculated with respect to the attenuation curve for the fission chamber with Th^{232} in beryllium, differs considerably from λ_{tr} = 4.5 cm, which was estimated by using the data from [4, 5]. The latter fact is probably connected with the major irregularities in the total cross section of beryllium in the energy range from 1.5 to 3 MeV.

The authors hereby acknowledge their indebtedness to V. V. Orlov for the discussion of the results and also to N. D. Lopata, V. F. Bashmakov, A. N. Nikolaev, and V. I. Popov for their help in the measurements.

LITERATURE CITED

1. M. Nakada, et al., Phys. Rev., 110, 1439 (1958).
2. H. Goldstein, Fundamental Aspects of Reactor Shielding, U.S.A., Addison–Wesley Publ. Co. (1959).
3. S. P. Belov, et al., Atomnaya Énergiya, 6, 663 (1959).
4. D. Huges and J. Harvey, Neutron Cross Sections, USA, BNL (1958).
5. M. Goldberg, V. May, and J. Stehn, Angular Distribution in Neutron-Induced Reactions, Vol. 1, USAEC, BNL-400 (1962).

REDUCTION OF THE CAPTURE γ RADIATION FROM THE REACTOR'S STRUCTURAL MATERIALS BY SCREENING THEM WITH BORON-CONTAINING SCREENS

(UDC 621.039.538.7)

B. F. Gromov, D. V. Pankratov, M. A. Solodyankin, and M. M. Sokolov

Translated from Atomnaya Énergiya, Vol. 18, No. 1, pp. 69-70, January, 1965
Original article submitted January 2, 1964

It is known that the leakage of neutrons with different energies from the reactor core may attain 20-30% of the total number of fission neutrons in the process of their moderation and diffusion. The "leakage" neutrons are subsequently absorbed by the structural materials of the reactor and its biological shield.

By using the multigroup method of calculation [1], the spatial and energy distributions of neutrons in all layers of the structural and shielding materials can be determined with sufficiently high accuracy. If the spatial and energy distributions are known, the sources of capture γ-radiation throughout the thickness of these materials can readily be determined.

Calculations of the γ-ray dose beyond the shield, which are performed by using the known spatial distribution of capture γ-radiation sources, show that a considerable contribution to the dose beyond the shield is made by γ-rays which are generated in the steel reflector, the "thermal" screen, and the reactor vessel, where the spectrum of neutrons that have leaked through is softened to a large extent due to the elastic and inelastic scattering on steel nuclei. For a thickness of $\sim$ 20 cm, the neutron spectrum which is characteristic for faily thick steel layers and is virtually invariable with respect to the corrdinate is formed.

The neutrons which have entered the low-energy region with an energy measured in tens of kiloelectron volts have a considerably larger relaxation length than fast neutrons: therefore, they pass through the steel screen with less attenuation.

Water is most often provided beyond the reactor vessel. Water effectively moderates neutrons to energies close to the thermal energy, thus producing a large splash in the flux of thermal and epithermal neutrons near the reactor vessel. A portion of neutrons that have been moderated as a result of diffision reach the reactor vessel. These neutrons are intensively absorbed by steel in the reactor vessel, whereby a strong source of secondary γ-rays is created in this boundary zone (Fig. 1).

Diffferent means for reducing the sources of such capture γ-rays are presently known and can be provided. In particular, these sources can be reduced by surrounding the reactor vessel with a screen made of a boron-containing material, which hinders the reverse flow of thermal and epithermal neutrons toward the reactor vessel.

The problem of reducing the capture γ-radiation from sources similar to those described above by means of boron-containing screens was treated in [2, 3]. The experimental results given in these papers are in satisfactory mutual agreement, and they show that, if a layer of boron carbide with a thickness of $\sim$ 20 mm is placed between steel (St. 3) and Plexiglas, the intensity of γ-radiation with an energy of 7.6 MeV will be reduced by a factor of 13.4, while the flux of γ-radiation from steel 1Kh18N9T will be reduced by a factor of 7.8.

A detailed analysis of the results of these experiments shows that the experimentally determined coefficients pertain to a particular case, namely, the case where the detector for recording γ-rays with E_γ = 7.6 MeV is located at a distance $\mu t \approx 0.5$ of the mean free path from the surface of the source.

If there is no boron screen at the interface between the reactor vessel and the hydrogenous material, the angular distribution of capture γ-rays at the surface of the source has a predominantly isotropic character. Besides

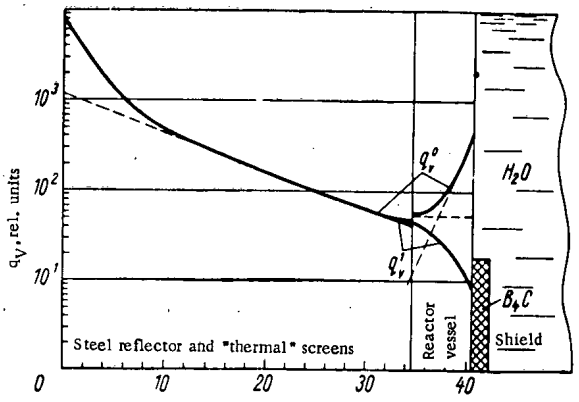

Fig. 1. Density of sources of capture γ-rays in steel. q_V^0) Without a boron screen; q_V^1) with a boron screen.

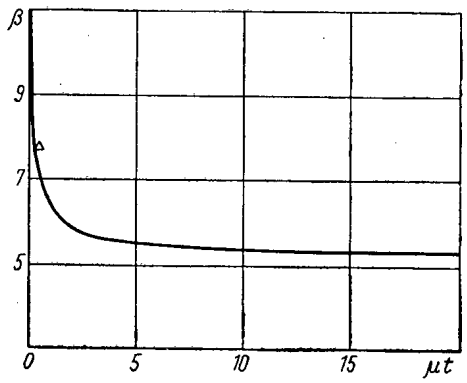

Fig. 2. Dependence of the reduction factor for capture γ-radiation secured by the boron screen on the "optical" thickness μt (in mean free path units) in the shield. Δ) Experimental result given in [2].

reducing the strength of sources of capture γ rays in the steel mass, a boron-containing screen also influences the form of their angular distribution at the steel surface. In this case, the angular distribution assumes a predominantly cosine character. It is well known that sources with equal strength, but different angular distributions (all other conditions being equal), produce different dose rates. This is due to the fact that, along the path of attenuation of γ-rays in the shield, isotropic sources are transformed into anisotropic sources due to intensive filtration, so that the reduction factor for the dose of capture γ radiation (the blocking factor) constitutes a function of the "optical" thickness μt (measured in mean free path units) between the sources and the detector.

For the confirmation of what has been said above, we calculated the spatial and energy distributions in steel screens and the reactor vessel by using the 18-group method in the P_2-approximation by means of an electronic computer for reactors with and without a boron-containing screen.

Figure 1 shows the spatial dependence of the density of capture γ-rays, calculated for the entire thickness of the steel mass with and without a boron screen. By using these sources of capture γ-rays, we can readily calculate the dose rate produced by these sources for different "optical" thicknesses μt (measured in mean free path units). The ratio of the dose rate produced by a source without the boron screen for the thickness μt to the dose rate produced by the same source with a boron screen characterizes the advantage provided by the boron screen. This factor is given by

$$\beta(\mu t) = \frac{\int\limits_{V_{\gamma\text{-sou}}} q_V^0(\mathbf{r}) \frac{e^{-\left|\int_0^{\mathbf{r}} \mu(\mathbf{r}')\,d\mathbf{r}'\right|}}{4\pi|\mathbf{r}|^2}\,dV}{\int\limits_{V_{\gamma\text{-sou}}} q_V^1(\mathbf{r}) \frac{e^{-\left|\int_0^{\mathbf{r}} \mu(\mathbf{r}')\,d\mathbf{r}'\right|}}{4\pi|\mathbf{r}|^2}\,dV}.$$

Figure 2 shows the reduction factor for the dose produced by capture γ-radiation in dependence on the "optical" thickness μt between the source and the detector. For $\mu t \approx 0.5$, the calculated value of the above factor is in satisfactory agreement with the experimental value given in [2, 3].

If a boron screen is provided in the reactor structure, the screen reduces the dose by a factor of $\beta(\mu t)$ for the thickness μt. This factor can be useful in selecting shield variants, where the dose at the point μt in question is calculated without considering a boron screen and is then reduced by a factor of β if a boron screen is to be provided.

It should be noted that the factor β depends on the composition and thickness of the steel screens and the reactor vessel as well as on the spec trum of incident neutrons.

The authors are deeply grateful to S. G. Tsypin and Yu. A. Kazanskii for their interest in the work and critical remarks.

LITERATURE CITED

1. G. I. Marchuk, Methods for Calculating Nuclear Reactors [in Russian] (Moscow, Gosatomizdat, 1961).
2. A. G. Bakov, et al., Atomnaya Énergiya, 13, No. 7 (1962).
3. D. L. Broder, et al., Atomnaya Énergiya, 8, 49 (1960).

DEPENDENCE OF THE DENSITY OF RADIATION DAMAGE TO THE REACTOR VESSEL ON THE COMPOSITION OF THE FERRO-AQUEOUS THERMAL SHIELD

(UDC 621.039.553.3)

K. K. Popkov and S. M. Rubanov

Translated from Atomnaya Énergiya, Vol. 18, No. 1,
pp. 70-71, January, 1965
Original article submitted January 15, 1964

The present article is concerned with an investigation of ferro-aqueous mixtures with different compositions for thermal shields from the point of view of the effect of the mixture composition on the radiation damage to the reactor vessel caused by neutrons. For this purpose, we considered a primary-shield composition consisting of 25 cm

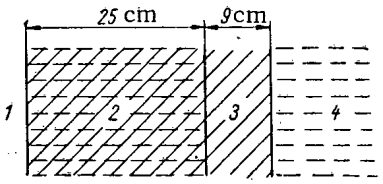

Fig. 1. Geometry of the compositions. 1) Reactor core; 2) ferro-aqueous mixture; 3) iron; 4) water.

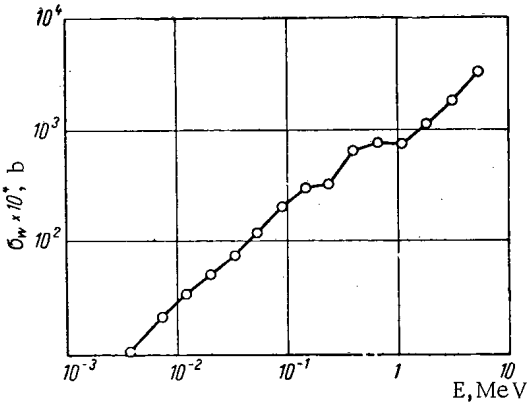

Fig. 2. Microscopic cross section of the generation of radiation damage [2].

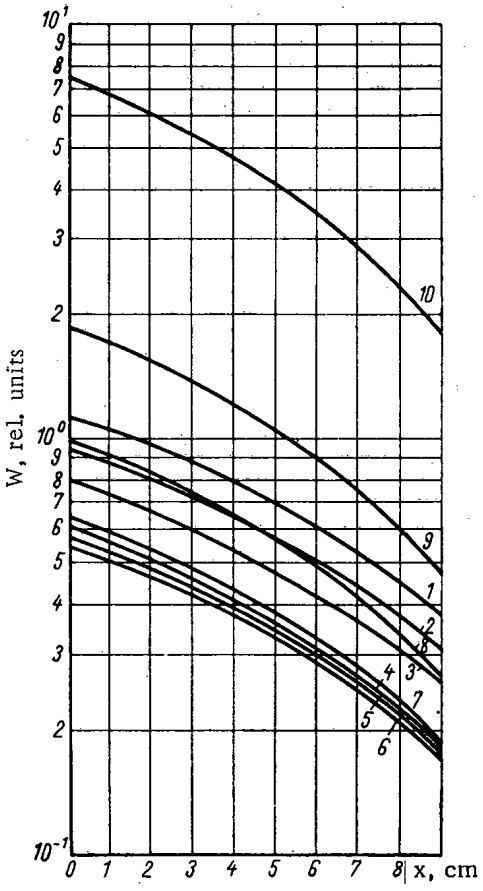

Fig. 3. Distribution of the density of radiation damage throughout the thickness of the iron layer. (Curves 1-10 pertain to compositions containing 0, 10, 20, 40, 50, 60, 70, 80, 90, and 100% iron in the ferro-aqueous thermal shield, respectively.)

TABLE 1. Group Cross Sections of the Formation of Radiation Damage

j	Energy interval of the group, eV	$\sigma_W(\Delta E_j)$, b
1	$1.5 \cdot 10^6 \div \infty$	1960
2	$9.0 \cdot 10^5 \div 1.5 \cdot 10^6$	790
3	$4.5 \cdot 10^5 \div 9.0 \cdot 10^5$	725
4	$3.0 \cdot 10^3 \div 4.5 \cdot 10^5$	182
5	$3.3 \cdot 10 \div 3.0 \cdot 10^3$	15 *

*Obtained by extrapolating the cross section given in [2].

of ferro-aqueous mixture, the composition of which varied, 9 cm of iron, which simulated the reactor vessel, and 30 cm of water, which corresponded to the primary-shield bath. The schematic diagram of the theoretical compositions is given in Fig. 1. The calculations were performed for ferro-aqueous mixtures with iron concentrations of 0, 10, 20, 40, 50, 60, 70, 80, 90, and 100% by volume. The core of a water-moderated water-cooled reactor was considered as the radiation source.

For these compositions, we calculated by means of an electronic computer the spatial-energy distribution of neutron fluxes in a two-dimensional geometry according to the seven-group method proposed in [1]. Moreover, we determined the mean group cross sections of formation of radiation damage (vacancies) in iron by using the energy dependence of this cross section given in [2] (Fig. 2).

The neutron spectrum with respect to which the averaging was performed was chosen for the first and the second groups in correspondence with the results of the ten-group calculations [1] performed for ferro-aqueous mixtures with the above concentrations. For $E_n > 2$ MeV, this spectrum differed only slightly from the fission spectrum. For the other groups, the spectrum with respect to which the cross sections were averaged was chosen on the basis of the spatial-energy distributions of neutron fluxes in ferro-aqueous mixtures obtained from 18-group calculations in the P_2-approximation. The program for these calculations was prepared on the basis of the recommendations given in [3]. The energy intervals from the second to the eighteenth group were taken from the 21-group calculation scheme given in [3]; the first group combined four fast groups of this scheme.

The group cross sections $\sigma_W(\Delta E_j)$ obtained as a result of calculations are given in the Table 1.

These cross sections were used for calculating the density distribution of radiation damage $W(\mathbf{r})$ in the iron layer simulating the reactor vessel:

$$W(\mathbf{r}) = \varrho \sum_j n v_j(\mathbf{r}) \sigma_W(\Delta E_j),$$

where ρ is the nuclear density of iron, and $nv_j(\mathbf{r})$ is the neutron flux of the j-th group at the point $\mathbf{r}$.

Figure 3 shows the function of the density distribution of radiation damage throughout the thickness x of the iron layer. It follows from the figure that, from the point of view of the minimum radiation damage, the optimum iron concentration in the primary shield lies in the range from 55 to 60%.

The authors are grateful to D. L. Broder for his interest in this project.

LITERATURE CITED

1. D. L. Broder, et al., Atomnaya Énergiya, 12, 129 (1962).
2. A. Rossin, Nucl. Sci. and Engng., 9, 137 (1961).
3. G. I. Marchuk, Methods for Calculating Nuclear Reactors [in Russian] (Moscow, Gosatomizdat, 1961).

ANTIFRICTION CHARACTERISTICS OF NEUTRON-IRRADIATED STEEL

(UDC 621.039.553.3/669.16)

E. A. Markovskii and M. M. Krasnoshchekov

Translated from Atomnaya Énergiya, Vol. 18, No. 1,
pp. 72-73, January, 1965
Original article submitted March 2, 1964

The aim of the experiments described here was to investigate changes in the antifriction properties of medium-carbon steel as a result of neutron irradiation under the actual operating conditions of a nuclear reactor and to determine the minimum integral neutron flux capable of producing changes in these properties.

Specimens with a diameter of 3 mm and a length of 10 mm, made of steel St. 45 (0.49% C, 0.56% Mn, and 0.27% Si), were irradiated and then tested. The specimens prepared were divided into four groups, each of which was subjected to a heat treatment: annealing at 850-870°C; hardening at 850°C in water; hardening at 850°C in water with subsequent tempering at 560-580°C; normalization at 850-870°C.

The specimens irradiated in different integral neutron fluxes and the specimens which were not irradiated were tested for hardness and wear. The wear tests were performed by means of a laboratory device [1] which made it possible to realize end-face friction of three specimens against a counterbase—a plate made of steel St. 45, which was hardened at 880°C in water and then tempered at 350-400°C. A special adapter with a reading instrument was used for determining the over-all wear of the three specimens with respect to the same base. The friction coefficient was measured by means of inductive data transmitters, which were connected to a self-recording galvanometer. Diesel oil, which was kept at a constant temperatture of 58°C, was pumped through the friction zone. The load was 60 kg/cm^2, while the sliding velocity was 4.1 m/sec. Each experiment lasted 1 h and was repeated five to six times.

Six sets of specimens were prepared, one of which was not irradiated, while five sets were irradiated in integral fluxes of 10^{16}, 10^{17}, 10^{18}, 10^{19}, and 10^{20} neutrons/cm^2 in the vertical channels of the nuclear reactor of the Institute of Physics, Academy of Sciences, Ukr. SSR. The dose was recorded with respect to thermal neutrons, while the share of neutrons with energies above 1 MeV amounted to 10-11%. Each set of specimens was packed in a container, which was made airtight by means of lead gaskets, and was then irradiated in the same channel.

For determining the thermal conditions, we used the data obtained earlier at the Institute of Physics, Academy of Sciences, Ukr. SSR, in measurements of the temperature of irradiated specimens of low-alloyed and structural steels for different reactor power levels and different clearances between the specimen and the container walls. Moreover, thermocolors for temperatures in the range from 85-380°C were deposited on the specimens in each container for recording the maximum temperature.

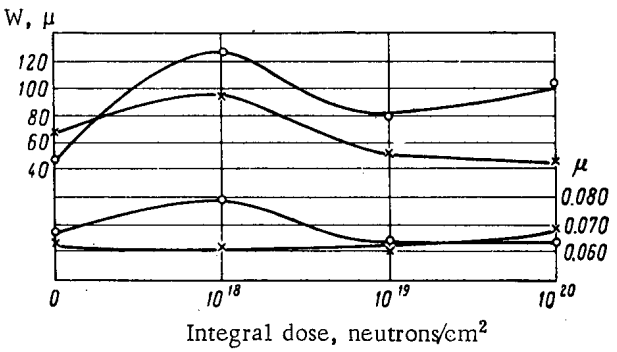

Fig. 1. Variation of the amount of wear W and of the friction coefficient μ of hardened (O) and annealed (x) steels in dependence on the irradiation dose.

We shall discuss some of the results obtained in testing specimens of hardened steel. The wear of specimens irradiated in a flux of 10^{18} neutrons/cm^2 was greater than the wear of unirradiated specimens. Further irradiation somewhat increased the wear resistance of the material. A maximum, which coincided with the maximum of the wear curve (Fig. 1), was also observed in the friction coefficient curve. These data are also in agreement with the variation of Vickers hardness for irradiated hardened-steel specimens (Fig. 2). The hardness of steel drops sharply as a result of irradiation in fluxes of 10^{16}-10^{17} neutrons/cm^2, and then, as a result of further irradiation,

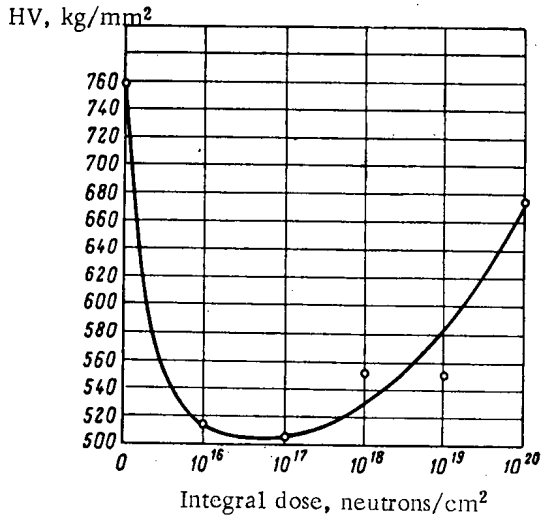

Fig. 2. Variation of the HV hardness of hardened steel in dependence on the irradiation dose.

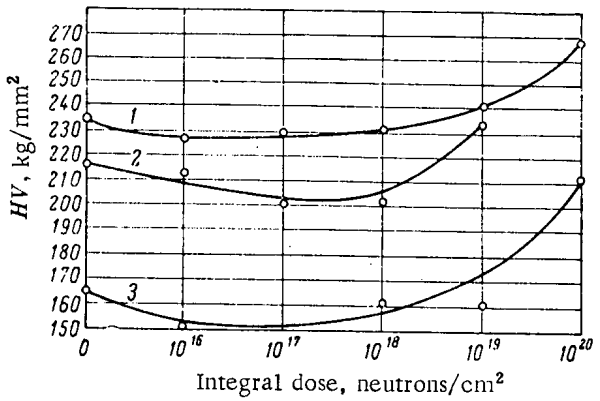

Fig. 3. Variation of steel hardness in dependence on the irradiation dose. 1) Tempered steel; 2) normalized steel; 3) annealed stee.

again increases, but still remains lower than the initial hardness, even for a flux of 10^{20} neutrons/cm^2. The microhardness varies in a perfectly similar manner.

During irradiation in fluxes of 10^{16}-10^{18} neutrons/cm^2, the temperature of the specimens attained 180-200°C. However, this heating could not have been the cause of the sharp decrease in hardness. For instance, it is known that the hardness of hardened steel St. 5 drops from HRC 55 to HRC 53 as a result of tempering at 200°C [2]. In our experiments, after irradiation in an integral flux of 10^{16} neutrons/cm^2, the hardness of hardened steel dropped from HV 756 to HV 514 (or from HRC 60 to HRC 48). Consequently, neutron bombardment rather than the thermal factor played the main role in the reduction in hardness of irradiated hardened steel.

As is known, neutron irradiation may accelerate the relaxation processes occurring in elastically stressed metals [3]. In our experiments, the internal stresses in the material were caused by heat treatment and not by elastic deformation. Hence we can conclude that the combination of the weakening process and the following strengthening process during neutron irradiation is present not only in the case of the material's deformation under stress, but also in the case of metastable hardening structures. This is also confirmed by the greater amount of wear of steel irradiated in integral fluxes of 10^{16}-10^{18} neutrons/cm^2.

Our experiments showed at the same time that, in the case of low irradiation doses, the wear resistance of annealed steel decreases (see Fig. 1): the maximum of the wear curve corresponds to a flux of 10^{18} neutrons/cm^2. The wear decreases with further irradiation, and, for an integral flux of 10^{20} neutrons/cm^2, the amount of wear is by 30% lower than the wear of unirradiated specimens; the friction coefficient changes only slightly during the irradiation process.

Figure 3 shows the diagram of changes in Vickers hardness for irradiated specimens of annealed, normalized, and tempered steel. The maximum initial hardness drop amounts to 6% for normalized steel and 8% for annealed steel. Twelve to fourteen readings were taken in hardness measurements. The scattering of these values relative to the mean value did not exceed ±2.5% for annealed steel and ±2% for normalized steel. This makes it possible to state that the hardness of annealed and normalized steels decreases in the case of small irradiation doses. Further irradiation of annealed steel promotes an increase in its wear resistance, which is in good agreement with the observed variation of the antifriction characteristics of these materials.

Since the structure of, for instance, annealed steel is not metastable, the weakening observed cannot be attributed to the effect of heating. Control annealing of unirradiated specimens of this steel at 180-220°C (the maximum temperatures in irradiation) during comparable periods of time did not produce changes in hardness.

LITERATURE CITED

1. E. A. Markovskii and V. I. Stetsenko, Zavodsk. laboratoriya, No. 4, 503 (1958).
2. Manual of Machine-Construction Materials [in Russian] (Moscow, Mashgiz, 1959), Vol. 1, p. 167.
3. P. A. Platonov, In the Collection: Effect of Nuclear Radiation on Materials [in Russian] (Moscow, Izd. AN SSSR, 1962), p. 106.

METHOD OF MEASURING RADIOACTIVE PREPARATIONS AND CHECKING STABILITY

(UDC 661.879)

V. M. Malykhin

Translated from Atomnaya Énergiya, Vol. 18, No. 1,
pp. 73-75, January, 1965
Original article submitted January 17, 1965

In continuous measurement of radioactive samples of approximately the same activity, it is possible, if the operation of the equipment is reliable and stable enough, to make the count using a single background measurement. If the number of preparations for one background measurement is equal to m, the measurement may be called a measurement of type m + 1. In this case, there is an optimum distribution of the total measuring time T between the operations of measuring the background count rate t_b and the count rate t_a of each of the preparations. This distribution is found as the one which, for a given value of T, gives the minimum relative error $\varepsilon(n_a)$ in % in the count rate of the preparation. The total time T required to measure m preparations of approximately equal activity shall be distributed as:

$$\frac{t_a}{T}=\sqrt{\frac{R}{m}}\cdot\frac{1}{1+\sqrt{mR}},\quad \frac{t_b}{T}=\frac{1}{1+\sqrt{mR}}, \tag{1}$$

where $R = (n_a + n_b)/n_b$ (here n_a is the count rate of the preparation, and n_b is the background count rate).

Naturally, in measuring more active preparations, a comparatively larger fraction of the total time should be allotted to recording the background count rate (for the same value of m). Similarly, with increase in m, less time is required for measuring the background, but it is greater as compared with the time required to measure each of the preparations:

$$\frac{t_b}{t_a}=\sqrt{\frac{m}{R}}\sim\sqrt{m}.$$

The way of measuring m is chosen on the basis of the stability of the apparatus during the time T, which gives acceptable accuracy $\varepsilon(n_a)$ in %. A preliminary determination of the count rate of the preparations makes it possible to find the ratio $r = n_a/n_b$. The values of m and $R = r + 1 = (n_a + n_b)/n_b$ determine the optimum distribution of the total measuring time T. Figure 1 shows the ratios t_a/T and t_b/T as a function of R for different values of m. For example, if, based on the reliability of the counting equipment, it is desired to make one background measurement for three preparation measurements, and the approximate value of the ratio is r = 1, we find in this case, from Fig. 1, for m = 3 and R = 2, $t_a/T = 0.23$ and $t_b/T \approx 0.32$. Thus, measuring the background should take ~32% of the total time T, where T is chosen in advance, based on the accuracy required.

The relative error $\varepsilon(n_a)$ for a reliability of P = 0.68 in the optimum distribution of the total measuring time T, is equal to:

$$\varepsilon(n_a),\ \%=\frac{\sqrt{m(1+r)}+1}{\sqrt{n_a r T}}\cdot 100\%, \tag{2}$$

where $\varepsilon(n_a) = \sigma(n_a)/n_a$; $r = n_a/n_b$.

The relative error for any other reliability P may be found by multiplying the right-hand side of Eq. (2) by the factor K corresponding to the reliability P:

P	0.68	0.87	0.95	0.99
K	1	1.5	2	2.5

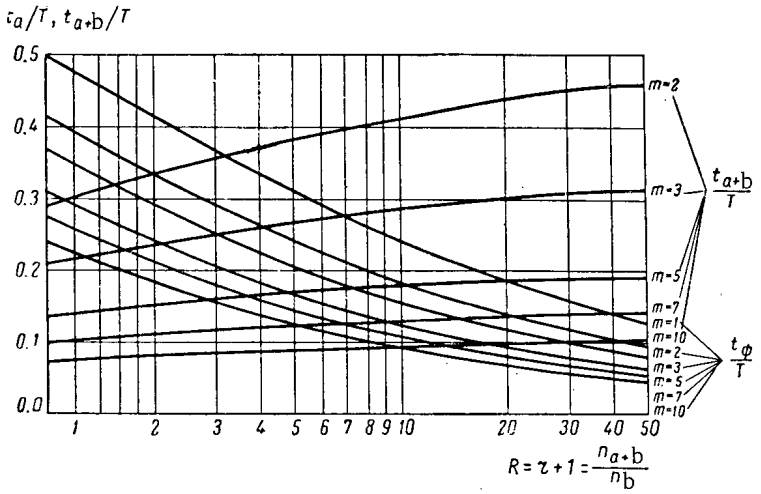

Fig. 1. Relative fractions of the time used in measuring the preparation t_{a+b}/T and the background t_b/T for an m + 1 type measurement.

Thus, the accuracy of measurement is determined by the type of measurement m, the total measuring time T, the absolute count rate n_a of the preparation, and the ratio of the rates of the preparation and background part, i.e., the quantity $r = n_a/n_b$. It may be seen from Eq. (2) that for a constant value of the ratio r, the relative error in the count rate of $\varepsilon(n_a)$ of the preparation is inversely proportional to the square root of the total measuring time T and the count rate of the preparation n_a, and is directly proportional approximately to the square root of the quantity m – the number of preparations per background measurement.

Equation (2) differs from the one usually given in hand books in that it contains fewer independent variables. For the optimum choice of t_a and t_b, the only independent variables are the total measuring time T and the ratio between the preparation and background count ratios $r = n_a/n_b$. Along with this, the formula is of great generality, since it is suitable for m + 1 type measurement. The magnitude of the error in this case will be more accurately determined. The radiometric equipment with a stable background should be provided with graphs for determining the relative error and the measuring time T. An example of a graph of this type for a counter with a mean background of 16 counts/min is given in Fig. 2.

In measuring the radioactive preparation, the count rate of the preparation and the background may be varied by adjusting the sensitivity of the radiometric equipment, as long as the changes in count rate of the preparation and the background are not proportional. It is very important that the maximum in the ratio between the count rates of the preparation and the background only gives the best measuring conditions for large values of r. For preparations of low activity (small values of r) conditions are better for the maximum value of the ratio n_a^2/n_b. Without getting into the question of the relative efficiency of the strictly optimum conditions as compared with the conditions for the maximum value of r, the best conditions for measuring preparations of different activity are found by means of the quality criterion Q:

TABLE 1. P% Critical Levels for the Experimental Value of χ^2_{exp}

P, %	per		
	10	15	20
10	14.7	21.1	27.2
5	16.9	23.7	30.1
1	21.7	29.1	36.2

TABLE 2. P% Critical Levels for the Experimental Value of R_{exp}

P, %	per		
	10	15	20
10	4.13	4.47	4.69
5	4.47	4.80	5.01
1	5.16	5.45	5.65

$$Q = \frac{1}{\varepsilon^2 T} = \frac{n_a r}{[\sqrt{m(1+r)}+1]^2}. \qquad (3)$$

This is the most general criterion, and corresponds to the familiar criteria of maximum r for high activity preparations and the maximum value of the ratio n_a^2/n_b for low activity preparations [1, 2]. An increase in Q means a reduction in $\varepsilon(n_a)$ (for the same values of T), or achieving the same accuracy in $\varepsilon(n_a)$ in a shorter time T. For low activity preparations, where $n_a \ll n_b$, i.e., $r \ll 1$,

$$Q = \frac{n_a^2}{n_b(\sqrt{m}+1)^2}.$$

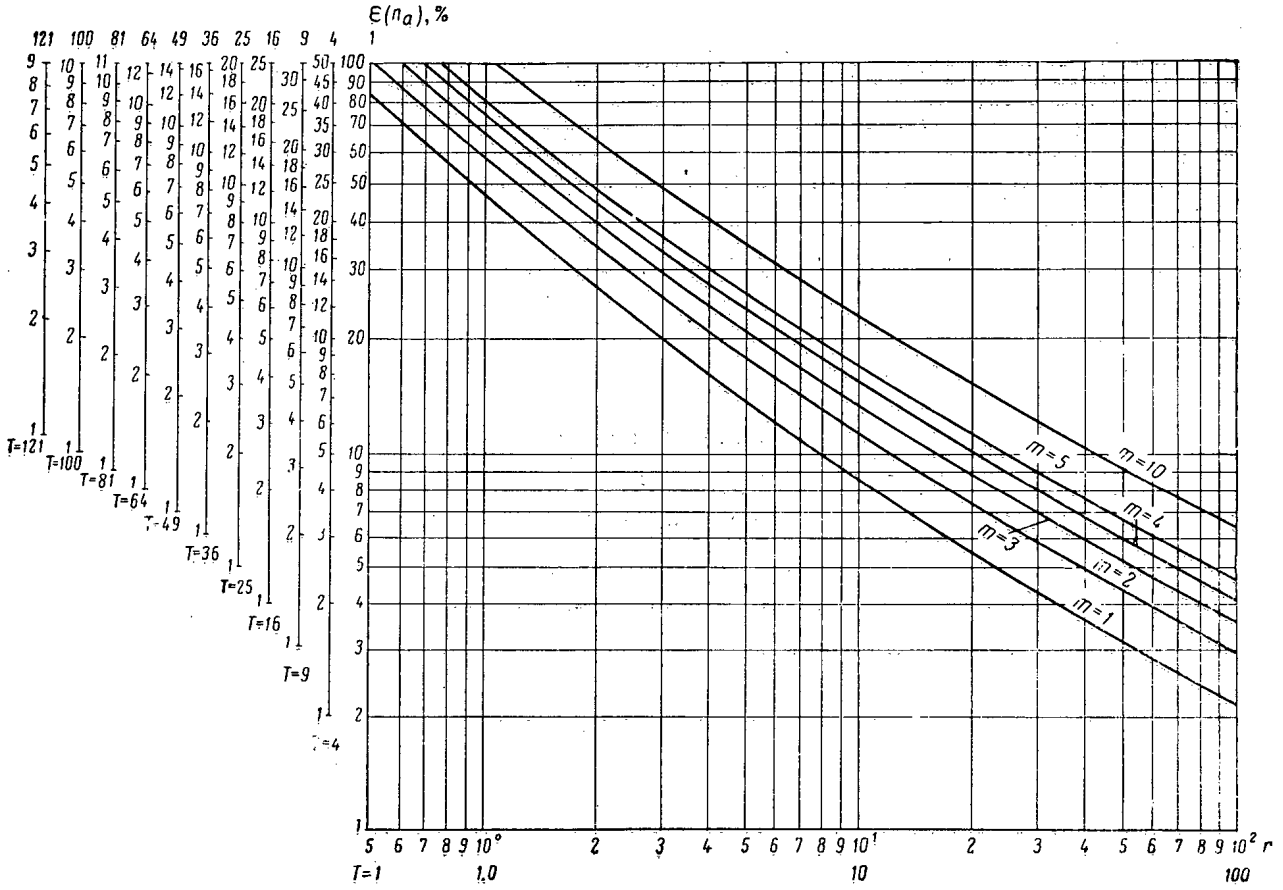

Fig. 2. The relative error $\varepsilon(n_a)$ in % for different values of the ratio between the count rates of the preparation and the background $r = n_a/n_b$. [The different values of T have their own scales of $\varepsilon(n_a)$, and the graph is plotted for $n_b = 16$.]

Thus, the background count rate can increase as the square of the preparation count rate without imparing the statistical accuracy of the measurement.

An important quality of the radiometric apparatus is the stability. Stability monitoring is based on checking how the distribution of the number of pulses in the subintervals of the total measuring time agrees with the Gaussian distribution. The χ^2 test and the method of amplitude control may be used for this purpose. From the number of pulses measured in different successive intervals of time, we calculate either the quantity χ^2:

$$\chi^2_{exp} = \frac{\sum_i (N_i - \bar{N})^2}{\bar{N}}$$

(Here, N_i is the number of pulses in the subinterval, $\bar{N} = \frac{\sum_i N_i}{n}$ is the mean number of pulses in the subinterval, and n is the number of subintervals), or the value of the amplitude:

$$R_{exp} = \frac{N_{i\,max} - N_{i\,min}}{\sqrt{\bar{N}}}.$$

After this, we have to turn to Tables 1 and 2, which give the critical levels of χ^2_{exp} and R_{exp} for 10, 15, and 20 subintervals.

For stable operation, the experimental value of χ^2_{exp} (or R_{exp}) may exceed the critical level of χ^2_p (or R_p) of the chosen significant level P only with the probability P. Thus, exceeding the experimental value of χ^2_{exp} of the 10% critical level, will indicate instability with 90% reliability.

Similarly, if the experimental value of R_{exp} exceeds the tabular 5% level, instability in the operation of the radiometric equipment may be assumed with 90% reliability.

It must be kept in mind when measuring preparations with small activity that a check on stability may be made during measurement as long as the total number of pulses is not less than 350-400. This is due to the necessity of having a quite accurate value of the dispersion in the amplitude method, and a normal distribution of the number of pulses in the subintervals in the χ^2-test. For example, if, in N subintervals, we successively obtain values of N_i equal to 38; 43; 31; 35; 30; 20; 36; 18; 35; 30, conditions are unstable with the reliability of 90%, since the amplitude ratio:

$$R_{exp} = \frac{N_{i\max} - N_{i\min}}{\sqrt{\bar{N}}} = \frac{43-18}{\sqrt{31.6}} = 4.46$$

exceeds the 10% critical level, $R_{10\%} = 4.13$.

LITERATURE CITED

1. A. Freedman and E. Anderson, Nucleonics, 10, 8 (1952).
2. Whole Body Counting. Proceedings of Symposium on Whole Body Counting, Vienna (1961), p. 184.

THE ROLE OF THERMAL PEAKS IN THE FORMATION OF DEFECTS

(UDC 621.039.553.3)

L. G. Gurvich and N. S. Bespalova

Translated from Atomnaya Énergiya, Vol. 18, No. 1,
pp. 76-77, January, 1965
Original article submitted February 13, 1964

In the paper by Seitz and Koehler [1], the concept is introduced of thermal peaks and displacement peaks, occurring in a lattice as a result of the thermal excitations produced by energy transfer from fast particles. Calculations show that this energy is sufficient to heat a region with a radius of 10 angstroms, containing not less than a thousand atoms, up to a temperature of the order of 1000°. Naturally, the reliability of calculations of this type is determined by whether or not it is possible to use the ordinary equations of heat conduction for such small regions. For this model of the thermal peaks and displacement peaks, use is made of the solution:

$$T(r, t)=T_0+\frac{Q}{(4\pi)^{3/2}cd}\frac{1}{(Dt)^{3/2}}\exp\left(-\frac{r^2}{4Dt}\right) \quad (1)$$

of the general equation of heat conduction:

$$\nabla^2 T=\frac{1}{D}\frac{\partial T}{\partial t}, \quad (2)$$

where T_0 is the equilibrium temperature, D = c/cd is the coefficient of diffusivity (C is the thermal conductivity of the lattice), c is the specific heat, d is the density, t is the time, and Q is the energy.

The number of transitions in a peak with the activation energy E' is defined in terms of the mean transition rate, referred to a single atom:

$$\nu=\nu_0 e^{-E'/kT}. \quad (3)$$

Then, the total number of transitions in a peak with the energy Q liberated is equal to:

$$\Delta n=n_0\nu_0\int_0^\infty dr\,4\pi r^2\int_0^\infty dt\left\{\exp\left[-\frac{E'}{kT(r, t)}\right]-\exp\left[-\frac{E'}{kT_0}\right]\right\} \quad (4)$$

where T(r, t) is found from Eq. (1). The integral (4) can not be taken in finite form, and is calculated approximately.

The number of transitions in the peaks is strongly dependent on the activation energy, and for a material with C = 0.2 cal/cm · sec · deg, c = 0.2145 cal/cm^3 · deg, and d = 2.328 g · cm^2 is approximately $4 \cdot 10^3$ for Q = 50 eV and E' = 0.1 eV, while for E' = 1 eV, the number of transition is not greater than $2 \cdot 10^{-4}$, and for E' = 3 eV, it is equal to only $6 \cdot 10^{-23}$. Similar results are obtained for other materials. These data are greatly different from those calculated from the formula:

$$\Delta n=0.016\left(\frac{\nu_0 r_s^2}{D}\right)\left(\frac{Q}{E'}\right)^{5/3}, \quad (5)$$

given previously in [1] as the expression obtained in an approximate calculation of the integral for the number of transitions. Actually, here, for values of E' equal to 0.1, 1, and 3 eV, the number of transitions is found to be equal to 6.71, 0.15, and 0.023 respectively.

In [1], a calculation is made of the formation of peaks in Cu_3Au for a diffusivity of D = 0.001 and an activation energy for the disordering process of 3 eV. The value of the upper limit of the integral (4) for this case gives

t	$D=0.001$				$D=0.04$			
	$e^{-r^2/4Dt}$	$\frac{Q}{A}(Dt)^{-3/2}$	T_{exact}, °K	$T(6)$, °K	$e^{-r^2/4Dt}$	$\frac{Q}{A}(Dt)^{-3/2}$	T_{exact}, °K	$T(6)$, °K
10^{-14}	10^{-110}	$1.4\cdot10^{7}$	300	0	$19\cdot10^{-3}$	$5.6\cdot10^{4}$	400	109
10^{-13}	$5\cdot10^{-12}$	$5\cdot10^{5}$	300	0	0.53	$1.8\cdot10^{3}$	1260	960
10^{-12}	$8.2\cdot10^{-2}$	$1.4\cdot10^{4}$	1200	0	0.94	56	825	525
10^{-11}	0,78	$5\cdot10^{2}$	690	500	0,99	2.8	300	0
$2\cdot10^{-11}$	0,88	$1.7\cdot10^{2}$	430	170	—	—	—	—
10^{-10}	1,00	14.2	314	14	—	—	—	—

the number of transitions in a peak with an energy of 50 eV which is not more than 10^{-3}, while according to (5), for each displaced atom, we get 10 disordered atoms. The reason for this difference is that inaccuracies were permitted in [1] in calculating the number of transitions resulting from increasing the temperature in the peak. Such are, first, the assumption that it is possible to approximate the temperature at the peak by the equations

$$T(t)=\begin{cases} \dfrac{Q}{(4\pi)^{3/2}cd}\dfrac{1}{(Dt)^{3/2}} & \text{for } 2\sqrt{Dt}>r; \\ 0 & \text{for } 2\sqrt{Dt}<r. \end{cases} \tag{6}$$

An exact calculation shows that the relation (6) does not apply in this case (see table). Actually, it is for practical purposes impossible to neglect the exponential coefficient in the solution of the equation of heat conduction. Since the temperature calculated by the correct formula is found to be higher than heat calculated from the approximate relation (6), the number of transitions will turn out to be greater then that given by Eq. (5), which, however, is only true for small values of E' (0.1 eV). The reason for this is to be found in incorrect evaluation of the integral for the number of transitions. It is assumed in [1] that in the region where the temperature is equal to zero in accordance with Eq. (6), there is no point in carrying out the integration over the time in Eq. (4). As this critical value of the time, we take the time $t' = r'^2/4D$, which simultaneously satisfies the equation:

$$1=\int_{t'}^{\infty} \nu_0 \exp\left(-\frac{E'}{kT(t)}\right) dt, \tag{7}$$

which is equivalent to the equation:

$$1=\frac{2}{3}\nu_0\alpha^{2/3}\int_{t'}^{\infty} e^{-x}x^{-1/3}\,dx, \tag{8}$$

where:

$$x=\frac{t^{3/2}}{\alpha}, \quad \alpha=\frac{Q}{E'}\frac{k}{cd(4\pi D)^{3/2}}.$$

As a result, to calculate the number of thermal jumps by atoms, we obtain an integral of the form:

$$n_T=\frac{2}{3}\nu_0\alpha^{3/2}\frac{4\pi}{3}(4D)^{3/2}\int_0^{\infty} dy\int_y^{\infty} e^{-x}x^{-1/3}\,dx, \tag{9}$$

in which:

$$y=\frac{r^3}{(4D)^{3/2}\alpha}.$$

Artificial introduction of a lower limit depending on the distance into the integral in question over the time, although it permits evaluation of the integral (9), nevertheless leads to a condition where t takes on all values from 0 to ∞. As a result of this, a value that is too high is obtained for the integral (9), implicitly con-

taining the expression $[Q/(4\pi)^{3/2}cd)(1/(Dt)^{3/2}]$, which may assume any large values as $t \to 0$. This is precisely the reason for the fact that Eq. (5), which is the result of evaluating the integral (9), gives values that are thousands and tens of thousands of times greater than the value of the integral (4), in which the exact solution of the equation of heat conduction is used.

The calculations just given show that in thermal peaks, only those transitions can occur in which the activation energy is of the value of tenths of an electron volt. If, however, the activation energy of the transition is greater than an electron volt, transitions in the volume of the thermal peak are of low probability. Accordingly, the role of the thermal peaks consists mainly in accelerating the diffusion and ordering processes, i.e., actually, in accelerating radiation annealing processes. The defect formation processes brought about by radiation are unquestionably of a pulsed nature. However, the pulse process by which defects are formed in solids cannot be discussed independently of the thermal motion of the atoms in the lattice, which is usually not taken into consideration.

The authors recognize their pleasant duty of expressing their gratitute to A. E. Kiv for discussing the work.

LITERATURE CITED

1. F. Seitz and I. Koehler, Displacement of Atoms During Irradiation in Solid State Physics, Ed. F. Seitz and D. Turnbull, N. Y. (1956), Vol. 2, p. 307.

AGREEMENT ON COLLABORATION IN DESALINIZATION EFFORTS

Translated from Atomnaya Énergiya, Vol. 18, No. 1,
pp. 78-79, January, 1965

An agreement between the USSR and the USA in the field of water desalinization, including the use of nuclear power for that purpose, was signed in Moscow on November 18, 1964. The agreement was signed in the name of the Soviet government by A. A. Gromyko, Foreign Minister of the USSR, and A. M. Petros'yants, representative of the State Committee on the Uses of Atomic Energy of the USSR. Signing for the USA were the US Ambassador to the USSR, F. Kohler, and the US President's special adviser in science and industry, D. Hornig.

Many countries throughout the world are known to be experiencing a shortage of fresh water for some time now. The dearth of water is felt with special acuteness in arid and desert regions. Many countries, including the United States, face a deficit of fresh water for the needs of industry and agriculture. The Soviet Union finds itself in the most favorable position in regard to fresh water resources (surface water and ground water), as compared to other nations, but the distribution of water throughout the vast territory of the USSR is uneven, so that certain regions in Central Asia and Kazakhstan are in dire need of fresh water supplies.

It is not surprising that this problem of desalting water, including sea water, has always been one of major import. The problem takes on added importance in our time because of the population expansion and the vigorous development of industry. Various techniques are at hand for desalting salt water: the use of ion exchange resins, freezing-out processes, distillation, etc. Distillation is the most promising of these methods.

Soviet scientists have been working constantly on the problem of desalting water. Certain advances have been registered in their endeavors. In the town of Shevchenko, on the shores of the Caspian Sea, in Kazakhstan, we have the example of a scaled-up pilot plant processing 4000 to 5000 cubic meters a day by the distillation method. Several pilot-plant desalinizers operating on a variety of flowcharts have been built at the same site. At Baku, in Azerbaidzhan, a desalinizer supplies an industrial electric power plant with water and utilizes the heat from the power plant.

Signing of the agreement on USSR-USA collaboration in desalinization projects.

Soviet scientists view the use of nuclear power for desalting purposes as timely. Theoretical calculations and experimental research alike demonstrate that the building of high-power nuclear reactors utilizing heat to generate electric power and to desalt water may provide a successful solution of that problem.

Even more promise is seen in the use of fast reactors. A first desalinizing reactor of this type, of 350 MW rating, is being built on the shores of the Caspian Sea.

American scientists are also working on water desalinization. They have built pilot desalinizing plants. Their feeling is that the use of nuclear power can be a great aid in solving this problem.

The agreement signed lays the groundwork for close collaboration between the scientists of the two countries in resolving this problem. The agreement provides for scientific and engineering collaboration on a broad scale in water desalinization, including projects involving nuclear power use. It is expected that the USSR and the USA will engage in mutual exchanges of scientific reports, papers, and other documents, including the findings of both Soviet and American pilot-plant research; symposia and scientific colloquia will be organized periodically to discuss engineering problems and plans; visits of technical experts to promote greater familiarization with existing plants, laboratories, and facilities will be encouraged.

INTERNATIONAL CONFERENCE ON THE QUANTUM THEORY OF SYSTEMS HAVING MANY DEGREES OF FREEDOM

Translated from Atomnaya Énergiya, Vol. 18, No. 1,
pp. 79-80, January, 1965

An international conference on selected topics in the quantum theory of systems having many degrees of freedom convened at Keszthély (Hungary) in September 1964, attended by approximately 80 delegates from Bulgaria, the German Democratic Republic, Poland, the USSR, and Czechoslovakia, and also from Austria, Belgium, Denmark, Italy, France, and West Germany. Representing the Soviet Uion and the Joint Institute for Nuclear Research were E. S. Fradkin (Lebedev Institute of Physics [FIAN], Moscow, S. V. Lordanskii and N. A. Potapkov (Steklov Institute of Mathematics [MIAN], Moscow, G. Domokos, P. S. Isaev, I. T. Todorov, G. Heber, P. Suranyi (all from Joint Institute for Nuclear Research, Dubna).

On the agenda of the conference were the basic topics:

a) nonequivalent representations in quantum field theory and in the theory of superconductivity;

b) approximate methods in the many-body problem and in the theory of nuclear structure;

c) certain aspects of the theory of elementary particles;

d) functional methods in field theory.

45 papers were submitted on these major topics. The large number of papers on the first two topics wad due to the application or development of the concepts and method of N. N. Bogolyubov elaborated during the years 1957 to 1961, on superconductivity theory and statistical mechanics.

In his report "The many-body problem in nuclear physics," P. Mittelstadt (Munich) proposed a combination of the Bogolyubov method and the Galitskii method to describe nuclear forces. The author thus introduces two different interaction potentials in such a way that the asymptotic behavior of the wave functions ψ^A and ψ^B becomes identical. He succeeded in selecting the required potential and in correcting the behavior of the wave function at zero. Different representations of ψ^A and ψ^B are associated with some canonical transformation. However, the potential found thereby turns out to be a nonlocal potential. There exist infinitely many such potentials. G. Fano (Bologna) studied systems of an infinite number of particles. Using the Gel'fand method, he performed a classification of all possible representations and found the equivalent representations. N. A. Potapkov (Moscow) considered the relaxation of an electron gas in the presence of a magnetic field, while S. V. Iordanskii (Moscow) dealt with the conditions under which equilibrium could be established in a superfluid liquid when there is relative motion of the normal and the superfluid components. A paper by P. Gombas (Budapest) proposed a simplification of the Hartree self-consistent method for calculating eigenfunctions and energies of atomic electrons. J. Nemec (Budapest) discussed the superconductive model with two kinetic energies. P. Szépfalusi (Budapest) constructed the Green's function and developed a diagram technique in a new representation in which an energy gap is provided for. The renormalized equation for the energy gap was completely derived in a paper by N. Menyhard (Budapest), the equation being stated with the aid of generalized Feynmann diagrams; an equation for the energy gap in the ladder graph approximation is discussed.

The audience showed interest in the papers submitted by H. Umezawa (Naples), G, Kuty and G. Marx (Budapest), J. Lopuszanski (Wroclaw), and G. Iona-Lazinio (CERN), on the existence of the Goldstone theorem, according to which a spontaneous breakdown of continuous symmetry is consistently associated with the appearance of a zero-mass boson. There is still no proof of this theorem in field theory, and its verification on the basis of several models cannot yet provide conclusive proof of the existence of such a theorem, nor of its refutation. The first paper dealt with the self-consistency of a method developed in an earlier paper by the author (Nuovo Cimento, 31, 439, 1964). The problem of self-consistency involves the correct determination of the passage to the limit and the conservation of commutative relationships imposed on the field operators in the transition from one rep-

resentation to another. The author showed that the Goldstone theorem does not hold under the assumptions which he formulated. Kuty and Marx considered two cases in the Goldstone model: a) Hermitian fields and b) non-Hermitian fields. Solutions violating symmetry and the physical significance of those solutions were discussed in the Schiff representation. The authors failed to obtain bosons of zero rest mass.

The Lopuszanski paper was devoted to the construction of nonequivalent representations in quantum field theory and in many-body theory. Iona-Lasinio's paper studied the relativistic model of field theory in which symmetry-violating solutions are present. The author successfully developed a criterion for the existence of the Goldstone theorem. The results obtained depend on the form of the model in question, however.

The discovery of parity nonconservation and the experimental research associated with searches for the vector meson have stimulated a need for deeper studies of the theory of weak interactions. It is now known that the four-fermion interaction results in a divergence. This poses the question of whether the theory of weak interactions is valid and whether the discrepancy in the theory could not be eliminated with some physical significance imparted to the solutions so obtained. In particular, the peratization method suggested over a year ago by Feinberg and Pais provides a positive solution to both problems. Several papers submitted to the conference dealt with these problems.

A paper by G. Domokos (Dubna) studied the four-fermion interaction in the ladder approximation for the case where the masses of all the fermions are zero. It was shown that their theory exists and is nonlocal, and that the coupling constant is singular. The case of nonzero mass changes nothing in the results.

J. Montvely (Budapest) showed that the peratization procedure of Feinberg and Pais in the theory of weak interactions leads to solutions satisfying the original nonregularized Bethe-Salpeter equation. J. Stern (Prague), in discussing the theory of weak interactions with a vector W-meson involved, found an integral equation relating the four-lepton amplitude and the form factor of the W-meson, and showed that the amplitude so found contains a resonance in an energy channel about 1 MeV wide. A. Frenkel and P. Graszko (Budapest) utilized the renormalized vector boson theory of Bialynicki-Birul to describe neutron decay. The authors reported excellent agreement with experimental evidence (on the energy spectrum of electrons). The difference from conventional Fermi theory consists in another form of distribution of the angle between the neutron spin direction and the electron momentum.

Several papers were devoted to the investigation of distinct facets of the current theory of strong interactions. H. Durr (Munich) made a formal treatment of a many-spurion system and derived several equations for computing the masses of unstable particles in nonlinear field theory. No concrete mass calculations were presented.

A paper by A. Bassetto, S. Ciccarello, M. Tonino (Padua), "Light-like solutions of the Bethe-Salpeter equation," revealed that the eigenvalues of equations in the ladder graph approximation for vacuum-like bound states ($P_\mu = 0$) are eigenvalues of the corresponding equation for a light-like bound state ($P_\mu^2 = 0$, $P_\mu \neq 0$) in the case where no degeneration occurs with respect to the four-dimensional angular momentum. The results are indicative of agreement with the Goldstone theorem. J. Bourdet (Lyons) constructed a potential in a nonrelativistic approximation giving the specified pole distribution in the l-plane. The nonsingular potential he derived ($\approx r^{-2+\varepsilon}$) was used to find a solution to the Schrödinger equation. P. S. Isaev (Dubna) considered the possible application of the quasipotential method proposed by A. A. Logunov and A. N. Tavkhelidze to the real case of π-meson scattering on nucleons. Quasipotential equations were shown to have resonant solutions. T. Fulton (Vienna) constructed finite SU_3 symmetry groups in his paper.

A review paper on asymptotic relationships linking the amplitudes of elastic and inelastic processes in local field theory was delivered by I. T. Todorov (Dubna). The work of Joint Institute scientists (A. A. Logunov, I. T. Todorov, Nguyen Van Hieu, et al.) using the Phragmen-Lindelof theorem to obtain important relationships between the differential cross sections of inelastic processes, was reflected amply in the paper.

Two reports were heard on the last topic. Functional methods in field theory make it possible to solve field equations (or the Green's function) in the form of continuous integrals. The integration of the field equations is carried out in a purely formal manner, and the problem can be solved ultimately, reducing in the given case to taking continuous integrals, only in certain particular cases. A paper by W. Thirring (Vienna) discussed the scalar field model and reported an exact solution of that model by functional methods. "Applications of functional methods in field theory," a paper by E. S. Fradkin (Moscow), stimulated intense interest. They ascertained the asymptotic behavior for the cross sections and the Green's function in the case of interaction with a vector meson.

The existence of a Regge pole and the existence of moving singularities was proved, in particular, in the case of scattering in a narrow angular region.

The proceedings of the symposium are to be published in 1965.

P. S. Isaev

ALL-UNION CONFERENCE ON NUCLEAR METEOROLOGY

S. G. Malakhov and I. V. Yagodovskii

Translated from Atomnaya Énergiya, Vol. 18, No. 1,
pp. 80-81, January, 1965

An all-union conference on nuclear meteorology was held at Obninsk in February 1964. Taking part in this conference were representatives of many institutes and establishments; about 60 papers were read on the natural radioactivity of the atmosphere and on its use in meteorological studies, on the global distribution and propagation of radioactive products of nuclear weapons tests in the atmosphere and in fallout reaching the ground, on the composition and properties of radioactive aerosols, on the propagation of radioactive aerosols and gases from local sources, on ways in which radioactive aerosols are washed out of the atmosphere, and on meteorological techniques.

The vertical distribution of radioactive emanations and their decay products in the troposphere, and estimates of the vertical turbulent mixing coefficient based on measurements of radon concentration, were discussed in papers on natural radioactivity, and results of measurements of the radon exhalation from the earth's surface were cited. B. I. Styro's report on investigations of the disperseness of particulates in a naturally radioactive aerosol should be noted. Data on Pb^{210} (Ra D) distribution in the atmosphere were discussed in some papers (V. D. Vilenski et al.). Data on this distribution were used in a report by I. L. Karol' to estimate the rate of mixing of an aerosol from the lower troposphere, the vertical turbulent mixing coefficient in the troposphere and stratosphere, and the rate of exchange between hemispheres in the troposphere.

In most papers on the global propagation of radioactive products of nuclear explosions in the atmosphere, results of systematic measurements of the level of radioactive pollution of the atmosphere and of fallout at various points throughout the Soviet Union are reported. Cases involving a rapid passage of radioactive fallout products from the stratosphere into the ground layer of the troposphere are analyzed in papers by G. V. Dmitrieva and V. I. Kasatkina. A synoptico-climatological pattern was proposed to account for the propagation of radioactive aerosols from nuclear explosions in the atmosphere. I. L. Karol' and S. G. Malakhov presented an analysis of the basic findings of research on patterns of global propagation of fission products ejected in the stratosphere, in a review paper.

Data on the sizes of radioactive particles in the stratosphere were cited in a paper on the disperse composition of radioactive aerosols (Ya. I. Gaziev, L. E. Nazarov); other papers on the disperse composition included one on fractionation of isotopes in the process of aerosol formation during a nuclear explosion (Yu. A. Izrael', M. P. Grechushkina), on the distribution of radioactive aerosols in size in the ground layer of the atmosphere (Ya. I. Gaziev, L. E. Nazarov, K. P. Makhon'ko).

An interesting communication submitted by B. I. Styro et al., was devoted to alpha-active "hot" particles in the atmosphere, their physical properties, composition, and sizes.

In papers dealing with the washing out of aerosols, estimates were made of parameters indicating the elimination of radioactive aerosols from the troposphere (K. P. Makhon'ko, G. S. Malakhov, I. I. Burtsev), and the role of clouds and precipitation in this process was evaluated (V. I. Baranov, N. G. Morozova).

In the next group of papers, we note some theoretical papers submitted by M. E. Berlyand et al., and the results of simulation experiments on the propagation of aerosols from a point source (N. L. Byzova et al.).

Papers dealing with techniques dealt with improvements in the quality of measurements of the total beta-activity of samples (L. I. Fedeonov et al., V. D. Spirin) and with fallout sampling (N. N. Aleksandrov, A. D. Pogudin et al.). A radiation-sedimentation method for investigating aerosols is proposed in a paper by E. E. Verzilov et al.

Complete texts are to be published in 1965.

APPLICATION OF METHODS OF NUCLEAR GEOPHYSICS IN ORE PROSPECTING, EXPLORATION, AND DEVELOPMENT

S. I. Savosin and V. I. Sinitsyn

Translated from Atomnaya Énergiya, Vol. 18, No. 1,
pp. 81-84, January, 1965

The use of nuclear geophysics methods has become an inseparable part of the set of geophysical tools in the prospecting, exploration, and development of deposits of coal, petroleum, and gas, as well as of several ore minerals, in the Soviet Union and in many other socialist countries.

The scope of radiometric investigations is consistently expanding in this area. In 1949, for example, 2 teams in the USSR were utilizing nuclear geophysics techniques; and performed investigation of 20,000 m of borehole; 29 teams used these techniques in 1954 to study a total of 4 million meters of borehole length; in 1960 the number of teams employing these techniques reached 185, and their work covered 12.4 million meters of borehole length.

Surveys made indicate that the utilization of nuclear geophysics techniques in the socialist countries has resulted in pronounced savings. For example, savings due to the use of nuclear geophysics in the petroleum and gas industry of the Soviet Union during 1960 amounted to roughly 60 million rubles, according to an estimate carried out by the Institute of Economics of the USSR Academy of Sciences. In addition, the use of these techniques made it possible to produce a million tons of petroleum by putting old abandoned wells back into production in some cases. The use of radioactive isotopes (tagged atoms and well as nuclear geophysic techniques making it possible to reactivate old wells) in Rumania brought about an increase of 300 thousand tons of oil in 1961. The use of radiometric logging techniques in the exploration of coal fields in Hungary resulted in savings on the order of 40 million forint, and savings of 20 million forint in the execution of hydrogeological studies. In Poland, nuclear geophysics techniques resulted in 8-12% increases in proved coal reserves, and a 10% increase in proved petroleum reserves. Petroleum production was upped 6% and coal reserves 6 to 90% in Czechoslovakia through the use of these methods.

The essence of the most popular techniques of nuclear geophysics in this field can be summed up in brief in the following.

Gamma-ray well logging is a technique based on recording the natural radioactivity of rocks pierced in drilling boreholes. It is generally acknowledged that all rocks present in the earth's crust contain (over the range studied) some amount of natural radioactive elements, viz., uranium, thorium, potassium-40. These elements and the products of the radioactive decay of some of them emit a penetrating gamma radiation. Because of certain geochemical conditions, various rocks have a specific average concentration of these radioactive elements. For example, the average radium content in limestones is $0.5 \cdot 10^{-12}$ g/g for dolomites, $0.11 \cdot 10^{-12}$ g/g, for clay shales $1.09 \cdot 10^{-12}$ g/g, for sandstones, from 0 to $1.5 \cdot 10^{-12}$ g/g. For any geological region or province taken as a whole, each lithological difference displays a characteristic radioactivity background.

Once the intensity of gamma rays characteristic of the given lithological difference has been established directly on a reference well or on drilled core material with the aid of equipment highly sensitive to gamma rays, the geological sections can be correlated and mapped in their continuity over wide areas without having to spend an inordinate amount of time and means on the extraction of borehole core material, making it possible thereby to effect a sharp delineation in clay fractions, sandstones, limestones, potassium salts, and make it possible to detect uranium and thorium deposits.

Geological domentation of petroleum fields in the Western Ukraine which had been destroyed during the Patriotic War with Hitlerite Germany was restored by nuclear geophysics techniques, backed up to a considerable extent by the use of gamma-ray logging. In Poland, gamma-ray logging techniques have acquired popularity in prospecting and exploration of potassium salts deposits. These methods are being used to define potassium salt beds in borehole sections, to ascertain the thickness of the beds, and the percentage content of potassium oxide.

Scattered gamma-radiation techniques include two variants of gamma-ray logging: gamma-gamma logging (GGL) and selective gamma-gamma loging (SGGL).

Isotopes emitting relatively hard gammas (e.g., Co^{60}) are employed in GGL work. The scattered gamma radiation, whose intensity is proportional to the density of the rock cored, is recorded by a field portable recorder. Strip chart lengths showing a lower gamma-radiation intensity are indicative of rocks of higher density (e.g., basalts), and higher intensity is indicative of friable rock (e.g., coals). Improved results were obtained in GGl work on uncased boreholes. This decides the range of application of gamma-gamma logging. This form of logging is employed in the USSR primarily as an aid in the exploration of coal fields, to ascertain the locations of coal beds and their thickness. GGL is useful in the petroleum and gas industry for shifting the position of the cement ring in the annular space of boreholes. In that case, the difference in the density of sectors filled with cement or free of cement is striking, and GGL will yield excellent results.

Isotopes emitting softer gamma rays (e.g., Cs^{137} and Se^{75}) are employed in SGGL work. The presence of such high-Z elements as lead, mercury, tungsten, antimony, iron, etc., in the rock alters the intensity and the back-scattered gamma-ray spectrum. The element and its percentage composition are determined from these parameters. This method is being used with success to effect a fairly simple differentiation in rocks without having to take samples or make a chemical analysis of points where certain heavy elements are present in higher concentration, and to monitor the content of these elements in the mined ore at various stages in the technological processing, and so forth.

Neutron gamma-ray logging (NGL) involves the measurement of gamma-ray emission appearing as a result of the capture of thermal neutrons by nuclei of various elements. NGL is employed in the Soviet Union to determine hydrogen content in rock. Information on this parameter is useful under favorable conditions in determining the porosity of the rock, in estimating water saturation level (which has particular importance not only in the field of geological exploration work, but also in engineering research).

Neutron-neutron logging (NNL) techniques are based on measurement of the density of neutrons slowed down in the rock surrounding the borehole. NNL is being carried out in two modifications at present: logging by measurement of the density of thermal neutrons (NNL_T) and measurement of the density of epithermal neutrons (NNL_{epi}). Information on the presence of elements presenting a high scattering and capture cross section for thermal neutrons in rocks may be gained by measuring the density of thermal neutrons. Measurement of the density of epithermal neutrons may have the effect of eliminating any influence of elements having a high capture cross section.

NNL_T techniques are being used on steadily widening scale in recent years in prospecting and assaying of the concentration of elements having a high thermal absorption cross section (chlorine, boron, etc.). One finding was that boron-bearing bedshaving boron content higher than 0.1% could be reliably detected and delineated in a borehole core by means of NNL_T. Data on the percentage content of boron in beds can be obtained without removing the core from the borehole when NNL_T and NNL_{epi} techniques are used in combination.

Pulsed neutron-neutron logging (PNNL) provides a new technique in nuclear subsurface borehole work. The idea of utilizing the nonstationary neutron distribution to investigate the properties of rocks under borehole field conditions was first advanced by G. N. Flerov and has been developed further at the All-Union Research Institute for Nuclear Geophysics and Geochemistry.

Periodic transmission and recording of neutron bursts provides a tool for detecting variations in the intensity of thermal neutrons scattered by the rock in the pulse separation in interval as a function of the content of rock-forming elements, particularly, H, Na, Mg, Cl, A. Fe, etc., affecting the mean lifetime τ of the neutrons. For example, τ is higher in oil-bearing and gas-bearing strata than in the water-bearing strata usually underlying them, because of the natural content of neutron-absorbing NaCl, KCl, etc., in the latter. The decay of the thermal neutron density n in those strata with time will take place at a different rate. As the delay time t following emission of the pulse is increased, the differences in neutron densities will become augmented and may increase to any level however high, theoretically speaking. In the NNL method, where a continuous-flux source is utilized, the thermal density in these media will not differ by anything greater than the ratio of the lifetime of thermal neutrons in the media $n_{oil}/n_{water} \propto \tau_{oil}/\tau_{water}$, and these may not exceed differences of two or three fold, which the reader may see by glancing at curves a, b, c in the diagram. The effect of an increase in delay time on the difference in thermal neutron densities is illustrated by the respective curves plotted at t= 360, 680, and 780 μsec. These

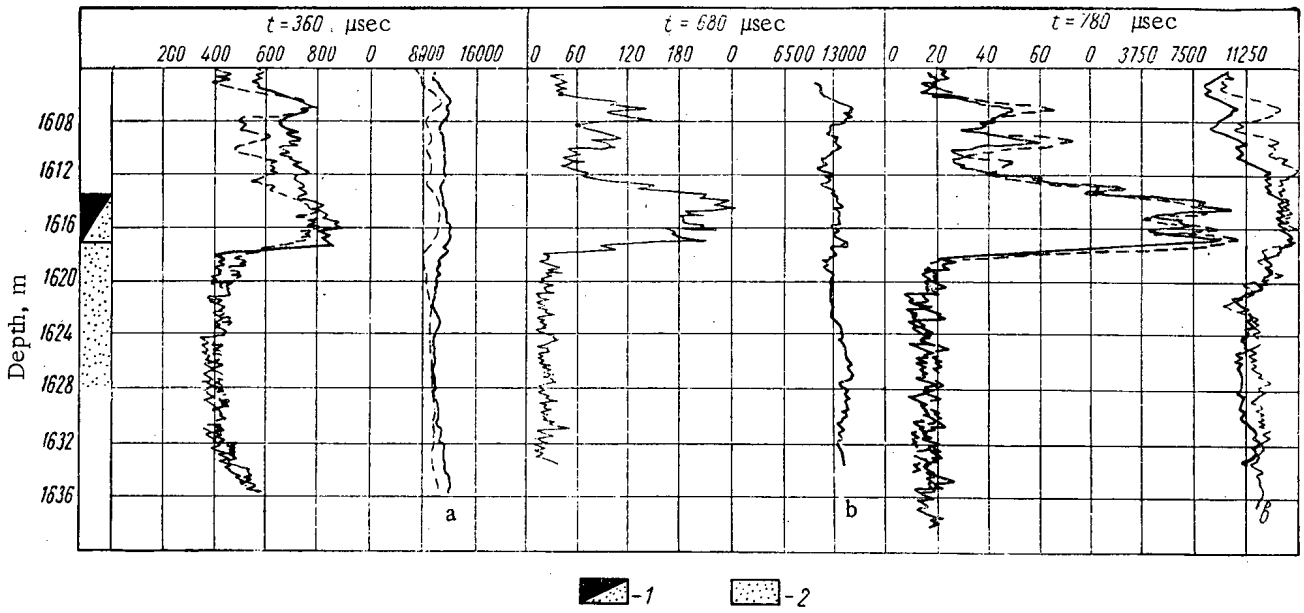

Results of PNNL measurements in well No. 803 of the Tuimazy oil field at various delay times (t). Curves a, b, c plotted on basis of NNL data; polonium-beryllium source employed (data supplied by Yu. S. Shimelevich and A. S. Shkol'nikov).

curves were plotted in PNNL measurements in a borehole at the Tuimazy oil fields, with a comparison to NNL results. It is evident from the diagram that the position of the water-bearing and oil-bearing sectors in sandstones was clearly demarcated by the recorder attached to the borehole pulsed neutron generator.

By varying the delay time, the position of an oil-bearing or gas-bearing stratum in the borehole and such basic parameters as the thickness, porosity and point of contact with the flooded portion of the stratum were determined by PNNL work. The effect of that part of the borehole filled with liquid, the effect of steel casing tubes, differences in the geological structure of that sector of the deposit, and degrees of salinity of the brine waters in the stratum were eliminated in the process. No other geophysical techniques, NNL included, are capable of eliminating the entire set of factors which distort or hamper the securing of reliable data so necessary in both exploration and development of oil and gas deposits.

The PNNL method has been in experimental use in the USSR since 1959. The high effectiveness of this method has made an impact on all industrial organizations which have tried it. A particularly warm appraisal of the method was given in the Tatneftegeofizika oil trust, where PNNL has become one of the principal techniques in keeping track of the development of the Romashki oil fields, largest in the USSR. Calculations indicate official cost of the neutron generator to be 7 to 8 thousand rubles, amortized over a very short period because of the savings achieved by its use.

Activation analysis or induced activity techniques are based on the phenomenon of neutron activation of nuclei of certain elements found in rock formations.

Activation analysis is used in experimental work in the exploration of aluminum, silicon, copper, indium, manganese, and other elements, appreciably curtails the volume of chemical analyses under field conditions, and speeds up the study of the quantitative content of pay ores in samples more than tenfold. The content of pay ores has been successfully assayed right in the process of field work by geological prospecting terms working with activation analysis techniques. Costs of activation analysis run 50% lower than costs incurred in conventional chemical analysis in aluminum and silicon assay work in the Irkutsk geological administration.

Geological organizations in Rumania are utilizing activation of manganese by means of a polonium-beryllium neutron source directly in prospecting and exploration boreholes, in investigation of iron ore fields. In Hungary, the method of neutron activation of minerals is being employed to detect bauxites and to determine the silicon modulus. This makes it possible to estimate the quality of bauxites found in the deposit.

The neutron activation analysis also makes it possible to detect and make quantitative determinations of some elements having a high thermal capture cross section. Such elements found in rocks include Na, Mn, Cl, Al, Ca, and others. This method is widely used in the USSR. Savings averaging up to 40,500 rubles for every thousands boreholes have been achieved by neutron activation analysis just in the work completed in 1960 at the Red October bauxite deposits.

There is reason to suppose that new advances in equipment will render activation analysis one of the most efficient techniques in the detection and investigation of the elements which are constituents of rocks on the earth's surface.

The method of radioactive isotopes is a geophysical technique par excellence (it is being used for research in chemistry, metallurgy, and biology as well). A batch of isotope-tagged material is lowered to a specified depth by a special device and is introduced into the stratum in the usual way, after which recurrent gamma-ray logging is employed to determine the site where the fraction of isotopes is absorbed.

Radioactive isotopes are meeting with greater acceptance in industrial geology and in engineering hydrogeology. Radioactive isotopes of comparatively short half-lives are pumped into the boreholes. These isotopes include I^{131}, Zr^{95}, Fe^{59}, Sb^{124}. An average of 3 to 5 mCi of the radioactive material is used in a single experiment involving pumping of isotope-tagged drilling mud. The thickness of the cement column in the annular space of the borehole can be measured readily by radioisotope techniques, which are equally effective in determining the height to which cement rises after being placed, the site of breaks or fractures in casing strings, monitoring hydraulic fracturing of strata, etc.

Gamma-emitter isotopes are useful in detecting water filtration zones through the main body of dams, reservoirs, etc. Tritium is a useful tool in tracking down the direction of flow of underground waters over great areas and over a large number of boreholes.

The high efficiency of radioactive isotopes can be demonstrated by the example of the monitoring by hydraulic fracturing in operating wells and injection wells in oil and gas fields. As the oil and gas is taken from the bed, the permeability of the stratum diminishes (the depleted stratum is filled with paraffins) and the oil yield from the paraffin-filled wells drops rapidly. An attempt is made to restore the normal output from these wells by working on the bottom face of the well through fracturing the stratum with a viscous fluid combined with coarse-grained sand pumped into the well hole under a high pressure. The normal crack structure and oil flow of the wells are restored after this pumping step. Hydraulic fracturing of the stratum can be monitored solely by tagging batches of sand with a radioactive isotope. The use of this method has resulted in the production of several million additional tons of petroleum.

RADIOACTIVE CHLORINE-36 IN MONITORING THE PRODUCTION AND PROCESSING OF HEXACHLORAN

G. M. Strongin and M. N. Kulikova

Translated from Atomnaya Énergiya, Vol. 18, No. 1,
pp. 84-85, January, 1965

The radioactive tracer Cl^{36} has been performing valuable services in monitoring the production hexachloran in several years of research at the M. I. Kalinin Chernorechenskoe chemical processing plant in the Gor'kii district of the national economy.

Hexachloran is a mixture of stereoisomers of 1-, 2-, 3-, 4-, 5-, 6-hexachlorocyclohexane, differing in their chemical properties, with admixtures of chlorinated hydrocarbons which have received meager study to date. The composition of hexachloran is inconstant and depends on the conditions prevailing when it was produced. The unavailability of any precise techniques of analysis which would be independent of the composition and independent of the amount of impurities present has stood in the way of making objective determinations of the basic parameters in the production technology of technical-grade and highly enriched hexachlorans. A decision was made to utilize Cl^{36}-labeled hexachlorocyclohexane stereoisomers, and a method of synthesis was elaborated involving the production of radioactive chlorine through chemical decomposition of $NaCl^{36}$ in an acidic medium in the presence of potassium permanganate.

In view of the high cost of Cl^{36} and the undesirability of allowing radioactive wastes to accumulate, another procedure was developed in order to allow for recovery of the material from hexachloran wastes by conversion to sodium chloride. The resulting pure radioactive isomers were utilized as tracers to determine amounts of analogous isomers of hexachlorocyclohexane in various hexachloran samples by the isotope dilution method. The activity of the samples was measured by a procedure developed at the plant, after coating a trichlorobenzene solution of the isomer onto filter paper and sealing the filter paper in a cellophane envelope. The error in the determination did not exceed 5% (relative) in any of the analytical procedures we elaborated.

(More detailed information on special aspects of the problem discussed here may be found in Trudy po khimii i khimicheskoi tekhnologii [Transactions in chemistry and chemical engineering], Gor'kii, 1958-1964.)

Definite improvements were obtained in the values of concentrations of constituents, determined earlier by chromatographic techniques, when several products were analyzed by the isotope dilution method. For example, it was demonstrated that the greasy waste left over in the production of highly enriched hexachloran contained not 3%, as hitherto supposed, but from 10 to 15% of the insecticide γ-isomer; this waste was directed to reprocessing to extract a low-value mixture of polychlorobenzenes, but on the basis of the new data it was decided to use it as an insecticide. The savings from this operation will be a million rubles annually, spread out over the entire Soviet Union.

In the analysis of technical-grade hexachloran, the isotope dilution method revealed that the standard chromatographic technique yields values on the low side, mainly because of incomplete extraction. Since attempts to improve the standard chromatographic method had led to no radical resolution of the problem, staff members of the plant decided in 1961 to propose a change in the GOST [All-Union State Standard] standard for technical-grade hexachloran, but to date, unfortunately, commercial hexachloran is being analyzed by a method acknowledged to be quite inaccurate.

Variants of the isotope dilution technique were also worked out at the plant for monitoring the production and processing of hexachloran, and particularly for monitoring the production of dusts of hexachloran-activated coal tar oils and creolins.

Radioactive tracers were proved irreplaceable in solubility determinations in multicomponent solvents, since data can be obtained thereby on solubility by simply measuring the radioactivity. In many cases in research work on the production of the technical grade γ-isomer, the use of Cl^{36} tracer facilitated and expedited the study of the kinetics of dissolution and crystallization of individual isomers. And in some cases the radiotracer method is being used as a standard method to check improvements in the precision of other methods of analysis: e.g., in the polarographic determination of hexachlorocyclohexane high precision may be obtained by using a standard which was been analyzed beforehand for the content of the γ-isomer, by means of Cl^{36} tracer.

Quite a few interesting problems have been successfully resolved by the use of Cl^{36}-labeled radioactive tracers. But Cl^{36} is applicable only in the study of chlorine-containing compounds.

It is evident that radioactive tracers tagged with C^{14} isotope can find an even wider range of applications in organic chemistry. At the present time, the radiochemical laboratory at the plant is working on a comparison of various methods for recording relatively weak C^{14} radiation with the object of selecting the most convenient variant.

Further, a radiometric technique for determining potassium by its natural beta-activity is being used in monitoring several potassium salt production streams at the plant. The precision of this technique was raised to 1% (relative) by measuring the activity with several counters placed in parallel. As we know, the method of determining potassium by its natural radioactivity is quite simple, and in practice is indifferent to the effect of varying impurity concentration, in addition requiring 10 to 20 times less time than chemical techniques.

All of the work mentioned was completed in a laboratory consisting of a counter room and preparations room occupying a total of 40 square meters floor space. The laboratory was staffed by four personnel. This laboratory differed from the usual chemical laboratory in that the floor in both rooms was lined with PVC panels, the walls and ceiling were painted with oil paints and corners joining wall to ceiling were all rounded. B-2 and B-3 counters and a scintillation measuring unit were employed to measure the radioactivity in the laboratory. A TISS dosimeter was used for health physics. Simple screens of plastic glass were used for shielding, along with small steel containers, protective plates of special steel, eye shields, etc. All of this equipment was obtained through the services of the All-Union IZOTOP organization or were fabricated directly at the plant.

This brief review of the work carried out demonstrates that the radiochemical laboratory enabled the parent plant to expand its activities in the field of research and analytical work and to achieve some practical results. Consequently, it seems quite beneficial to organize laboratories in-plant for working with labeled atoms at each large chemical processing enterprise.

BIBLIOGRAPHY

NEW BOOKS

Translated from Atomnaya Énergiya, Vol. 18, No. 1,
pp. 86-88, January, 1965

Atomizdat Releases

10 let Pervoi v mire atomnoi elektrostantsii SSSR [Ten years of on-line performance of the world's first nuclear electric power station]. 1964, 215 pages. 53 kopeks.

Articles by specialists in their own fields and on the study of the reactor in the First nuclear electric power station are made available in this collection. The articles describe the results of research and experimental work directed to the study of the properties of this type of reactor and its components. The articles do not cover the entire field, but are of interest insofar as they elucidate the engineering solutions adopted for the reactors in the I. V. Kurchatov power station at Belyi Yar.

The articles take up reactor operation, process channels, absorbing rods, steam generators, and other topics. Tests for starting up power stations are described: the effect of gamma-radiation on the electrical conductivity of water, neutron radiographic research, investigation of the thermostability of organic coolants, and other subjects are considered.

Trudy Mezhdunarodnoi konferentsii po uskoritelyam [Proceedings of the international accelerator conference]. Dubna, August 21-27, 1963. Edited by A. A. Kolomenskii et al., 1964. 1092 pages. 5 rubles, 72 kopeks.

The reports of Soviet and foreign specialists included herein discuss the design of superhigh-energy charged-particle accelerators (150 to 1000 GeV) and colliding-beam work. Papers by foreign scientists appear in English. The conference was held in August 1963 at the Dubna Joint Institute for Nuclear Research.

Issledovaniya po primeneniyu organizheskikh teplonositelei-zamedlitelei v energeticheskikh reaktorakh [Investigations in the use of organic moderator-coolants in power reactors]. 1964. 244 pages. 82 kopeks.

One of the areas of brightest prospects in power reactor design is the design of reactors using organic coolant-moderators. In the Soviet Union, this work is being carried out in the design of low-power units. One such unit, the ARBUS organic-cooled organic-moderated reactor, rated at 750 kW(e), has been in successful operation since August 1963.

The work being conducted by various organizations in the USSR in investigating organic moderator-coolants for the ARBUS and other installations has been well reflected in this collection of articles. Four sections appear: I. Radiation-chemical research; II. Heat transfer research; III. Interaction with materials; IV. Neutron physics research.

The first section contains five articles. All of these deal to some extent with how to cope with the major disadvantage of organic fluids: radiolysis and pyrolysis. Yu. N. Aleksenko and V. A. Khramchenkov discuss the radiation stability of monoisopropyldiphenyl at different temperatures. A study of a mixture of incompletely hydrated terphenyls by Yu. N. Aleksenko, A. M. Brodskii, K. P. Lavrovskii, and V. A. Khramchenkov follows. The possible use of petroleum gas-oil fractions as coolant was probed by A. M. Brodskii et al. A. B. Vol'f-Epshtein et al., considered a coolant based on cumene wastes. The last article in this section (A. M. Brodskii et al.) deals with hydrogenization recovery of organic coolants.

The second section contains six articles. The use of organic coolants as the working fluid in nuclear power facilities is discussed in a paper by Yu. I. Koryakin, A. A. Loginov et al. Heat transfer characteristics of monoisopropyldiphenyl and hydroterphenyl in radiolysis and their modifications are taken up in an article by Yu. N. Aleksenko et al. An investigation of heat exchange when organic fluids are used is discussed in other articles in this section (L. S. Sterman and V. V. Petukhov investigation of heat output; L. S. Sterman, V. D. Mikhailov et al.—burnout flux in boiling in tubes; L. E. Mikhailov and K. V. Naboichenko—boiling in the annular gap; F. F. Bogdanov—heat removal from a bundle of helical heated rods).

Two articles make up the third section. Yu. F. Bychkov et al., discuss corrosion attack by diphenyl on metals and oxides, and A. A. Nevzorova et al., study the compatibility of organic fluids and certain structural materials.

The first of five articles in the fourth section is devoted to critical experiments with monoisopropyldiphenyl and gas-oil. (Yu. N. Aleksenko et al.). L. N. Yurova et al., discussed several physical characteristics of uranium-organic lattices investigated on a critical assembly. The behavior of neutrons when organic fluids are used was taken up in the remaining three articles (L. N. Yurova et al.—dependence of square of diffusion length and of neutron diffusion coefficient on temperature in organic fluids; V. I. Mostovoi et al.—scattering of slow monochromatic neutrons on monisopropyldiphenyl; V. S. Dikarev et al.—measurement of thermal neutron spectra in a uranium-organic lattice).

This book is the first collection of articles on organic-cooled organic-moderated reactors in the Soviet or foreign nucleonic literature. The heavy load of theoretical and experimental data derived from the latest available research renders the book highly useful for practical purposes.

V. I. Krasnikov. Geologicheskie predposylki poiskov mestorozhdenii urana [Geological prerequesites in prospecting uranium deposits]. 1964. 187 pages. 73 kopeks.

This book generalizes upon the experience acquired in geological prospecting studies of ore-bearing districts and considers a wide range of factors influencing the choice of effective prospecting techniques in uranium prospecting at the current state of scientific and engineering art. The book reflects the new theoretical basis of prospecting derived from scientific data and practice. A portion of the book is devoted to discussion.

An ample reference list of literature is given at the end of the book.

N. G. Gusev, V. P. Mashkovich, and B. V. Verbitskii. Radioaktivnye izotopy kak gamma-izluchateli [Radioactive isotopes as gamma-emitters]. 1964. 279 pages. 70 kopeks.

This handbook cites tabulated material on the calculations pertaining to the ionization and energy gamma-constants of a large number of radioisotopes, enabling us thereby to determine the gamma-constants of preparations with initial filters, daughter emissions, and other factors taken into account. All the characteristics of radioisotopes are brought up to date in line with the most recent literature data.

The list of pertinent literature includes 467 titles.

A. A. Moiseev and V. I. Ivanov. Kratkii spravochnik po radiatsionnoi zashchite i dozimetrii [Concise shielding and dosimetry handbook]. 1964. 182 pages. 57 kopeks.

This book provides reference material on radiation shielding and dosimetry of ionizing radiations, compiled from data published in the Soviet and foreign literature.

Information is cited on the content of natural radioactive isotopes in the external environment and in the human organism; the data required for calculating exposure dosage due to natural and to artificial radioactivity, in work with radioactive isotopes and sources of ionizing radiations, are supplied.

Critical tolerance levels for exposure and critical tolerance concentrations of radioactive isotopes in air and in water are given.

The handbook consists mainly of graphs and tables. A list of literature used in its compilation appears.

L. A. Pertsov. Prirodnaya radioaktivnost' biosfery [Natural radioactivity of the biosphere]. 1964. 315 pages. 1 ruble, 24 kopeks.

This monograph assembles material on the natural radioactivity of the external environment published in recent years. Descriptions of phenomena and patterns which apparently aid a more complete understanding of the basic causes of the dynamics of indices of the natural radioactivity of the biosphere and consequently will contribute to a more correct interpretation of radiation hygiene facts in each concrete case are offered.

A. N. Protsenko. Pokorenie atoma [Taming of the atom]. 1964. 175 pages. 28 kopeks.

The reader learns the fundamentals of nuclear techniques in popular form and with no slighting of scientific accuracy. The author presents a lively and interesting account of various types of nuclear reactors, their operating principles, their function and the interrelation of control systems, heat removal systems, radiation shielding. No complicated mathematical formulae appear.

I. M. Bekkerman. Nevidimoe ostavlyaet sled [Footprints left by the invisible]. 1964. 155 pages. 24 kopeks.

This book presents a popular account of cloud chambers and bubble chambers, instruments in wide use in the physics of the atomic nucleus and of elementary particles. As is well known, these instruments enable scientists to "see" nuclear particles, or rather to see the tracks left by those particles, and thereby to study the interaction of particles. The physical fundamentals and the design of cloud chambers and bubble chambers, and some results of their use, are elucidated in clearcut manner in the book.

L. V. Bobrov. Teni nevidimogo sveta [Shadows left by invisible light]. 1964. 114 pages. 18 kopeks.

This book contains little known biographical details filling out the picture of Roentgen, the scientist and the man, standing on the frontier between classical and modern physics.

Related literature is listed.

K. Spurny, C. Jech, B. Serdlacek, and O. Storch. Aerozoli [Aerosols]. Translated from the Czech, 1964. 360 pages. 1 ruble, 75 kopeks.

The book describes the physicochemical and biological properties of aerosols, methods for measuring concentrations of dust, smoke, and vapor in the air, and methods for making determinations of radioactive dust. A detailed description of the possible engineering use of aerosols and of methods for coping with dust in industry appears.

The book is the first monograph of this type to appear in the Russian language.

A list of related literature is appended.

G. Thomson. Zashchita mlekopitayushchikh ot ioniziruyushchikh izluchenii. Translation from the English [Protection of mammals against ionizing radiations]. 1964. 178 pages. 93 kopeks.

This book presents a survey of a sector of modern radiobiology of high practical and theoretical importance: chemical protection and treatment of mammals from the injurious effects of external ionizing radiation. The book centers the brunt of its attention on the chemical prophylaxis of radiation injuries.

É. Cotton. Sem'ya Kyuri i radioaktivnost'. Translation from the French [The Curie family and radioactivity]. 1964. 175 pages. 51 kopeks.

The author, Eugenie Cotton, is a physicist who has been an active participant in the international women's democratic movement, and was intimately acquainted with the Curie family. She renders a lively and captivating account of the history of the discovery of radioactivity, of the scientific activities and life of this glorious family. Warm words of sincerity sketch a portrait of Marie Curie, an outstanding researcher and remarkable person who devoted her entire lifetime to science and to the cause of progress of human reason.

K. Zelig. Albert Einstein. Abridged translation from the German. 1964. 205 pages. 63 kopeks.

This book by Selig, who knew Einstein well, gives a detailed account of the life and career of the scientist. The principal merit of the book is the abundance of factual material. Einstein's meetings with many persons in various professions are described. The portrait of Einstein presented in the book is the portrait of a living person, replete with his character and contradictions, a person educated in the XIX century who completely changed the world's outlook in the XX century.

Releases by Other Publishers

International Electrotechnical Vocabulary (2nd edition), Group 65, Radiology and Radiological Physics. Publ. by the central office of the International Electrotechnical Commission, Geneva, 1964, 110 pp.

This book is the official edition of a list of terms and their definitions prepared by the International Standards Organization. Included are over 500 entries from radiology, dosimetry, radiometry, and related fields. Each entry is presented in parallel format in eight languages in this edition (English, French, German, Spanish, Italian, Dutch, Polish, Swedish), and the definitions are bilingual (French and English).

The terms are those recommended by the International Standards Organization for international usage.

Polonii, materialy po toksikologii, klinike i terapii porazhenii [Polonium: toxicology, clinical treatment and therapy of injuries]. Edited by V. A. Sanotskii. Moscow. Meditsina press, 1964. 276 pages. 1 ruble, 32 kopeks.

A collection of papers devoted to the biological effects of the α-radioactive isotope Po^{210}, this book consists of two parts. The first contains 18 papers making a balance sheet of many years of research on the pathology of polonium-induced injuries, and on the toxicity of polonium under a variety of conditions. The second part publishes 10 investigations on the therapy of lesions by polonium. The book ends with a generous list of literature extending to 16 pages.

Materialy po toksikologii radioaktivnykh veshchestv, vyp. 4 (torii-232, uran-238). [Toxicology of radioactive materials, No. 4 (thorium-232, uranium-238)]. Edited by A. A. Letavet and E. B. Kurlyandskaya. Moscow, Meditsina press, 1964. 120 pages. 61 kopeks.

This publication includes 12 papers on work completed at the radiotoxicological laboratory of the Institute of Industrial Hygiene and Occupational Diseases of the Academy of Medical Sciences of the USSR; the papers deal with the toxicology of insoluble thorium and uranium compounds, viz. with thorium dioxide $Th^{232}O_2$ and the uranic-uranous oxide $U_3^{238}O_8$. A comparison of soluble and insoluble compounds is made in some of the papers.

A. I. Nikolaev. Mikroelementy v patogeneze i lechenii luchevoi bolezni [Trace elements in the pathogenesis and treatment of radiation sickness]. Tashkent, publ. by Meditsina press, Uzbek SSR, 1964. 126 pages. 48 kopeks.

The effect of trace elements on regeneration in an organism exposed to irradiation is studied on the basis of Soviet and foreign research. Material dealing with clinical tests of complex cobalt compounds in general radiation complications in telegammatherapy patients is presented.

Radiatsionnaya avtomatika, izotopy i yadernye izlucheniya v nauke i tekhnike [Radiation-based automatic control, isotopes and nuclear radiations in science and industry]. Kiev, publ. by Academy of Sciences of the Ukrainian SSR, 1964. 196 pages. 93 kopeks.

This book is a collection of articles on the applications of radioactive isotopes and ionizing radiations in science and industry.

M. F. Yudin and V. I. Fominykh. Neitronnaya dozimetriya [Neutron dosimetry]. Moscow, Standards press, 1964. 216 pages.

This book presents the basic conditions mandatory in order to achieve unity in neutron measurements, without which it would be impossible to compare the results of neutron flux and neutron dose measurements. After a brief introduction elucidating the concepts of neutron dose and describing the basic properties of the neutron, there follows the first chapter, devoted to the characteristics of neutron sources. Both radioactive sources and accelerators of charged particles or nuclear reactors are described there. The second and third chapters analyze the major processes occurring in the interaction of neutrons with matter, biological tissue included.

Techniques for neutron flux measurements are in the fourth chapter; special sections here take up detectors showing a constant recording efficiency for neutrons of various energies and absolute measurements of the flux of thermal, intermediate, and fast neutrons. Neutron dosimetry is considered in the fifth chapter. Sections dealing with neutron dosimetry units, applications of special ionization chambers and other equipment, and different techniques in neutron dose determinations are also found there.

The sixth chapter in which methods for converting flux density units to neutron exposure dose and the related equipment (checking circuits, standard and reference neutron emitters, neutron counters and dosimeters, are analyzed) is of particular interest. The book ends in a special section on neutron radiation shielding. The list of literature used contains 240 titles.

Several appendices give the relationships between the units used in the dosimetry of ionizing radiations, recommended forms for inspection of neutron sources and dosimeters, dose absorption curves for neutrons of different energies at different depths in a tissue-equivalent phantom, and miscellaneous useful data.

The book is written for technicians engaged in the checking and calibration of counters and neutron dosimeters, and for those utilizing these instruments in practice or specializing in dosimetry of ionizing radiations.

Soviet Journals Available in Cover-to-Cover Translation

ABBREVIATION	RUSSIAN TITLE		TITLE OF TRANSLATION	PUBLISHER	TRANSLATION Vol.	Issue	BEGAN Year
AÉ	Atomnaya énergiya		Soviet Journal of Atomic Energy	Consultants Bureau	1	1	1956
Akust. zh.	Akusticheskii zhurnal		Soviet Physics – Acoustics	American Institute of Physics	1	1	1955
	Astronomicheskii zhurnal		Soviet Astronomy – AJ	American Institute of Physics	34	1	1957
Astr(on). zh(urn).	Avtomaticheskaya svarka		Automatic Welding	Br. Welding Research Assn. (London)	12	1	1959
Avto(mat). svarka	Avtomatika i Telemekhanika		Automation and Remote Control	Instrument Society of America	27	1	1956
	Biofizika		Biophysics	National Institutes of Health**	6	1	1961
	Biokhimiya		Biochemistry	Consultants Bureau	21	1	1956
Byull. éksp(erim). biol. (i med.)	Byulleten' éksperimental'noi biologii i meditsiny		Bulletin of Experimental Biology and Medicine	Consultants Bureau	41	1	1959
		Life Sciences	Doklady Biological Sciences Sections (includes: Anatomy, biochemistry, biophysics, cytology, ecology, embryology, endocrinology, evolutionary morphology, genetics, histology, hydrobiology, microbiology, morphology, parasitology, physiology, zoology)	National Science Foundation*	112	1	1957
		Life Sciences	Doklady Botanical Sciences Sections (includes: Botany, phytopathology, plant anatomy, plant ecology, plant embryology, plant physiology, plant morphology)	National Science Foundation*	112	1	1957
DAN (SSSR) Dokl(ady) AN SSSR	Doklady Akademii Nauk SSSR	Chemical Sciences	Proceedings of the Academy of Sciences of the USSR, Section: Chemical Technology	Consultants Bureau	106	1	1956
		Chemical Sciences	Proceedings of the Academy of Sciences of the USSR, Section: Chemistry	Consultants Bureau	106	1	1956
		Chemical Sciences	Proceedings of the Academy of Sciences of the USSR, Section: Physical Chemistry	Consultants Bureau	112	1	1957
		Earth Sciences	Doklady Earth Sciences Sections (includes: Geochemistry, geology, geophysics, hydrogeology, lithology, mineralogy, oceanology, paleontology, permafrost, petrography)	American Geological Institute	124	1	1959
		Earth Sciences	Proceedings of the Academy of Sciences of the USSR, Section: Geochemistry	Consultants Bureau	106-123	1 6	1956-1958
		Earth Sciences	Proceedings of the Academy of Sciences of the USSR, Section: Geology	Consultants Bureau	112-123	1 6	1957-1958
		Mathematics	Soviet Mathematics – Doklady	American Mathematical Society	130	1	1960
		Physics	Soviet Physics – Doklady (includes: Aerodynamics, astronomy, crystallography, cybernetics and control theory, electrical engineering, energetics, fluid mechanics, heat engineering, hydraulics, mathematical physics, mechanics, physics, technical physics, theory of elasticity sections)	American Institute of Physics	106	1	1956
	Elektrosvyaz'		Telecommunications	Am. Inst. of Electrical Engineers		1	1957
Entom(ol). oboz(r).	Entomologicheskoe obozrenie		Entomological Review	National Science Foundation**	37	1	1958
FMM	Fizika metallov i metallovedenie		Physics of Metals and Metallography	Acta Metallurgica	5	1	1957
FTT, Fiz. tv(erd). tela	Fizika tverdogo tela		Soviet Physics – Solid State	American Institute of Physics	1	1	1959
Fiziol. Zh(urn). SSSR	Fiziologicheskii zhurnal imeni I.M. Sechenov		Sechenov Physiological Journal USSR	National Institutes of Health**	47	1	1961
Fiziol(ogiya) rast.	Fiziologiya rastenii		Plant Physiology	National Science Foundation*	4	1	1957
	Geodeziya i aerofotosyemka		Geodesy and Aerophotography	American Geophysical Union			1962
	Geokhimiya		Geochemistry	The Geochemical Society	1	1	1956
Geol. nefti i gaza	Geologiya nefti i gaza		Petroleum Geology	Petroleum Geology	2	1	1958
	Geomagnetizm i aeronomiya		Geomagnetism and Aeronomy	American Geophysical Union	1	1	1961
	Iskusstvennye sputniki zemli		Artificial Earth Satellites	Consultants Bureau	1	1	1958
Izmerit. tekhn(ika)	Izmeritel'naya tekhnika		Measurement Techniques	Instrument Society of America	7	1	1958

The translation of this journal is published in sections

Declassified and Approved For Release 2013/09/24 : CIA-RDP10-02196R000700010001-6

Izv. AN SSSR O(td). Kh(im). N(auk)	Izvestiya Akademii Nauk SSSR: Otdelenie khimicheskikh nauk	Bulletin of the Academy of Sciences of the USSR: Division of Chemical Science	Consultants Bureau	16	1	1952
Izv. AN SSSR O(td). T(ekhn). N(auk): Metall). i top.	(see Met. i top)					
Izv. AN SSSR Ser. fiz(ich).	Izvestiya Akademii Nauk SSSR: Seriya fizicheskaya	Bulletin of the Academy of Sciences of the USSR: Physical Series	Columbia Technical Translations	18	3	1954
Izv. AN SSSR Ser. geofiz.	Izvestiya Akademii Nauk SSSR: Seriya geofizicheskaya	Bulletin of the Academy of Sciences of the USSR: Geophysics Series	American Geophysical Union	7	1	1957
Izv. AN SSSR Ser. geol.	Izvestiya Akademii Nauk SSSR: Seriya geologicheskaya	Bulletin of the Academy of Sciences of the USSR: Geologic Series	American Geological Institute	23	1	1958
Iz. Vyssh. Uch. Zav., Tekh. Teks. Prom.	Izvestiya Vysshikh Uchebnykh Zavedenii Tekhnologiya Tekstil'noi Promyshlennosti	Technology of the Textile Industry, USSR	The Textile Institute (Manchester)	4	1	1960
Kauch. i rez.	Kauchuk i rezina	Soviet Rubber Technology	Palmerton Publishing Company, Inc.	18	3	1959
	Kinetika i kataliz	Kinetics and Catalysis	Consultants Bureau	1	1	1960
	Koks i khimiya	Coke and Chemistry, USSR	Coal Tar Research Assn. (Leeds, England)		8	1959
Kolloidn. zh(urn).	Kolloidnyi zhurnal	Colloid Journal	Consultants Bureau	14	1	1952
	Kristallografiya	Soviet Physics – Crystallography	American Institute of Physics	2	1	1957
Metallov: i term.	Metallovedenie i termicheskaya obrabotka metallov	Metals Science and Heat Treatment of Metals	Acta Metallurgica	6	1	1958
	Metallurg	Metallurgist	Acta Metallurgica		1	1957
Met. i top.(gorn.)	Metallurgiya i toplivo (gornoye delo)	Russian Metallurgy and Fuels(mining)	Scientific Information Consultants, Ltd.		1	1960
Mikrobiol.	Mikrobiologiya	Microbiology	National Science Foundation*	26	1	1957
	Ogneupory	Refractories	Acta Metallurgica	25	1	1960
OS, Opt. i spektr.	Optika i spektroskopiya	Optics and Spectroscopy	American Institute of Physics	6	1	1959
Paleontol. Zh(urn)	Paleontologicheskii Zhurnal	Journal of Paleontology	American Geological Institute		1	1962
	Pochvovedenie	Soviet Soil Science	National Science Foundation**	53	1	1958
	Poroshkovaya Metallurgiya	Soviet Powder Metallury and Metal Ceramics	Consultants Bureau	2	1	1962
	Priborostroenie	Instrument Construction	Taylor and Francis, Ltd. (London)	4	1	1959
Pribory i tekhn. éks(perimenta)	Pribory i tekhnika éksperimenta	Instruments and Experimental Techniques	Instrument Society of America	3	1	1958
Prikl. matem. i mekh(an).	Prikladnaya matematika i mekhanika	Applied Mathematics and Mechanics	Am. Society of Mechanical Engineers	22	1	1958
PTE	(see Pribory i tekhn. éks.)					
	Problemy Severa	Problems of the North	National Research Council of Canada		1	1958
	Radiokhimiya	Radiochemistry	Consultants Bureau	4	1	1962
Radiotekh.	Radioteknika	Radio Engineering	Am. Institute of Electrical Engineers	16	1	1961
Radiotekhn. i élektron(ika)	Radiotekhnika i électronika	Radio Engineering and Electronic Physics	Am. Institute of Electrical Engineers	6	1	1961
	Stal'	Stal (in English)	Iron and Steel Institute	19	1	1959
	Stanki i instrument	Machines and Tooling	Production Engineering Research Assoc.	30	1	1959
Stek. i keram.	Steklo i keramika	Glass and Ceramics	Consultants Bureau	13	1	1956
Svaroch. proiz-vo	Svarochnoe proizvodstvo	Welding Production	Br. Welding Research Assn. (London)	5	4	1959
Teor. veroyat. i prim.	Teoriya veroyatnostei i ee primenenie	Theory of Probability and Its Application	Soc. for Industrial and Applied Math.	1	1	1956
Tsvet. metally	Tsvetnye metally	The Soviet Journal of Nonferrous Metals	Primary Sources	33	1	1960
UFN	Uspekhi fizicheskikh nauk	Soviet Physics – Uspekhi (partial translation)	American Institute of Physics	66	1	1958
UKh, Usp. khimi	Uspekhi khimii	Russian Chemical Reviews	Chemical Society (London)	29	1	1960
UMN	Uspekhi matematicheskaya nauk	Russian Mathematical Surveys	Cleaver-Hume Press, Ltd. (London)	15	1	1960
Vest. mashinostroeniya	Vestnik mashinostroeniya	Russian Engineering Journal	Production Engineering Research Assoc.	39	4	1959
Vop. onk(ol).	Voprosy onkologii	Problems of Oncology	National Institutes of Health**	7	1	1961
Zav(odsk). lab(oratoriya)	Zavodskaya laboratoriya	Industrial Laboratory	Instrument Society of America	24	1	1958
ZhAKh, Zh. anal(it). Khim(ii)	Zhurnal analiticheskoi khimii	Journal of Analytical Chemistry	Consultants Bureau	7	1	1952
ZhETF Zh. éksperim. i teor. fiz.	Zhurnal eksperimental'noi i teoreticheskoi fiziki	Soviet Physics – JETP	American Institute of Physics	28	1	1955
ZhFKh Zh. fiz. khimii	Zhurnal fizicheskoi khimii	Russian Journal of Physical Chemistry	Chemical Society (London)	33	7	1959
ZhNKh Zh. neorg(an). khim.	Zhurnal neorganicheskoi khimii	Journal of Inorganic Chemistry	Chemical Society (London)	4	1	1959
ZhOKh Zh. obshch. khim.	Zhurnal obshchei khimii	Journal of General Chemistry USSR	Consultants Bureau	19	1	1949
ZhPKh Zh. prikl. khim.	Zhurnal prikladnoi khimii	Journal of Applied Chemistry USSR	Consultants Bureau	23	1	1950
ZhSKh Zh. strukt(urnoi) khim.	Zhurnal strukturnoi khimii	Journal of Structural Chemistry	Consultants Bureau	1	1	1960
ZhTF	Zhurnal tekhnicheskoi fiziki	Soviet Physics – Technical Physics	American Institute of Physics	26	1	1956
Zh. tekhn. fiz.	Zhurnal vychislitel'noi matematika i matematicheskoi fiziki	U.S.S.R. Computational Mathematics and Mathematical Physics	Pergamon Press, Inc.	1	1	1962
Zh. vyssh. nervn. deyat. (im. Pavlova)	Zhurnal vysshei nervnoi deyatel'nosti (im I. P. Pavlova)	Pavlov Journal of Higher Nervous Activity	National Institutes of Health**	11	1	1961

*Sponsoring organization. Translation published by Consultants Bureau.
**Sponsoring organization. Translation published by Scripta Technica.

Declassified and Approved For Release 2013/09/24 : CIA-RDP10-02196R000700010001-6

SIGNIFICANCE OF ABBREVIATIONS MOST FREQUENTLY ENCOUNTERED IN SOVIET PERIODICALS

FIAN	Phys. Inst. Acad. Sci. USSR.
GDI	Water Power Inst.
GITI	State Sci.-Tech. Press
GITTL	State Tech. and Theor. Lit. Press
GONTI	State United Sci.-Tech. Press
Gosenergoizdat	State Power Press
Goskhimizdat	State Chem. Press
GOST	All-Union State Standard
GTTI	State Tech. and Theor. Lit. Press
IL	Foreign Lit. Press
ISN (Izd. Sov. Nauk)	Soviet Science Press
Izd. AN SSSR	Acad. Sci. USSR Press
Izd. MGU	Moscow State Univ. Press
LEIIZhT	Leningrad Power Inst. of Railroad Engineering
LET	Leningrad Elec. Engr. School
LETI	Leningrad Electrotechnical Inst.
LETIIZhT	Leningrad Electrical Engineering Research Inst. of Railroad Engr.
Mashgiz	State Sci.-Tech. Press for Machine Construction Lit.
MEP	Ministry of Electrical Industry
MES	Ministry of Electrical Power Plants
MESEP	Ministry of Electrical Power Plants and the Electrical Industry
MGU	Moscow State Univ.
MKhTI	Moscow Inst. Chem. Tech.
MOPI	Moscow Regional Pedagogical Inst.
MSP	Ministry of Industrial Construction
NI ZVUKSZAPIOI	Scientific Research Inst. of Sound Recording
NIKFI	Sci. Inst. of Modern Motion Picture Photography
ONTI	United Sci.-Tech. Press
OTI	Division of Technical Information
OTN	Div. Tech. Sci.
Stroiizdat	Construction Press
TOE	Association of Power Engineers
TsKTI	Central Research Inst. for Boilers and Turbines
TsNIEL	Central Scientific Research Elec. Engr. Lab.
TsNIEL-MES	Central Scientific Research Elec. Engr. Lab.-Ministry of Electric Power Plants
TsVTI	Central Office of Economic Information
UF	Ural Branch
VIESKh	All-Union Inst. of Rural Elec. Power Stations
VNIIM	All-Union Scientific Research Inst. of Metrology
VNIIZhDT	All-Union Scientific Research Inst. of Railroad Engineering
VTI	All-Union Thermotech. Inst.
VZEI	All-Union Power Correspondence Inst.

Note: Abbreviations not on this list and not explained in the translation have been transliterated, no further information about their significance being available to us. — Publisher.